Performance of Spectrum Sensing Schemes in Cognitive Radio for Static and Dynamic Primary Users in Additive Laplacian Noise

A Thesis Submitted To

Nirma University

In Partial Fulfillment Of The Requirements For

The Degree Of

Doctor of Philosophy

In

Technology & Engineering

BY

KHUSHBOO SINHA

(18FTPHDE24)

Department of Electronics & Communications Engineering

Institute of Technology, Nirma University,

Ahmedabad, Gujarat, India

February 2023

Nirma University
Institute of Technology
Certificate

This is to certify that the thesis entitled **Performance of Spectrum Sensing Schemes in Cognitive Radio for Static and Dynamic Primary Users in Additive Laplacian Noise** has been prepared by **Ms. Khushboo Sinha** under my supervision and guidance. The thesis is her own original work completed after careful research and investigation. The work of the thesis is of the standard expected of a candidate for Ph.D. Programme in **Electronics and Communication Engineering** and I recommend that it be sent for evaluation.

Date: Feb. 8, 2023

Signature of the Guide

Forwarded Through:

9/2/23
(i) Head, Department of Electronics and Communication Engineering

9/2/23
(ii) Dean, Faculty of Technology and Engineering

13-2-23
(iii) Dean, Faculty of Doctoral Studies and Research

To:
Executive Registrar
Nirma University

14/2/22

Nirma University
Institute of Technology

Declaration

I, **Khushboo Sinha**, registered as Research Scholar, bearing Registration No. **18FTPHDE24** for Doctoral Programme under the Faculty of **Technology and Engineering** of Nirma University do hereby declare that I have completed the course work, pre-synopsis seminar and my research work as prescribed under R. Ph.D. 3.5.

I do hereby declare that the thesis submitted is original and is the outcome of the independent investigations / research carried out by me and contains no plagiarism. The research is leading to the discovery of new facts / techniques / correlation of scientific facts already known. This work has not been submitted to any other University or Body in quest of a degree, diploma or any other kind of academic award.

I do hereby further declare that the text, diagrams or any other material taken from other sources (including but not limited to books, journals and web) have been acknowledged, referred and cited to the best of my knowledge and understanding.

Date: Feb. 8, 2023

Khushboo Sinha

Khushboo Sinha
(18FTPHDE24)

I endorse the above declaration made by the student.

Y N Trivedi

Dr. Y N Trivedi
(Guide)

Enclosure - V

Specimen 'D'

Nirma University
Institute of Technology
<u>Certificate</u>

This is to certify that the thesis entitled **Performance of Spectrum Sensing Schemes in Cognitive Radio for Static and Dynamic Primary Users in Additive Laplacian Noise** has been prepared by me, under the supervision and guidance of **Dr. Y. N. Trivedi**. The thesis is my own original work completed after careful research and investigation. The work of the thesis is of the standard expected of a candidate for Ph.D. Programme. The final hard bound copy of the thesis is submitted after incorporating all the suggestions / corrections suggested by the referees.

Date: 07/02/2024

Khushboo Sinha

Khushboo Sinha

Date: 07/02/2024

YNTrivedi

Dr. Y. N. Trivedi (Guide)

Forwarded Through:

(i) 8/2/24

Dr. R. N. Patel
Dean - Faculty of Technology and Engineering

9-2-'24

(ii)

Dr. P. N. Tekwani
Dean - Faculty of Doctoral Studies and Research

(iii) 9/2/24

Shri G. Ramachandran Nair
Executive Registrar, Nirma University

Dedicated

To

My Grandparents

Who nurtured my childhood with unconditional love and care

&

My Husband (Pravin Kumar)

Whose motivations and criticism make me stronger!

Acknowledgements

First and foremost, I praise and thank God, the almighty for his divine grace and showers of blessing. He has given me the strength to overcome all the challenging moments during my research work. It would have been very difficult to accomplish the work without immense love and support from many wonderful people. Although I am sure my words would fall short, I would like to extend my sincere gratitude with open arms to each of them.

I would like to express my sincere gratitude to my supervisor, Professor Y. N. Trivedi for introducing me to the field of statistical signal processing and wireless communications through his theory classes. His profound insights in wireless communications, along with the crucial ability to review the research work minutely, have been a source of inspiration. He has always shown a great deal of faith in my talent and given me the freedom to work fairly independently. He provided invaluable and constructive guidance whenever I needed it. He will inspire me as a role model for my future career with his unique blend of technical expertise, foresight, patience, and generosity. I shall be forever obliged for the opportunity to work with him during my Ph.D.

I would like to express my gratitude to each of the faculty at the ECE department of the IT-NU for their direct or indirect support. I would like to offer special thanks to Prof. Ruchi Gajjar, Prof. Vaishali Dhare, Prof. Twinkle Bhavsar, Prof. Piyush Bhatsana, and Prof. Rachna Sharma for their invaluable academic support. I am deeply indebted to Late Prof. Tanish Zaveri and former IT-NU faculty Prof. Dhaval Pujara for the fruitful discussions we had on several technical ideas.

I want to thank Nirma University, the Director-IT-NU, the Registrar-IT-NU, and the Directorate of Research and Innovation. Special thanks to the Vice-Chancellor of NU and the President of NU for their assistance during my period as a full-time research scholar. I would like to express my thanks to the IT-NU administrative and technical staff members. I want to offer special thanks to Ms. Krupaxi Patel, Ms. Kajal Shah, and lab assistant Mr. Prasann Shukla.

I would like to express my gratitude to research advisory committee members Dr. Y. B. Acharya and Dr. Manjunath Joshi for their constructive suggestions.

I want to thank my former colleagues Mr. Dharam Shah and Mr. Jay Gupta for guiding me in many ways during my initial days as a research scholar and for all the fun interactions we had.

I thank my grandparents for teaching me valuable lessons in life. I thank my parents for their love and care.

Finally, to my husband Pravin and devotee son Talin, thank you for being my pillars of strength. Your unconditional love and support have helped me to overcome the ups and downs in the past few years.

Last but not the least, the journey to this point was not easy. I would like to thank all mentioned and unmentioned who helped me on the way.

Khushboo Sinha
18FTPHDE24

List of Tables

List of Figures

List of Abbreviations

ALN	Additive Laplacian Noise
ASIC	Application Specific Integrated Circuit
AVCD	Absolute Value Cumulation Detection
ALR	Averaged Likelihood Ratio
AWGN	Additive White Gaussian Noise
BBP	Batch Bernoulli Process
BHT	Binary Hypothesis Testing
BPSK	Binary Phase Shift Keying
CSGN	Circularly Symmetric Gaussian Noise
CLT	Central Limit Theorem
CR	Cognitive Radio
CRs	Cognitive Radios
CRN	Cognitive Radio Network
CSS	Cooperative Spectrum Sensing
CuSum	Cumulative Sum
DDTHED	Dynamic Double Threshold Energy Detection
DTMC	Discrete Time Markov Chain
ED	Energy Detection
EGC	Equal Gain Combining
FCC	Federal Communications Commission
FLOM	Fractional Lower Order Moment

FHOM	Fractional Higher Order Moment
FSA	Fixed Spectrum Allocation
FC	Fusion Center
GED	Generalized Energy Detection
GGD	Generalized Gaussian Distribution
GGN	Generalized Gaussian Noise
GLRT	Generalized Likelihood Ratio Test
GMN	Gaussian Mixture Noise
GoF	Goodness-of-Fit
GRCR	Gerschgorin Radii and Center Ratio
HPUN	Hidden Primary User Node
i-AVCD	improved Absolute Value Cumulation Detection
iED	Improved ED
IEEE	Institute of Electrical and Electronics Engineers
iid	Independent and Identically Distributed
IoT	Internet of Things
ISM	Industrial Scientific and Medical
LSCP	Last Status Change Point
LRT	Likelihood Ratio Test
LSMD	Logarithmic Similarity Measure Detector
LSTP	'L'-step transition probability
MAI	Multiple Access Interference
MCA	Middleton Class A
MCMC	Markov Chain Monte-Carlo
MCD	Modified Correlation Detector
MCP	Markov Chain Parameter

MD	Moment based Detector
MDS	Modified Detection Schemes
MF	Matched Filter
MGC	Maximum Generalized Correntropy
MGN	Mixed Gaussian Noise
MIMO	Multiple Input Multiple Output
ML	Maximum Likelihood
MLE	Maximum Likelihood Estimation
M**-QAM**	'M'- Quadrature Amplitude Modulation
NP	Neyman Pearson
NR	New Radio
NSS	Narrowband Spectrum Sensing
OSA	Opportunistic Spectrum Access
OSTP	One-step transition probability
PCA	Polarity Coincidence Array
PCC	Polarity Coincidence Correlator
PDF	Probability Density Function
PRSCD	Phase-Rotated Spectral Correlation Detector
PMF	Probability Mass Function
PU	Primary User
PUs	Primary Users
QAM	Quadrature Amplitude Modulation
QoS	Quality of service
QPSK	Quadrature Phase Shift Keying
RDCA	Rayleigh Distributed Channel Attenuation
RMH	Refined Metropolis-Hastings

RF	Radio Frequency
ROC	Receiver Operating Characteristics
SDR	Software Defined Radio
SL-PCA	Soft Limiting-Polarity Coincidence Array
SMD	Sample Mean Detector
SNR	Signal-to-Noise Ratio
SSR	Suprathreshold Stochastic Resonance
SU	Secondary User
TD	Threshold Detector
TS	Threshold System
TP	Transition Probability
TV	Television
TPM	Transition Probability Matrix
3GPP	Third Generation Partnership Project
UWB	Ultra-Wideband
ULAD	Unilateral Left-Tail Anderson Darling
WLAN	Wireless Local Area Network
WRAN	Wireless Regional Area Network
WSS	Wideband Spectrum Sensing

Nomenclature

α	Scale parameter of Rayleigh distributed channel attenuation
$\Gamma(\cdot)$	Gamma function
γ	Average signal-to-noise ratio
$\hat{\vartheta}'_1$	Estimated first transition point of the PU under hypothesis H_1
$\hat{\vartheta}'_o$	Estimated first transition point of the PU under hypothesis H_o
κ	Scale parameter of Laplacian noise
$\mathbf{y}$	Array of N received observations at the cognitive terminal
Ψ	Detection Threshold
θ_A	Arrival rate of the PU
θ_D	Departure rate of the PU
$\Upsilon(\mathbf{y})$	Decision statistic
ϑ'_1	Second transition point of the PU under hypothesis H_1
ϑ_1	First transition point of the PU under hypothesis H_1
ϑ'_o	Second transition point of the PU under hypothesis H_o
ϑ_o	First transition point of the PU under hypothesis H_o
$E[\cdot]$	Expectation/Mean operator
$f_{n_m}(v)$	Probability density function of Laplacian noise at m_{th} sample
$f_n(v)$	Probability density function of Generalized noise
g_{ij}	One step transition probability of PU from i_{th} state to j_{th} state
H_1	Alternate hypothesis
H_o	Null hypothesis

l_{ij}	Sensing samples corresponding to one step transition of PU from i_{th} state to j_{th} state
l_{scp}	Last status change point of the PU
N	Total aggregate sensing samples
n_m	Laplacian noise at m_{th} sample
N_{ij}	Sensing samples corresponding to $(N-m)$ step transition of PU
P	exponent of the symbols received at the cognitive terminal
P_D	Detection probability
P_F	False alarm probability
P_o	Optimum P
P_{error}	Total error probability
s_m	Primary user symbol at m_{th} sample
$var[\cdot]$	variance operator
P_M	Missed detection probability
Q_d	Localized detection probability at surrounding cognitive terminals in CSS scheme
Q_f	Localized false alarm probability at surrounding cognitive terminals in CSS scheme
U_l	Single-bit hard decision at l_{th} CR in CSS scheme
y_m	Received PU observation at m_{th} sample

Contents

Abstract

Due to the evolution in wireless communications, the RF spectrum is overcrowded as it is scarce and expensive. However, it has been observed that the licensed spectrum remains underutilized. In the literature, various spectrum sensing schemes have been proposed for efficient spectrum utilization. In this case, the cognitive radio (CR) terminal senses the licensed spectrum of the primary user (PU). If the spectrum is found vacant, then the unlicensed user or secondary user (SU) can utilize the spectrum without interfering with the PU. The performance of the spectrum sensing techniques is presented and evaluated using receiver operating characteristics (ROC). The ROC for different spectrum sensing techniques is presented and compared with the literature assuming different scenarios such as coherent and non-coherent detections, different channel environments, PU with different waveforms, and various diversity schemes. A majority of the papers have assumed additive white Gaussian noise (AWGN) and static behavior of PU in the sensing interval. However, in a real-time scenario, these assumptions are difficult to follow. For example, in the multi-user environment, the interference from different sources such as multiple access interference (MAI) can be well approximated by additive Laplacian noise instead of AWGN. Further, due to the large density of PU and their frequent transitions, the static nature of PU in the sensing interval may not be followed. The dynamic behavior of the PU degrades the ROC performance of detection schemes, which assumed static behavior.

In this thesis, we assume additive Laplacian noise (ALN) channel instead of AWGN channel. We assume static PU and use a modified correlation detector (MCD) with cooperative spectrum sensing (CSS) scheme. We compare our proposed correlation detection scheme with the other state-of-the art of the correlation detection schemes. Dynamic behavior of the PU, where PU may randomly change its states within sensing period, has not been analyzed with ALN in the literature. We assume the dynamic behavior of PU, where the Poisson process models the rate of arrival and departure of the PU in the prescribed spectrum sensing interval. In this case, we use a non-coherent scheme using improved absolute value cumulation detection (i-AVCD). Subsequently, we assume more than one transition of PU in the sensing interval. The two transitions of PU have been modeled using weighted samples, which are further based on Cumulative Sum (CuSum) for detection. In this case, we use the sample mean detection (SMD) and i-AVCD as detection schemes. The multiple transitions of PU are modeled using the Markov chain. Further, we assume PU with different modulation order M such as M-QAM and show the effect of M on the ROC performance. Finally, we consider attenuation in the channel by Rayleigh distribution with diversity schemes such as Equal Gain Combining (EGC) and Soft limiting Polarity Coincidence Array (SL-PCA). In all the cases, we present ROC using simulations. We also derive analytical expressions of detection probability (P_D) and false alarm probability (P_F). A close match between simulations and their analytical counterparts validates our analytical approach. Further, a significant improvement in performance of the detection schemes is achieved using the CSS and receive diversity schemes.

Chapter 1

Introduction

Due to limited spectrum availability and increasing surge in the demand by users for wireless applications, such as multimedia services and industrial Internet of Things (IoT), spectrum scarcity has emerged as one of the most critical problems in the field of wireless communications [1]. The Fixed Spectrum Allocation (FSA) policy adopts a static mode for allocating the Radio Frequency (RF) spectrum [2, 3]. According to the Federal Communications Commission (FCC) report, FSA policy results in poor spectrum utilization where a major portion of the spectrum bands is not efficiently utilized that results in poor spectrum efficiency [4]. Spectrum utilization below 6 GHz, particularly in Ultra-Wideband (UWB) is very low which varies from 4.54% in Singapore to 17.4% in Chicago [5]. Unlicensed spectrum bands, such as Industrial Scientific and Medical (ISM) bands (2.4 GHz and 5 GHz) are used by Bluetooth, ZigBee, and Wireless Local Area Network (WLAN) [6–8]. With recent releases of the Third Generation Partnership Project (3GPP), i.e., Releases 16 and 17, these unlicensed bands have been proposed to be used by 5G New Radio (NR) [9]. Many countries in the US and Europe use 60 GHz millimeter wave band as an unlicensed band [10]. On the other hand, licensed spectrum bands such as Television (TV) bands, include white spaces in the range of 300 MHz - 3 GHz [11]. These TV white spaces are unoccupied or idle frequency bands used for television broadcast [12]. They have been assigned to mobile communications in order to efficiently use the increasingly scarce spectrum resource [13]. In an effort to mitigate the constraints of the spectrum, such as spectrum scarcity, congestion, and under-utilization, J. Mitola in 1999, proposed the notion of Cognitive radio which is based on the fundamentals of Software Defined Radio (SDR) [14, 15].

Cognitive Radio [16, 17]: The Cognitive Radio (CR) is a smart wireless radio that can automatically sense and detect the unoccupied spectrum and use it without interfering with licensed users [18, 19]. In the Opportunistic Spectrum Access (OSA) model of a Cognitive Radio Network (CRN) based communication systems, an unlicensed user or Secondary User (SU) makes opportunistic access to the under-utilized licensed band and can use the band until a licensed user or PU occupies the band [20]. The CR automatically detects available bands in the wireless spectrum and adjusts its transmission parameters accordingly [21]. The Institute of Electrical and Electronics Engineers (IEEE) 802.22 has been widely accepted as the first CR based Wireless Regional Area Network (WRAN) standard [22]. Wireless standards such as ECMA-392, IEEE 802.11af, and IEEE 802.15.4m operate in an OSA based CR model. Spectrum sensing is one of the major functions of a CR system where the spectrum is continuously monitored by the cognitive terminal to decide the presence or absence of PU and thus, reliably find the vacant spectrum [23].

Spectrum Sensing [24, 25]: In a CR system, SU at the cognitive terminal uses a technique known as "spectrum sensing" to sense the presence of the PU in the licensed spectrum. Spectrum sensing is a process of identifying unused portions of the spectrum, known as spectrum holes. In addition to this, the SU must exit the channel once the PU reappears in order to reduce the effect of adverse influence on the licensed users. Based on the span of the considered frequency band, spectrum sensing is classified as Wideband Spectrum Sensing (WSS) and Narrowband Spectrum Sensing (NSS). The wideband sensing involves scanning the wideband to determine the availability of the PU [26]. Narrowband sensing, on the other hand, focuses on scanning and monitoring a single segment of the band. In this case, the spectrum sensing problem is formulated as Binary Hypothesis Testing (BHT) problem.

Binary Hypothesis Testing: In this testing problem, the null hypothesis is denoted as H_o and the alternate hypothesis is denoted as H_1. At the cognitive terminal, each received symbol y_m from the PU can be expressed as [27]

$$\begin{aligned} H_o &: y_m = n_m; \\ H_1 &: y_m = s_m + n_m, \end{aligned} \tag{1.1}$$

where $m = 1, 2, \ldots, N$. The N denotes aggregate sensing samples. The s_m denotes the PU signal and $n_m \sim L(0, \kappa)$, i.e., Laplacian distribution with mean 0 and variance $2\kappa^2$, where κ is the scale parameter. The Probability Density Function (PDF) of the Laplacian noise can be expressed as [28]

$$f_{n_m}(v) = \frac{1}{2\kappa} \exp\left(-\frac{|v|}{\kappa}\right). \tag{1.2}$$

The detection probability P_D and false alarm probability P_F can be expressed as [29]

$$\begin{aligned} P_D &= Prob\Big\{\Upsilon(\mathbf{y}) > \Psi | H_1\Big\}, \\ P_F &= Prob\Big\{\Upsilon(\mathbf{y}) > \Psi | H_o\Big\}, \end{aligned} \tag{1.3}$$

where $\Upsilon(\mathbf{y})$ is the decision statistic and Ψ is the detection threshold obtained using the Neyman Pearson (NP) test [30]. The main focus of the spectrum sensing schemes is to improve the P_D. A brief description of research in the field of spectrum sensing in the past couple of years is presented in the following section.

1.1 Research in the field of Spectrum Sensing

Several spectrum sensing schemes have been analyzed in the literature. For example, in a spectrum sensing scheme, such as the Energy Detection (ED), square of the absolute value of the received observations is computed over the sensing period to obtain the final decision statistic [31,32]. The ED has been further modified to improved ED, where the received observations are raised to a positive real exponent P over the sensing period to get the final decision statistic [33]. The improved ED outperformed conventional ED significantly with an increase in the parameter P [34]. In the centralized CSS scheme, multiple Cognitive Radios (CRs) exist which send their hard or soft decisions to a central controlling center known as Fusion Center (FC) [35]. The FC combines the local decisions received from the surrounding CRs based on standard fusion schemes and gives the final decision on the presence or absence of the PU [36]. Thus, the CSS scheme offers space diversity through sensing channels to improve the detection performance [37–39]. The Covariance based spectrum sensing scheme has been analyzed in [40, 41], where decision statistic is formed from the covariance matrix of the received signal. The Eigenvalue based spectrum sensing has been proposed in [42–45], where decision statistic is derived as the ratio of maximum to minimum eigenvalues obtained from the covariance matrix of the received signal. The deep learning based detector has been proposed in [46,47], where the detection framework has been modeled using a deep neural network.

In the context of our country India, several researchers from different parts of the country have been involved in the field of spectrum sensing in cognitive radio. The improved ED has been analyzed for a multiple antenna scenario at the CR [48]. The CSS based on Gerschgorin Radii and Center Ratio (GRCR) algorithm has been proposed in [49]. In this paper, the VLSI architecture of the CSS scheme has been presented in the Rayleigh Fading environment. Subsequently, an Application Specific Integrated Circuit (ASIC) chip has been fabricated based on the GRCR based CSS scheme. Using the majority fusion scheme over an erroneous control channel, the CSS scheme has been introduced in [50]. The optimum number of surrounding CR users has been derived using different threshold selection approaches in [51]. The energy efficiency has been achieved in the collaborating scenario by optimizing CR users in [52]. For this, the relay assistance model has been proposed. Soft decision fusion scheme using a radix 2 decision fusion strategy has been proposed in [53]. It has been revealed that this soft fusion scheme inherits a hard decision fusion part and there is a mutual connection between the two. The spectrum sensing schemes proposed in [37–53] have assumed static PU with Gaussian noise.

In real communication systems, noise cannot be always Gaussian, especially in an impulsive noise environment and long range communications [54]. Several spectrum sensing schemes proposed in the literature have assumed non-Gaussian noise under the scenario of static PU. For example, the goodness-of-fit based detection scheme has been analyzed with symmetric alpha-stable noise based on the concept of geometric power [55]. The Middleton Class A (MCA) noise has been analyzed using the goodness-of-fit based detection scheme [56]. However, in the dense traffic areas, the PU possesses dynamic behavior [57]. The case of dynamic PU based on the Markov chain has been proposed in Nakagami-m fading channel [58]. In this paper, a correlated multiple antenna scenario has been addressed with ED scheme. Apart from this, several other spectrum sensing schemes with dynamic PU have been analyzed in the literature [59, 60]. The spectrum sensing schemes proposed in [58–60] have assumed Gaussian noise. The research in the field of spectrum sensing during the past couple of years has motivated us in many ways which are presented in the following section.

1.2 Motivation

Many spectrum sensing schemes have been proposed in the past couple of years, with a focus on developing suitable detection schemes to detect the existence of the PU with high detection probability. Followings are highlighted as key motivations based on the study of spectrum sensing schemes in Additive Laplacian Noise (ALN) environment.

(a) In general, there exist three models of a CR based communication systems. They are interweave, overlay, and underlay [61, 62]. In an interweave model, also known as OSA model, the SU opportunistically accesses the licensed spectrum. While opportunistically accessing the spectrum, only the SU is allowed to use the spectrum if it is idle, or not in use by the PU. This model does not allow the sharing of the band by PU and SU at the same time, hence interference effects are highly mitigated. Thus, this model provides the most assured Quality of service (QoS) and the highest level of reliability. It is of interest to consider OSA model of a CR, where SU opportunistically accesses the licensed band only after being assured of the absence of the PU.

(b) Many natural and man-made events, such as thunderstorms, lightning, microwave emissions, motor engines, etc. cause a high spike impulsive noise [63]. The impulsive noise is a train of high amplitude and low probable narrow impulses. These impulses can have a short or long duration. Further, they have fatter tails. The AWGN fails to characterize these impulsive environments. Non-Gaussian noises, such as MCA noise, Bernoulli Gaussian noise and Gaussian Mixture Noise (GMN) model impulsive noise scenario. By varying different parameters of these noises, the degree of impulse can be varied from a high impulse scenario (Dirac's distribution) to a no impulse scenario (Gaussian). Owing to fat tails, the Laplacian noise models impulsive noise precisely [64]. Further, in time-hopped UWB communication systems, Laplacian noise has been shown to model Multiple Access Interference (MAI) precisely as compared to other non-Gaussian models [65]. The MAI is the interference from the surrounding multiple users. Hence, it is of interest to observe the performance of spectrum sensing schemes in ALN.

(c) A majority of the available spectrum sensing schemes assume the existence of the PU in static state [66]. In the real world, PU cannot remain static under all circumstances, especially when PU traffic varies widely [67]. In order to align with practical scenarios, for example, in densely populated areas with high mobile traffic or in the war-prone border areas, the PU possesses dynamic behavior. As a result, achieving high detection probability while paying special attention to the dynamic behavior of the PU is of relevance.

1.3 Our Research Contributions

In this thesis, we have considered seven different system models. In all the models, we have assumed ALN channel. We have presented the performance using a plot between P_D and P_F, referred to as Receiver Operating Characteristics (ROC). The significant contributions made in this thesis are as follows:

(a) We have proposed a modified version of a general correlation detector known as Modified Correlation Detector (MCD). In the proposed MCD scheme, Binary Phase Shift Keying (BPSK) modulated static PU signal is corrupted with the Laplacian Noise. The received signal then correlates with the known PU signal at the cognitive terminal. Finally, it is raised to an exponent P with its range defined as $0 < P \leq 2$. Raising the received signal to an exponent P gives non-linearity to the detector with the condition $P \neq 1$. At $P = 1$, the proposed detector behaves as a Matched Filter (MF) detector which is linear in nature. The performance of this detection scheme has been shown using simulations. The MCD detector outperforms MF detector and Threshold Detector (TD) for $P < 1$. We have derived the closed-form expressions of P_D and P_F, presented ROC for different values of P and shown that performance improves as P decreases.

(b) In the second model, we have extended the first one with CSS using MCD as a localized detection scheme at each CR. The impact of different CSS fusion schemes on the detection probability has been discussed. We have derived closed-form expressions of P_D and P_F and presented ROC.

(c) In the third model, we have presented dynamic and unknown PU with one transition within the sensing period. Dynamic PU refers to the condition where PU randomly transits from 'ON' state to 'OFF' state and vice-versa within sensing period. The transitions are assumed as random arrival and random departure. Further, they are modeled using the Poisson distribution. Here, CR is not aware of any information about PU. Hence, we have used Generalized Likelihood Ratio Test (GLRT) together with Maximum Likelihood Estimation (MLE) of the PU. Further, the transition points are unknown and random. So, they are averaged out over the Likelihood Ratio Test (LRT). The Averaged Likelihood Ratio (ALR) is further simplified to get the final detection scheme, which corresponds to the improved Absolute Value Cumulation Detection (i-AVCD) scheme used with dynamic parameters, such as arrival rate ($\theta_A T$) and departure rate ($\theta_D T$) of the PU. We have presented the ROC using simulations. The performance of the i-AVCD scheme with Absolute Value Cumulation Detection (AVCD) and ED as its special cases, has been shown in the dynamic PU scenario. We found that the performance of the detection schemes in the dynamic PU scenario is better than the performance with static PU scenario, when the arrival rate and departure rate of the PU are beyond 1.

(d) In the fourth one, we have extended the third one with CSS using i-AVCD as a localized detection scheme at each CR. The impact of different CSS fusion schemes on the detection probability has been discussed. Finally, the simulation results are presented using ROC.

(e) In the fifth model, we have further increased the transition point of the unknown PU from 1 to 2, i.e, PU makes two transitions within the sensing period. The MLE has been used to jointly estimate the unknown PU and its Last Status Change Point (LSCP) under both hypotheses H_o and H_1. Further, Cumulative Sum (CuSum) based detection schemes, such as Sample Mean Detector (SMD) and i-AVCD have been presented. We have derived closed-form expressions of P_D and P_F and presented the results with ROC. Besides this, the comparison of one transition point of the PU with two transition points of the PU is presented. We observed that one PU status change outperforms the two PU status changes due to less estimation error in LSCP.

(f) In the sixth model, we overcome the limitations of a limited number of PU transitions. A scenario of multiple transitions of the PU has been presented within the sensing period. A modified detection scheme based on i-AVCD has been proposed. The Transition Probability Matrix (TPM) is used to calculate the transition probabilities when PU makes a transition from one state to another. In this case, 'M'- Quadrature Amplitude Modulation (M-QAM) for PU has been considered. Further, it has been assumed that the SU knows the Markov parameters a priori. Finally, we have derived closed-form expressions of P_D and P_F and presented the ROC.

(g) In the seventh model, we have modified the sixth one by including channel attenuation. It has been assumed that the channel attenuation follows Rayleigh distribution. Here also, M-QAM modulation has been considered for the PU. Further, a multiple antenna system has been analyzed at the CR. We have used diversity techniques, such as the Equal Gain Combining (EGC) and Soft Limiting-Polarity Coincidence Array (SL-PCA), derived P_D and P_F, and presented the results with ROC.

1.4 Organization of the Thesis

The thesis is organized as follows.

Chapter 2 presents a detailed overview of the diverse spectrum sensing techniques in cognitive radio. This chapter describes various coherent and non-coherent spectrum sensing schemes. Further, the cases of static PU and dynamic PU have been analyzed.

Chapter 3 proposes a modified, non-linear correlation detector MCD in ALN when PU is static. The performance of the proposed detection scheme has been presented with ROC.

Chapter 4 presents the CSS scheme when MCD is used as a localized detection scheme by each of the CRs present around the FC.

Chapter 5 presents the detection schemes, such as i-AVCD and SMD, when PU makes only one transition in ALN environment. Further, special cases of i-AVCD, such as AVCD and ED have been analyzed.

Chapter 6 presents the CSS scheme when PU makes one transition. The i-AVCD and SMD are used as localized detection schemes.

Chapter 7 presents the i-AVCD and sample mean detector SMD using CuSum based weighted samples in dynamic PU environment. Two transitions of the PU are assumed within the sensing period. Further, the detection performance with two transitions of the PU has been compared to the performance with one transition of the PU.

Chapter 8 presents modified i-AVCD scheme with M-QAM modulated PU. Further, multiple transitions of the PU are modeled using two state Discrete Time Markov Chain (DTMC). The detection performance has been compared with modified AVCD and modified ED.

Chapter 9 presents the modified i-AVCD scheme for M-QAM modulated PU. Besides this, multiple transitions of the PU are considered with Rayleigh distributed channel attenuation. Further, diversity schemes, such as EGC and SL-PCA are also presented.

Chapter 10 concludes our research work with a summary of the contributions and future scope.

1.5 Conclusion

In this chapter, we briefy discussed spectrum sensing schemes available in the literature for static and dynamic PUs. Spectrum sensing schemes for static PU were discussed with non-Gaussian noise. Further, sensing schemes for dynamic PU were discussed with Gaussian noise. Apart from this, the motivation of using impulsive noise such as Laplacian noise in the dynamic PU scenario was also presented followed by our contribution in the field of spectrum sensing. We conclude that in order to address the knowledge gap in the current research, it is important to analyze the performance of spectrum sensing schemes in the scenario of dynamic PU with additive Laplacian noise. In the next chapter, we will present an extensive literature survey on state-of-the-art of the spectrum sensing schemes.

Chapter 2

Literature Survey

Over the past few decades, demand for the available spectrum has remarkably increased manifold in the field of wireless communications [68]. For efficient spectrum utilization, spectrum sensing has gained a lot of attention. In this section, we present a detailed survey of the spectrum sensing schemes. We also discuss non-Gaussian noise models which have been considered in the literature, such as Laplacian noise and Generalized noise. Further, we present details of static and dynamic Primary Users (PUs).

2.1 Laplacian Noise

Impulsive noise is a sudden man-made or naturally occurring noise. Impulsive noise is a train of narrow impulses with high amplitude and low probability of occurrence [69]. It possesses high spikes and fatter tails. Some common examples are man-made noises, such as machine motors, microwave ovens, neon signs, etc [70].

The Probability Density Function (PDF) of the Laplacian noise can be expressed as [71]

$$f_{n_m}(v) = \frac{1}{2\kappa} \exp\left(-\frac{|v|}{\kappa}\right), \tag{2.1}$$

where κ is the scale parameter of the Laplacian noise. In section 2.2, we will present a few Generalized noise models which result in Laplacian, Gaussian, and other impulsive noises as their special cases.

2.1.1 Preference of Laplacian noise over AWGN

Avalanches, ice-cracking, etc. are naturally occurring phenomena that have impulsive characteristics of noise [72]. Noise such as AWGN is non-impulsive in nature and it models thermal noise. It possesses thinner tails, low amplitude and a high probability of occurrence [73]. However, noise does not remain Gaussian and possesses impulsive behavior in long-range communications. Further, PDF of noise in discrete time domain is similar to the Laplacian distribution which can be seen in Figure 10 of [74].

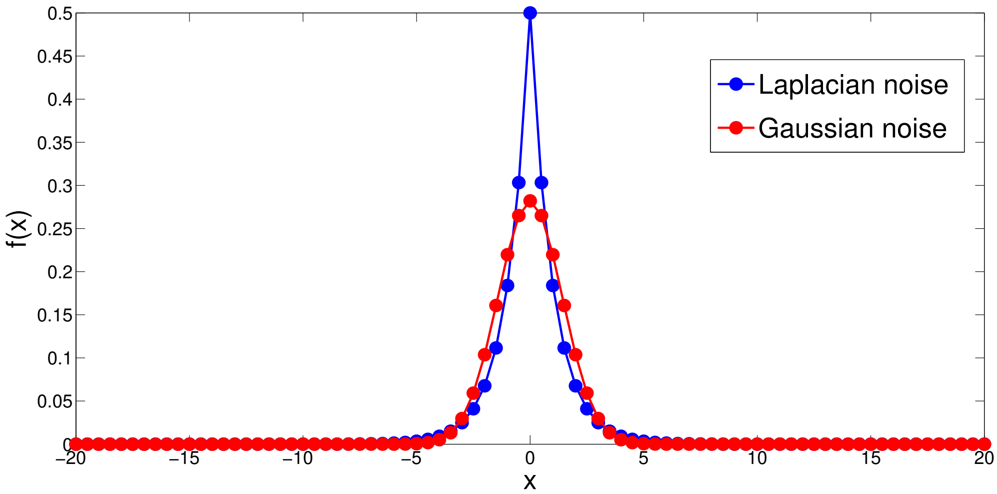

Figure 2.1: PDF showing impulsiveness of Laplacian noise for mean=0, variance=2.

Figure 2.1 shows the PDFs of Laplacian noise and Gaussian noise with mean equals to 0 and variance equals to 2. It can be seen that Laplacian noise possesses a high spike in the distribution at 0 mean while Gaussian noise has a comparatively low spike. Similarly, Figure 2.2 is zoomed view of Figure 2.1, showing the thickness of tails of Gaussian and Laplacian noises. It can be clearly observed that Laplacian noise has fatter tails than Gaussian noise which proves to be a better option to model impulsive noise scenario. In Figure 1 of [75], it has been shown that the discrete time model of MAI is accurately modeled using Laplacian distribution instead of Middleton Class A (MCA) noise and AWGN in time-hopped UWB systems.

2.2 Generalized Noise Models

In this section, we present two Generalized noise models, such as McLeish noise and Generalized Gaussian noise.

2.2.1 McLeish Noise

McLeish distribution is a generalized circularly symmetric distribution model with mean μ, variance σ^2, and a non-Gaussian parameter c, which is denoted as $\mathcal{CML}(\mu, \sigma^2, c)$ [76]. It is used to model noise ranging from highly impulsive noise, such as Dirac's distribution to non-impulsive noise, such as AWGN. The degree of impulsiveness can be varied by varying the impulsive parameter c. The PDF of McLeish noise can be represented as [76]

$$f_n(v) = \frac{2\sqrt{c}|v|^{c-1}}{\sqrt{2\sigma_v^2}\pi\Gamma(c)} K_{c-1}\left(\sqrt{\frac{2c}{\sigma_v^2}}|v|\right), \tag{2.2}$$

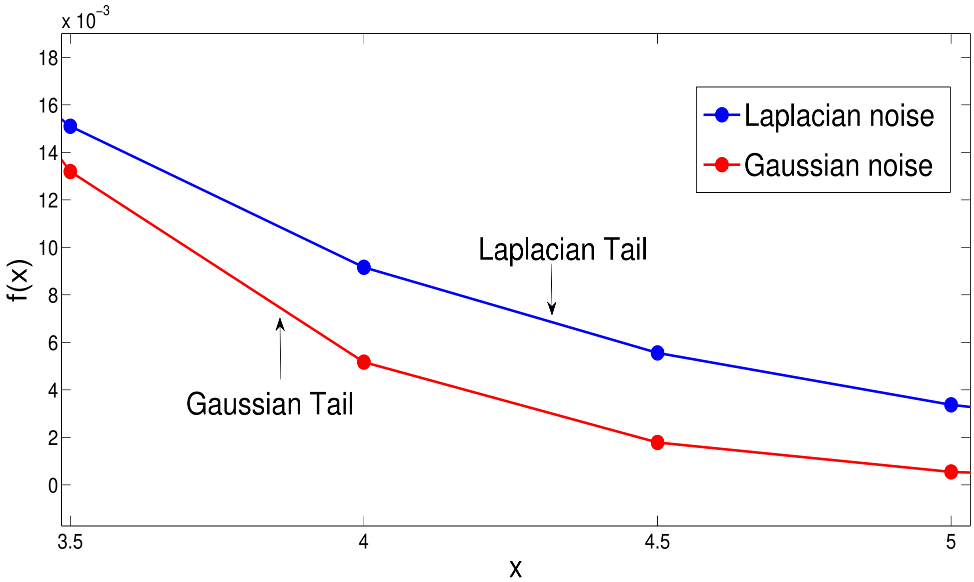

Figure 2.2: Zoomed view of the tails of Gaussian and Laplacian noises showing their thickness.

where $K_c(\cdot)$ denotes c_{th} order modified Bessel function of second kind. The complex and circularly symmetric Laplacian, Gaussian, and Dirac's distributions can be obtained as the special cases of McLeish noise at $c = 1$, $c \to +\infty$ and $c \to 0^+$, respectively. The $\Gamma(\cdot)$ represents Gamma function defined as $\Gamma(v) = \int_0^{+\infty} e^{-t} t^{v-1} dt$ [77].

2.2.2 Generalized Gaussian Noise

The Generalized Gaussian Noise (GGN) characterizes certain types of atmospheric and impulsive noises [78,79]. The PDF of Generalized Gaussian Noise (GGN) can be represented as [80]

$$f_n(v) = \frac{1}{2\Gamma\left(1 + \frac{1}{\kappa_o}\right) A(\kappa_o, \sigma)} \exp\left\{-\left|\frac{v}{A(\kappa_o, \sigma)}\right|^{\kappa_o}\right\}, \tag{2.3}$$

where $A(\kappa_o, \sigma)=\sigma^2 \left\{\frac{\Gamma\left(1/\kappa_o\right)}{\Gamma\left(3/\kappa_o\right)}\right\}$, is known as the scale parameter with variance σ. The κ_o is known as the shape parameter with $0 < \kappa_o \leq 2$ for heavy-tailed noise, such as Laplacian noise, and $\kappa_o > 2$ for short-tailed noise. The special cases are formed at $\kappa_o = 1$, $\kappa_o = 2$, and $\kappa_o = 0.5$ which result in Laplacian, Gaussian, and certain atmospheric impulsive noises, respectively [81]. Several spectrum sensing schemes which considered Laplacian noise have been proposed in the literature. In the following section, we present a few coherent spectrum sensing schemes in additive Laplacian noise (ALN).

2.3 Coherent Spectrum Sensing Schemes

In a coherent spectrum sensing scheme, the SU has prior information about the PU. In this section, we briefly explain several coherent spectrum sensing schemes available in the literature in ALN environment.

2.3.1 Matched Filter detector

The Matched Filter (MF) detector is used if the SU has prior knowledge about numerous attributes of the physical implementation of the PU [82]. The MF can be used in this situation using cross-correlation between the known sequence of the PU and the signal that is received at the cognitive terminal [83]. The detector confirms the presence of the PU signal whenever a true correlation peak arises, else it claims an empty band. The MF detector offers the best performance, especially at low SNR. Besides this, the MF detector also recognizes the power levels of the PU. The SU can adjust its power levels to avoid unnecessary interference with the PU signal [84]. The hybrid MF detector as a double MF detector has been proposed in [85]. It has been shown that the hybrid MF detector outperformed MF detector for $P_F < 0.5$. The MF detection scheme can be represented as [86]

$$\Upsilon(\mathbf{y}) = \sum_{m=1}^{N} \left(s_m^* y_m \right) \underset{H_o}{\overset{H_1}{\gtrless}} \Psi, \tag{2.4}$$

where $\Upsilon(\mathbf{y})$ denotes the decision statistic. The s_m^* represents the conjugate of s_m and Ψ denotes the detection threshold obtained using the NP test.

2.3.2 Threshold Detector

The Threshold Detector (TD) has been proposed in [87] which has a much simplified practical implementation due to the need for low resource equipment. In addition to this, the TD outperformed MF detector in term of detection performance. The TD has been widely discussed as a sub-optimal detector [88, 89]. In TD, the received observation y_m is quantized by a Threshold System (TS) at a fixed threshold of $t_m = s_m/2$ to obtain z_m. Finally, a linear correlation is performed between z_m and s_m. The result is then compared with the detection threshold Ψ. The detection scheme can be represented as [90]

$$\Upsilon(\mathbf{y}) = \sum_{m=1}^{N} \left(s_m z_m \right) \underset{H_o}{\overset{H_1}{\gtrless}} \Psi, \tag{2.5}$$

where for $s_m > 0$

$$z_m = \begin{cases} 1, & y_m \geq t_m \\ 0, & y_m < t_m, \end{cases} \tag{2.6}$$

and for $s_m < 0$

$$z_m = \begin{cases} 0, & y_m \geq t_m \\ 1 & y_m < t_m. \end{cases} \tag{2.7}$$

2.3.3 Other coherent spectrum sensing schemes

The two blind correlation detectors, known as the Phase-Rotated Spectral Correlation Detector (PRSCD) and the complex decomposition based PRSCD have been explored in [91]. It has been shown that the two blind detectors outperformed the MF detector. Besides MF detector, Feature detectors such as Waveform detector and Cyclostationary detectors are the two other coherent detectors [92, 93]. Based on the different applications of correlation, several coherent spectrum sensing schemes have been analyzed in [94–96]. The coherent detection schemes proposed in [82–96] have assumed noise as AWGN. Further, in these cases, full or partial information on PU was available at the cognitive terminal a priori. However, in a real-time scenario, it is not always possible for a CR to know prior information about PU. Hence, in the following section, we present some non-coherent spectrum sensing schemes where information about PU is not available at the CR a priori.

2.4 Non-Coherent Spectrum Sensing Schemes

Non-coherent spectrum sensing schemes do not need information about the PU signal a priori. The i-AVCD, with AVCD and ED as its special cases, is a non-coherent spectrum sensing scheme available in the literature in the Laplacian noise environment. Although ED is one of the special cases of i-AVCD, we explain it separately in the following sections.

2.4.1 improved Absolute Value Cumulation Detection

The improved Absolute Value Cumulation Detection (i-AVCD) refers to the detection scheme where the received observations at the cognitive terminal are raised to a positive exponent P over the range defined as $0 < P \leq 2$. The detection scheme can be represented as [97]

$$\Upsilon(\mathbf{y}) = \sum_{m=1}^{N} |y_m|^P \underset{H_o}{\overset{H_1}{\gtrless}} \Psi, \tag{2.8}$$

where $\Upsilon(\mathbf{y})$ is the decision statistic. The AVCD and ED are special cases of i-AVCD at $P = 1$ and $P = 2$, respectively. The AVCD scheme can be represented as [98]

$$\Upsilon(\mathbf{y}) = \sum_{m=1}^{N} |y_m| \underset{H_o}{\overset{H_1}{\gtrless}} \Psi, \tag{2.9}$$

where $\Upsilon(\mathbf{y})$ is the decision statistic. The Ψ is the detection threshold that can be obtained using NP test.

2.4.2 Energy Detector

The Energy Detector (ED) is a classical non-coherent detection scheme. No prior information about PU is required in this scheme [99–102]. Besides this, it is one of the frequently used detection scheme as it offers very low computation complexity. This scheme is used in different channel conditions. An important disadvantage of ED is that it performs poorly at low Signal-to-Noise Ratio (SNR) and is unable to distinguish between signals from PU and interference [103]. Multipath fading and Shadowing result in power fluctuations of the received signal. The noise uncertainty and the channel effect have to be thoroughly investigated in order to obtain sustainable performance in these scenarios. As the SU does not use the estimation of SNR in the ED, it results in an SNR wall problem. The SNR wall and noise uncertainty have been investigated in [104], where noise levels were estimated to achieve a reduced level of uncertainty under Gaussian noise. The detection scheme can be expressed as

$$\Upsilon(\mathbf{y}) = \sum_{\mathrm{m}=1}^{\mathrm{N}} |\mathrm{y_m}|^2 \underset{\mathrm{H_o}}{\overset{\mathrm{H_1}}{\gtrless}} \Psi, \tag{2.10}$$

where $\Upsilon(\mathbf{y})$ is the decision statistic. The Ψ is the detection threshold that can be obtained using the NP test. These spectrum sensing schemes have explored a non-collaborative scenario, where only one CR is present and communication takes place between a CR and PU. In the next section, we will present a collaborative spectrum sensing scheme where multiple CRs communicate with PU. This scheme is known as the Cooperative Spectrum Sensing (CSS) Scheme. The CSS scheme mitigates the Hidden Primary User Node (HPUN) problem which occurs under the severe effect of multipath fading.

2.5 Cooperative Spectrum Sensing Scheme

The most challenging issue in spectrum sensing is the HPUN problem which occurs when the CR is under the severe effect of multipath shadowing [105, 106]. In CSS, multiple CRs are considered to mitigate the fading effect. This scheme offers space diversity via sensing channels, also known as sensing diversity, and provides a good solution to mitigate the HPUN problem. The CSS utilizes two channels. The first one is the sensing channel, while the other is reporting channel [107]. The sensing channel is the channel between PU and CR, while the reporting channel is the channel between CR and the controlling center known as the FC. The CSS scheme has been classified into three different categories. The first is centralized CSS, the second is distributed CSS, and the third one is Relay assisted CSS [108]. Figure 2.3 shows a collaborative scenario of CSS scheme where M_o CRs are available out of which k_o CRs are active. Active CRs refer to a minimum number of CRs which infer the presence of the PU. The M_o CRs use some localized detection schemes to produce local hard decisions for detection of the PU signal. Then, the hard decisions are individually communicated to the FC via reporting channel. After collecting hard decisions in the form of '0' and '1', the FC uses standard fusion schemes, such as the 'OR rule', 'AND rule', and 'majority rule'. These fusion schemes combine the received hard decisions in a specific and unique way to deliver final judgement on the availability of the PU. We have used specific terminologies for these fusion rules. They are CSS: OR, CSS: AND, and CSS: majority for OR rule, AND rule, and majority rule, respectively. All

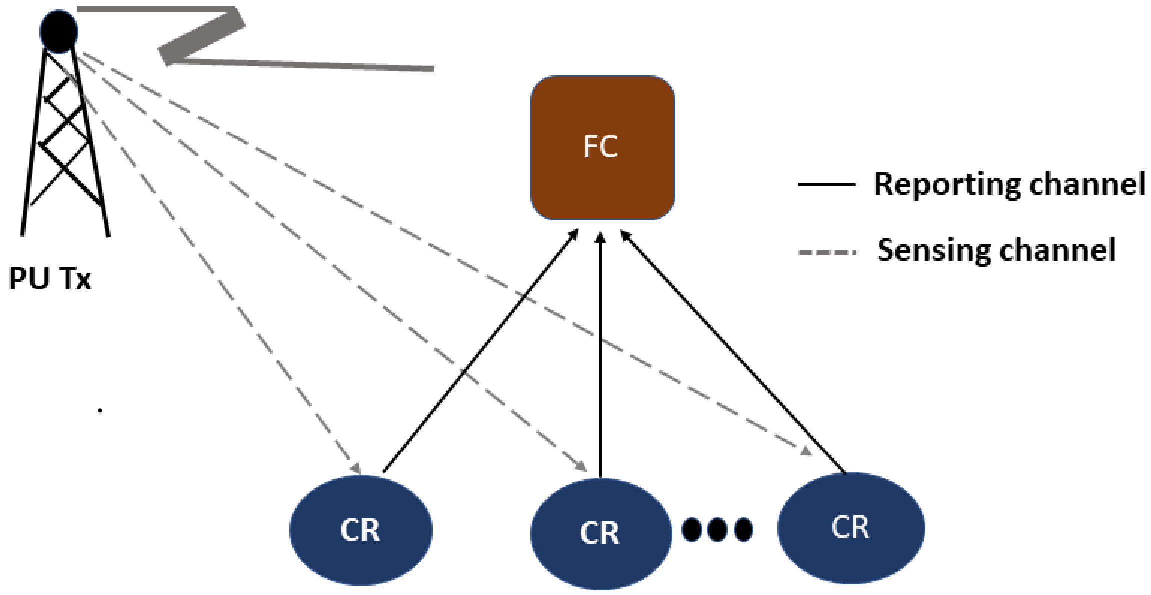

Figure 2.3: Centralized cooperative sensing scheme in cognitive radio

the single-bit hard decisions from each M_o CR are combined at the FC according to a decision rule expressed as

$$U = \sum_{l=1}^{M_o} U_l \underset{H_o}{\overset{H_1}{\gtrless}} k_o, \tag{2.11}$$

where U_l is the hard decision from each CR. Finally, at the FC, P_F and P_D can be expressed as [109]

$$\begin{aligned} P_F &= \sum_{l=k_o}^{M_o} \binom{M_o}{l} Q_f^l (1 - Q_f)^{M_o - l}, \\ P_D &= \sum_{l=k_o}^{M_o} \binom{M_o}{l} Q_d^l (1 - Q_d)^{M_o - l}, \end{aligned} \tag{2.12}$$

where Q_f and Q_d denote the false alarm probability and detection probability, respectively, using some localized detection schemes at each M_o CR. Here, $k_o = 1$ represents CSS: OR rule, $k_o = M_o$ indicates CSS: AND rule, and $k_o < M_o$ signifies CSS: majority rule. Substituting $k_o = 1$ in (2.12), P_F and P_D for 'CSS: OR' fusion scheme can be expressed as

$$\begin{aligned} P_F &= 1 - \left\{1 - Q_f\right\}^{M_o}, \\ P_D &= 1 - \left\{1 - Q_d\right\}^{M_o}. \end{aligned} \tag{2.13}$$

Similarly, substituting $k_o = M_o$ in (2.12), P_F and P_D for 'CSS: AND' fusion scheme can be expressed as

$$\begin{aligned} P_F &= Q_f^{M_o}, \\ P_D &= Q_d^{M_o}. \end{aligned} \tag{2.14}$$

The 'CSS: OR' fusion scheme allows the FC to infer that there exists at least one CR with its hard decisions based on the two hypotheses. In the CSS: OR scheme, there is a minimal chance of the PU getting affected by interference from the surrounding CRs.

The CSS scheme based on various localized detection schemes has been proposed in the literature. The CSS based on Dynamic Double Threshold Energy Detection (DDTHED) has been proposed in [110] considering Circularly Symmetric Gaussian Noise (CSGN). It has been shown that CSS-DDTHED performed better than CSS-ED. The Priority based polarized transmission scheme has been proposed in [111] to improve the detection performance of the polar coded CSS scheme in Rayleigh fading channel with BPSK modulated PU. The principle of polarization which gives near Shannon-limit performance at a low value of average SNR has been applied. The local decision bits were transmitted over noisy or near noiseless channels depending on the used or idle sub-bands, respectively. The CSS: OR and CSS: AND rules were used as fusion schemes at the FC. It has been shown that the Priority-based polarized transmission scheme outperformed the polar coded CSS scheme. The subcarrier modulation based CSS (SMCSS) has been proposed in [112], where local decision bits were sent over orthogonal subcarriers to the FC. The FC makes a final decision on the availability of the PU based on two-level decision fusion, which includes user-level fusion and network-level fusion. The CSS scheme in Nakagami-q/n fading channel has been presented in [113]. The CSS scheme with a multiple antenna scenario at each CR has been analyzed in [114]. Further, rewards and punishment based collaborative spectrum sensing has been proposed in [115]. The CSS schemes presented in [110–115] have assumed additive noise AWGN with static PU. These schemes have been explored with only one antenna at the CR. The performance of the sensing schemes can be greatly improved by using multiple antennas at the CR. The spectrum sensing schemes for a multiple antenna scenario are presented in the following section.

2.6 Spectrum Sensing Schemes for a Multiple Antenna Scenario

In this section, we present spectrum sensing schemes available in the literature when a CR is equipped with multiple antennas.

2.6.1 Polarity Coincidence Array

The Polarity Coincidence Correlator (PCC) is a well-known detection scheme when a CR is equipped with two antennas. The decision statistic can be represented as [116]

$$\Upsilon(\mathbf{y}) = \sum_{m=1}^{N} u\Big(y_{m,1} y_{m,2}\Big), \tag{2.15}$$

where $\mathbf{y} = [y_1, y_2, \ldots, y_N]$ represents an array of N observations of PU. The $u(\cdot)$ represents the unit step function. Further, $y_{m,1}$ and $y_{m,2}$ represent received observations at the first and second antennas, respectively. The Polarity Coincidence Array (PCA) is an extension of PCC for multiple antenna systems. The decision statistic can be represented as [116]

$$\Upsilon(\mathbf{y}) = \sum_{m=1}^{N} \left\{ \sum_{k=1}^{K} sgn(y_{m,k}) \right\}^2, \tag{2.16}$$

where $sgn(\cdot)$ represents signum function, K represents total number of antennas at the CR terminal with $K > 1$. Finally, the PCA detection scheme can be represented as

$$\Upsilon(\mathbf{y}) \underset{H_o}{\overset{H_1}{\gtrless}} \Psi, \tag{2.17}$$

where Ψ is the detection threshold that can be obtained using the NP test.

2.6.2 Soft-Limiting Polarity Coincidence Array

The soft-limiting Polarity Coincidence Array (SL-PCA) has been proposed as an improved detection scheme for a multiple antenna system for static PU. The decision statistic can be represented as [117]

$$\Upsilon(\mathbf{y}) = \sum_{m=1}^{N} \left\{ \sum_{k=1}^{K} F_S(y_{m,k}) \right\}^2, \tag{2.18}$$

where soft limiting function $F_S(v)$ can be expressed as

$$F_S(v) = \begin{cases} 1, & S < v \\ \frac{1}{S} v, & -S \leqslant v \leqslant S \\ -1, & v < -S, \end{cases} \tag{2.19}$$

where S is the soft limiting factor with its range defined as $0 \leq S < \infty$. Finally, the SL-PCA detection scheme can be represented as

$$\Upsilon(\mathbf{y}) \underset{H_o}{\overset{H_1}{\gtrless}} \Psi, \tag{2.20}$$

where Ψ is the detection threshold obtained using the NP test. In the next section, we will present spectrum sensing schemes where PU follows different behaviors, such as static and dynamic. Further, different behaviors of noise, such as Gaussian and non-Gaussian are also explained.

2.7 Critical Analysis on State-of-the-Art Work

Many spectrum sensing schemes have been proposed in the literature where PU operates in different modes, i.e, static and dynamic modes. Conventional spectrum sensing techniques presume that the PU operates in static mode during the sensing period [118]. It signifies that the PU is either present or absent during the period of sensing. The case of static PU is acceptable for slow fluctuation of PU traffic, similar to television (TV) transmission [119]. However, in the case of rapid fluctuation of PU traffic, as observed in cellular communication or WLAN, the scenario of dynamic PU is considered [120]. In this case, during a prescribed sensing time interval, several times the PU becomes active and inactive. Hence, the assumption of static PU may deteriorate the ROC performance.

On the other hand, several spectrum sensing schemes have been proposed with the assumption of background noise as Gaussian [121–124]. However, in a real-time scenario, it may not be followed. For example, a non-Gaussian noise is caused by a variety of sources, such as thunderstorms, lightning, microwave oven emissions, etc [125]. Impulsive noise models, such as the symmetric alpha-stable distribution noise, Middleton Class A noise, and Bernoulli-Gaussian noise are some of the examples [126] of non-Gaussian noise models. The MAI in UWB communication systems has been investigated and proven to be impractical to be modeled as AWGN [75]. In the time-hopped UWB communication system, Laplacian noise is shown to be effective in modeling of the MAI. Spectrum sensing schemes which have addressed the static behavior of the PU with non-Gaussian noise are presented in the following section.

2.7.1 Static PU With Non-Gaussian Noise

Several spectrum sensing schemes have been proposed in the literature which considered the scenario of static PU with non-Gaussian noise. Detection schemes such as Suprathreshold Stochastic Resonance (SSR) assisted ED has been proposed in [127], where a non-linear technique has considered both Fractional Higher Order Moment (FHOM) and Fractional Lower Order Moment (FLOM) in the Laplacian noise. The PCA detector has been proposed where noise followed Generalized Gaussian Distribution (GGD), known as Generalized Gaussian Noise (GGN). The PCA detector has considered a multiple antenna system where the number of antennas at CR is greater than 2. Expressions of

P_D and P_F were derived for Rayleigh fading and no fading channels. The SL-PCA detection scheme has been introduced as an improvement over PCA detection scheme for a multiple antenna scenario. Unlike the case of the PCA detector, the SL-PCA detector is valid for a minimum number of antennas greater than or equal to 1.

The i-AVCD and AVCD have been proposed in the Laplacian noise environment. The CSS scheme has been used to improve detection performance using a collaborative scenario of CRs. It has been shown that the CSS based on Rao detector (CSS-Rao) outperformed the CSS based on conventional ED (CSS-ED), where noise followed GGD [128]. The Maximum Generalized Correntropy (MGC) based spectrum sensing has been discussed, where noise followed symmetric alpha-stable distribution [129]. The MGC reduced the negative effect of symmetric alpha-stable noise on the detection performance. Further, the CSS scheme has been considered to improve detection performance.

The non-linear Kernel function has been proposed using the CSS scheme in [130], where both higher order and lower order moments were considered in Laplacian noise. The CSS scheme applies standard fusion schemes on the collective decisions received from the surrounding CRs. The majority rule (k_o out of M_o rule, where $k_o < M_o$) has been used to analyze the performance in the Laplacian noise environment [131]. In this case, the Rayleigh fading channel has been explored with ED as a detection scheme. It was observed that the CSS: OR rule outperformed other CSS fusion schemes at $K_o = 3$. On the contrary, in the case of AWGN, CSS: OR outperformed other fusion schemes at $K_o = 1$. The Logarithmic Similarity Measure Detector (LSMD) based CSS scheme has been proposed in [132], where the logarithmic similarity measure converted all logarithmic operations into multiplicative operations in the environment of symmetric alpha-stable noise. In an impulsive noise environment, large magnitudes of the received observations are due to the noise component itself. The CSS scheme under bivariate isotropic symmetric alpha-stable noise has been proposed in [133], where received observations with smaller magnitudes were selected via a non-linear selection scheme.

The CSS scheme has been analyzed with Mixed Gaussian Noise (MGN) in [134]. The MGN noise is the summation of Gaussian noises with different mixing coefficients and variances. These mixing coefficients add non-Gaussian behavior to the noise. The hyperbolic tangent based ED has been proposed in [135]. In this detection scheme, the hyperbolic tangent function was explored to suppress the impulsive noise by non-linear behavior. The Unilateral Left-Tail Anderson Darling (ULAD) detector has been proposed in [136], where the Goodness-of-Fit (GoF) test was used in Laplacian noise. The Generalized Energy Detection (GED) has been proposed in [137], where noise followed McLeish distribution. These detection schemes have assumed static PU with non-Gaussian noise. However, the assumption of static PU is valid for slow-moving traffic. In heavy traffic scenarios, such as in densely populated industrial areas, the assumption of static PU no longer remains valid [138–142]. Hence, in the following section, we present sensing schemes, where dynamic PU has been considered under Gaussian noise.

2.7.2 Dynamic PU with Gaussian Noise

Several spectrum sensing schemes have been proposed in the literature, where the dynamic behavior of the PU is considered in an AWGN environment. The scenario of a single transition of PU during the sensing period has been addressed in [143], where PU transits from one state to another state only once. In this case, the random transitions of PU followed the Poisson distribution. This work has been extended in [144] to multiple antenna scenarios. The Average Log LRT (ALLRT) has been proposed in [145] with ED as a detection scheme. The performance of ALLRT has been improved significantly over classical ED.

The case of two transitions of the PU has been proposed in [146] with an extension to three PU transitions in [147] during the sensing period. The CuSum based ED scheme has been proposed in [146, 147]. The case of multiple transitions of the PU has been presented in [148], where PU changed its status multiple times. In this case, the spectrum sensing schemes were analyzed in terms of throughput versus sensing period. It has been shown in [149] that multiple PU changes caused significant degradation in the detection performance using ED. The random transition of the PU has been analyzed in [150], where the transition followed Batch Bernoulli Process (BBP). Besides this, Markovian evolution was followed for the vacant licensed band. The performance of the dynamic PU under both the sensing period and transmission period has been discussed in [151]. The effect of deep sensing has been proposed in [152], where flat-fading gains and locations of the PU were jointly estimated at the same time. The Markov chain-based sensing has been proposed in [153], where the on-off status of the PU was modeled using the Markov chain. The Partially observed Markov decision process has been addressed in [154], where occupancies of the vacant licensed band followed Markovian evolution. A Defense strategy based on the Markov chain has been proposed against an off-sensing attack on the SU, where the zero-sum Markov game modeled the interaction between the attacker and the SU [155]. Collaborative spectrum sensing based on hard and soft decision fusion schemes has been proposed in [156], where hidden bivariate Markov chain estimation has been explored. The Refined Metropolis-Hastings (RMH) algorithm has been proposed in [157], which worked similar to Markov Chain Monte-Carlo (MCMC) way. In the next section, we will briefly present our research work, where the dynamic behavior of the PU is considered in ALN.

2.8 Our research work: Dynamic PU with Non-Gaussian Noise

The performance of i-AVCD improves with Laplacian noise as compared to their performance with Gaussian noise. Further, MAI is accurately modeled using Laplacian noise, and not AWGN. Apart from this, i-AVCD scheme and its special cases, have not been analyzed for dynamic PU with MAI, where MAI is modelled using Laplacian noise. Hence, in this thesis, we have assumed that background noise follows Laplacian distribution in all the system models considered. A new coherent detection scheme is proposed for the case of static PU in ALN and the closed-form expressions of P_D and P_F

are derived. We present ROC for this new scheme and compare it with the MF detector and TD. The proposed scheme outperforms both the schemes for $P < 1$, where P denotes the real and positive exponent to which received observations at the CR terminal are raised. Apart from this, cooperative sensing diversity is used and expressions of P_D and P_F have been derived.

The dynamic behavior of PU is assumed by taking one transition during the sensing interval. The arrival and departure of the PU are modeled by the Poisson distribution. Then, two transitions of PU are modeled using weighted samples, which are further based on CuSum for detection. Further, multiple transitions are modeled using the two-state Markov chain. The effect of the Markov parameters on the detection performance has been analyzed. In this case, we use a non-coherent detection scheme, i-AVCD and present the ROC.

The effect of higher order modulation scheme, such as M-QAM for the PU signal has been explained in [158] for the case of static PU using ED and Moment based Detector (MD). The noise followed McLeish distribution. The performance of detection schemes, such as ED and MD was compared for $M = 2$ (BPSK) and $M = 16$ (16-QAM). It was shown using ROC that the BPSK outperformed 16-QAM. However, the effect of Quadrature Phase Shift Keying (QPSK) and higher order modulation, such as 64-QAM was not addressed. It motivated us to consider higher order modulation scheme, such as M-QAM for the dynamic PU, instead of static PU. Here, we use a modified i-AVCD scheme. We consider M with values 2, 4, 16, and 64 corresponding to BPSK, QPSK, 16-QAM, and 64-QAM. In literature, the Rayleigh distributed channel attenuation has been presented in GGN for static PU using the SL-PCA detection scheme. We present the modified i-AVCD for dynamic PU when channel attenuation is modeled using Rayleigh distribution in ALN. In the next chapter, we will present our first proposed coherent spectrum sensing scheme based on a Modified Correlation Detector in additive Laplacian noise.

2.9 Conclusion

In this chapter, we discussed several state-of-the art spectrum sensing schemes available in the literature. Further, we also discussed the motivation of using Laplacian noise instead of AWGN. Apart from this, the performance of sensing schemes for the case of static PU was discussed in non-Gaussian noise environment. Static PU refers to the case where PU remains in a single state, i.e., either 0 or 1 within sensing period. Similarly, the performance of several spectrum sensing schemes was discussed with dynamic PU in Gaussian noise. Dynamic PU refers to the case when PU may transit from 'ON' state to 'OFF' state and vice-versa in random fashion within sensing period. We conclude that Laplacian noise proves to be a better fit to model MAI in discrete time model. The i-AVCD scheme with Laplacian noise outperforms its performance with Gaussian noise. Further, we also conclude that the research gap exists for the scenario of dynamic PU in non-Gaussian noise such as ALN. Hence, our research focuses to fill-up this knowledge gap and to evaluate and analyze the performance of i-AVCD scheme and its special cases in dynamic PU environment.

Chapter 3

Spectrum Sensing Using Modified Correlation Detector in ALN

In this chapter, a Modified Correlation Detector (MCD) based spectrum sensing scheme has been proposed assuming additive Laplacian noise. In the proposed modified detector, the received signal at the cognitive terminal is correlated with the BPSK modulated PU signal. Then, the received signal is raised to an arbitrary exponent P, whose value ranges from 0 to 2, i.e, $0 < P \leq 2$. The Matched Filter (MF) detector is a special case of MCD detector at $P = 1$. Considering the proposed detection scheme, the analytical expressions of detection probability and false alarm probability have been derived. Performance of the proposed MCD scheme has been presented using ROC and detection probability versus average SNR. Further, the optimum value of P for different values of average SNR and false alarm probability has been obtained using simulations. The analytical expressions are validated by comparing the results with simulation results. Finally, the chapter ends with a brief conclusion.

3.1 Introduction

A correlation detector is a form of coherent detector, where the received signal at SU is correlated with the known sequence of the PU signal [159]. This detector can be used if the SU has prior knowledge about numerous attributes of the physical implementation and structure of the PU [160]. The MF detector is a linear correlation detector, where decision statistic is formed using cross-correlation between the known sequence of the PU and the signal that is received at the cognitive terminal [161]. The detector confirms the presence of the PU whenever a true correlation peak arises, else it claims an empty band [162]. Unlike in the case of Gaussian noise, the performance of linear MF detector in non-Gaussian noise is poor as compared to the performance of another linear correlation detector available in the literature such as TD [87]. The TD is a form of linear correlation detector that has been proposed in non-Gaussian noises such as Generalized Gaussian noise (GGN) and Gaussian Mixture Noise (GMN) [87,163]. The TD outperformed MF detector for a wide range of parameters of GGN and GMN [87,163]. It has been shown that for $\kappa_o \in [0.42, 1]$, the TD outperformed MF detector while for $\kappa_o < 0.42$, the MF detector outperformed TD [163]. The κ_o in GGN is known as the shape parameter. It is to be noted here that Laplacian noise is a special case of GGN at $\kappa_o = 1$.

In this chapter, we present a modified version of a general correlation detector known as MCD. In the MCD scheme, the PU signal is corrupted with ALN. The received signal then correlates with the known PU signal at the cognitive terminal. Finally, it is raised to a real and positive exponent P with $0 < P \leq 2$. Raising the received signal to an exponent P gives non-linearity to the detector with the condition $P \neq 1$. At $P = 1$, the proposed detector behaves as the MF detector which is linear in nature. The closed-form expressions of P_D and P_F for the proposed detector have been derived. The impact of P on detection probability has been shown using simulations. The optimum P for different values of average SNR and P_F has been obtained using simulations. The proposed detector shows improved performance over detectors such as MF detector and TD for $P < 1$. Nevertheless, similar to TD, the proposed scheme serves as a unique method to improve the detection performance of the MF detector.

The rest of the chapter is presented as follows. The system model for the MCD scheme is presented in Section 3.2. Section 3.3 presents the performance analysis of the MCD scheme. In this section, the MF detection scheme, which is a specific case of MCD at $P = 1$, is also discussed. Finally, results are presented in Section 3.4 before a brief conclusion of our work in Section 3.5.

3.2 System Model

Let $\mathbf{y} = [y_1, y_2, \ldots, y_N]$ be a vector of N observations of the PU received at the cognitive terminal, where $N \geq 1$. It has been assumed that all the received observations are real, Independent and Identically Distributed (iid). Each received observation y_m can be represented as

$$\begin{aligned} H_o &: y_m = n_m; \\ H_1 &: y_m = \sqrt{\gamma} s_m + n_m, \end{aligned} \tag{3.1}$$

where $m = 1, 2, \ldots, N$. The H_o denotes the null hypothesis, i.e., PU is not present and H_1 denotes the alternate hypothesis when PU is present. The γ denotes the average SNR, where $\gamma = (1/N) \sum_{m=1}^{N} s_m^2 / 2\kappa^2$. The $s_m \in \{-1, 1\}$ denotes the BPSK PU signal similar to [97]. The $n_m \sim L(0, \kappa)$, i.e., Laplacian distribution with mean 0 and variance $2\kappa^2$, and its PDF can be expressed as [97]

$$f_n(v) = \frac{1}{2\kappa} \exp\left(-\frac{|v|}{\kappa}\right). \tag{3.2}$$

The proposed MCD scheme can be represented as

$$\Upsilon(\mathbf{y}) = \sum_{\mathrm{m=1}}^{\mathrm{N}} \left(\sqrt{\gamma}\mathrm{s_m y_m}\right)^{\mathrm{P}} \underset{\mathrm{H_o}}{\overset{\mathrm{H_1}}{\gtrless}} \Psi, \tag{3.3}$$

where $\Upsilon(\mathbf{y})$ is the decision statistic which is obtained by assuming that the SU knows information about the PU, Ψ is the detection threshold which is obtained using the NP test. The received sample y_m at the SU is correlated with the PU signal s_m and average SNR γ, assuming the two are known at the SU. Finally, it is raised to P with $0 < P \leq 2$, where $P = 1$ corresponds to the general correlation detector which is linear in nature. The impact of P on the performance of the proposed detection scheme has been discussed in the results section. In the next section, we will present the performance analysis of the proposed MCD scheme.

3.3 Performance Analysis

In this section, closed-form expressions of P_D and P_F have been derived. For large N, especially when $N \geq 30$, the distribution of decision statistic $\Upsilon(\mathbf{y})$ can be well-approximated as Gaussian using Central Limit Theorem (CLT) [63], [116], [158]. Therefore,

$$\begin{aligned} H_o &: \Upsilon(\mathbf{y}) \sim \mathrm{N}\left(\mu_{\mathrm{o}}, \sigma_{\mathrm{o}}^2\right), \\ H_1 &: \Upsilon(\mathbf{y}) \sim \mathrm{N}\left(\mu_1, \sigma_1^2\right), \end{aligned} \tag{3.4}$$

where μ_o and μ_1 denote the mean under hypotheses H_o and H_1, respectively, whereas σ_o^2 and σ_1^2 denote the respective variance under the two hypotheses. The main contribution of CLT is to approximate the distribution of the decision statistic $\Upsilon(\mathbf{y})$, where random variables present in $\Upsilon(\mathbf{y})$ are iids. The P_D and P_F are detection probability and false alarm probability, respectively, which can be represented as

$$\begin{aligned} P_D &= Prob\Big\{\Upsilon(\mathbf{y}) > \Psi | H_1\Big\}, \\ P_F &= Prob\Big\{\Upsilon(\mathbf{y}) > \Psi | H_o\Big\}. \end{aligned} \tag{3.5}$$

Under H_o, $\Upsilon(\mathbf{y})$ can be represented as

$$\begin{aligned} \Upsilon(\mathbf{y}) = \sum_{m=1}^{N} \left\{\sqrt{\gamma}\mathrm{s_m y_m}\right\}^{\mathrm{P}} &= \sum_{m=1}^{N} \left\{\sqrt{\gamma} s_m n_m\right\}^{P} \\ &= \sum_{m=1}^{N} w_m^P, \end{aligned} \tag{3.6}$$

where $w_m = \sqrt{\gamma} s_m n_m$.

The PDF of w_m can be derived and expressed as [164]

$$f_{w_m}(x) = \frac{1}{2\kappa\sqrt{\gamma}} \exp\left(-\frac{|x|}{\kappa\sqrt{\gamma}}\right). \tag{3.7}$$

As $w_1, w_2, \ldots, w_N$ are iid, μ_o can be expressed as

$$\mu_o = E\left\{\sum_{m=1}^{N} w_m^P\right\} = N \times E\left[w_1^P\right], \tag{3.8}$$

where $E[\cdot]$ is the mean operator. Similarly, variance σ_o^2 can be expressed as

$$\sigma_o^2 = N \times var\left[w_1^P\right], \tag{3.9}$$

where $var[\cdot]$ is the variance operator. The mean $E\left[w_1^P\right]$ can be expressed as

$$\begin{aligned} E\left[w_1^P\right] &= \frac{\kappa^P}{2\sqrt{\gamma}}\left\{\left(-1\right)^P\Gamma\left(P+1\right)\left(\sqrt{\gamma}\right)^{P+1} + \Gamma\left(P+1\right)\left(\sqrt{\gamma}\right)^{P+1}\right\} \\ &= \frac{\kappa^P}{2\sqrt{\gamma}}\left\{\Gamma\left(P+1\right)\left(\sqrt{\gamma}\right)^{P+1}\left\{1+\left(-1\right)^P\right\}\right\}, \end{aligned} \tag{3.10}$$

where $\Gamma(v) = \int_0^{+\infty} e^{-t} t^{v-1} dt$ [77]. Similarly, variance $var\left[w_1^P\right]$ can be expressed as

$$\begin{aligned} var\left[w_1^P\right] &= E\left[w_1^{2P}\right] - E^2\left[w_1^P\right] \\ &= \frac{\kappa^{2P}}{2\sqrt{\gamma}}\left\{\Gamma\left(2P+1\right)\left(\sqrt{\gamma}\right)^{2P+1}\left(-1\right)^{2P} + \Gamma\left(2P+1\right)\left(\sqrt{\gamma}\right)^{2P+1}\right\} \\ &- \frac{\kappa^{2P}}{4\gamma}\left\{\Gamma\left(P+1\right)\left(\sqrt{\gamma}\right)^{P+1}\left\{1+\left(-1\right)^P\right\}\right\}^2 \\ &= \frac{\kappa^{2P}}{2\sqrt{\gamma}}\left\{\Gamma\left(2P+1\right)\left(\sqrt{\gamma}\right)^{2P+1}\left\{1+\left(-1\right)^{2P}\right\}\right\} - \frac{\kappa^{2P}}{4\gamma}\left\{\Gamma\left(P+1\right)\left(\sqrt{\gamma}\right)^{P+1}\left\{1+\left(-1\right)^P\right\}\right\}^2. \end{aligned} \tag{3.11}$$

The proofs of $E\left[w_1^P\right]$ and $var\left[w_1^P\right]$ are given in Appendix I.1 and Appendix I.2, respectively. Using (3.8) and (3.9), the μ_o can be expressed as

$$\mu_o = \frac{N\kappa^P}{2\sqrt{\gamma}}\left\{\Gamma\left(P+1\right)\left(\sqrt{\gamma}\right)^{P+1}\right\}\left\{1+\left(-1\right)^P\right\} \tag{3.12}$$

and σ_o^2 can be expressed as

$$\sigma_o^2 = \frac{N\kappa^{2P}}{2\sqrt{\gamma}}\Bigg\{\Gamma\big(2P+1\big)\big(\sqrt{\gamma}\big)^{2P+1}\Bigg\{1+\big(-1\big)^{2P}\Bigg\}\Bigg\} - \frac{N\kappa^{2P}}{4\gamma}\Bigg\{\Gamma\big(P+1\big)\big(\sqrt{\gamma}\big)^{P+1}\Bigg\{1+\big(-1\big)^{P}\Bigg\}\Bigg\}^2. \tag{3.13}$$

Finally, using CLT, the final expression of P_F can be represented as

$$P_F = Prob\Big\{\Upsilon(\mathbf{y}) > \Psi|H_o\Big\} = Q\bigg(\frac{\Psi-\mu_o}{\sigma_o}\bigg), \tag{3.14}$$

where $Q(\cdot)$ represents the Q-function which can be mathematically expressed as

$$Q(v) = \frac{1}{\sqrt{2\pi}}\int_v^{+\infty} \exp\bigg(-\frac{t^2}{2}\bigg)dt.$$

Similarly, under hypothesis H_1, $\Upsilon(\mathbf{y})$ can be represented as

$$\begin{aligned}\Upsilon(\mathbf{y}) = \sum_{\mathrm{m=1}}^{\mathrm{N}}\Big\{\gamma\mathrm{s_m^2} + \sqrt{\gamma}\mathrm{n_m s_m}\Big\}^{\mathrm{P}} &= \sum_{m=1}^{N}\Big\{\alpha_o + \sqrt{\alpha_o}n_m\Big\}^P \\ &= \sum_{m=1}^{N} u_m^P,\end{aligned} \tag{3.15}$$

where $\alpha_o = \gamma s_m^2$, $u_m = \Big(\alpha_o + \sqrt{\alpha_o}n_m\Big)$.
The PDF of u_m can be derived as

$$f_{u_m}(x) = \frac{1}{2\kappa\sqrt{\alpha_o}}\exp\left(-\frac{\big|x-\alpha_o\big|}{\kappa\sqrt{\alpha_o}}\right). \tag{3.16}$$

As $u_1, u_2, \ldots, u_N$ are iid, μ_1 can be expressed as

$$\mu_1 = E\Bigg\{\sum_{m=1}^{N} u_m^P\Bigg\} = N \times E\Big[u_1^P\Big]. \tag{3.17}$$

Similarly, variance σ_1^2 can be represented as

$$\sigma_1^2 = N \times var\Big[u_1^P\Big]. \tag{3.18}$$

The mean $E\Big[u_1^P\Big]$ and variance $var\Big[u_1^P\Big]$ can be expressed as

$$E\Big[u_1^P\Big] = \frac{1}{2\kappa\sqrt{\alpha_o}}\Bigg\{a_o^{P+1}\Gamma\big(P+1\big)\Big\{\exp\left(\frac{\alpha_o}{c_o}\right) + \big(-1\big)^P\exp\left(-\frac{\alpha_o}{c_o}\right)\Big\}\Bigg\}$$
$$= \frac{c_o^P}{2}\Bigg\{\Gamma\big(P+1\big)\Big\{\exp\left(\frac{\alpha_o}{c_o}\right) + \big(-1\big)^P\exp\left(-\frac{\alpha_o}{a_o}\right)\Big\}\Bigg\},$$

$$var\Big[u_1^P\Big] = \frac{1}{2\kappa\sqrt{\alpha_o}}\Bigg\{a_o^{2P+1}\Gamma\big(2P+1\big)\Big\{\exp\left(\frac{\alpha_o}{c_o}\right) + \big(-1\big)^{2P}\exp\left(-\frac{\alpha_o}{c_o}\right)\Big\}\Bigg\} \tag{3.19}$$
$$-\frac{1}{4\kappa^2\alpha_o}\Bigg\{a_o^{P+1}\Gamma\big(P+1\big)\Big\{\exp\left(\frac{\alpha_o}{c_o}\right) + \big(-1\big)^P\exp\left(-\frac{\alpha_o}{a}\right)\Big\}\Bigg\}^2$$
$$= \frac{c_o^{2P}}{2}\Bigg\{\Gamma\big(2P+1\big)\Big\{\exp\frac{\alpha_o}{c_o} + \big(-1\big)^{2P}\exp\left(-\frac{\alpha_o}{c_o}\right)\Big\}\Bigg\}$$
$$-\frac{c_o^{2P}}{4}\Bigg\{\Gamma\big(P+1\big)\Big\{\exp\left(\frac{\alpha_o}{c_o}\right) + \big(-1\big)^P\exp\left(-\frac{\alpha_o}{c_o}\right)\Big\}\Bigg\}^2, \tag{3.20}$$

where $c_o = \kappa\sqrt{\alpha_o}$. The proofs of $E\Big[u_1^P\Big]$ and $var\Big[u_1^P\Big]$ are given in Appendix I.3 and Appendix I.4, respectively. The μ_1 and σ_1^2 can be derived as

$$\mu_1 = \frac{Nc_o^P}{2}\Bigg\{\Gamma\big(P+1\big)\Big\{\exp\left(\frac{\alpha_o}{a}\right) + \big(-1\big)^P\exp\left(-\frac{\alpha_o}{c_o}\right)\Big\}\Bigg\} \tag{3.21}$$

and σ_1^2 can be derived as

$$\sigma_1^2 = \frac{Nc_o^{2P}}{2}\Bigg\{\Gamma\big(2P+1\big)\Big\{\exp\left(\frac{\alpha_o}{c_o}\right) + \big(-1\big)^{2P}\exp\left(-\frac{\alpha_o}{c_o}\right)\Big\}\Bigg\}$$
$$-\frac{Nc_o^{2P}}{4}\Bigg\{\Gamma\big(P+1\big)\Big\{\exp\left(\frac{\alpha_o}{c_o}\right) + \big(-1\big)^P\exp\left(-\frac{\alpha_o}{c_o}\right)\Big\}\Bigg\}^2. \tag{3.22}$$

Now, CLT is invoked to get final expression of detection probability as

$$P_D = Prob\Big\{\Upsilon(\mathbf{y}) > \Psi|H_1\Big\} = Q\Big(\frac{\Psi-\mu_1}{\sigma_1}\Big). \tag{3.23}$$

The sum of P_F and missed detection probability P_M yields the overall total error probability P_{error} as

$$P_{error} = P_F + P_M, \tag{3.24}$$

where $P_M = 1 - P_D$. Now, optimum value of P, i.e., P_o is determined so that P_{error} is minimum. The optimum value of P can be obtained analytically by differentiating the above expression with respect to P as

$$P_o = \arg\min_P\left(P_{error}\right) = \arg\min_P\left(P_F + P_M\right). \tag{3.25}$$

P_o can be obtained by solving $\frac{\partial P_{error}}{\partial P} = 0$. However, the solution to this equation is stubborn, therefore an alternative option of simulations has been used. The optimum P varies with P_F as well as average SNR. Hence, to get optimum P using simulations, we plot a graph between P_{error} and P, keeping γ constant for the first time and then, keeping P_F constant for the second time. Then the minimum value of P_{error} obtained in the graph is regarded as the minimum error probability and this value of P for which minimum P_{error} is obtained, is denoted as P_o.

3.4 Simulation Results

In this section, we present the performance of the proposed MCD scheme with ROC. We also present P_D versus average SNR for the proposed scheme. Further, total error probability and optimum P have been obtained using simulations for different values of average SNR and P_F. For simplicity, the value of κ is assumed to be 1 in simulations. Table 3.1 shows simulation parameters which have been used to obtain Figure 3.1.

Table 3.1: Simulation Parameters for Figure 3.1

Parameters	**Values**
Number of iterations	10000
P_F	0.01 : 0.05 : 1
N	30
γ	-8 dB
κ	1

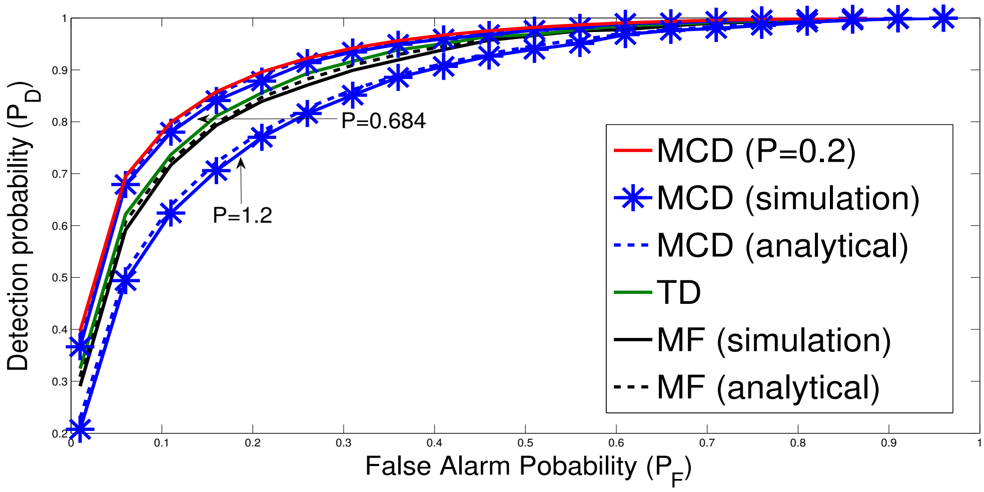

Figure 3.1: ROC for MCD scheme at $\gamma = -8$ dB and $N = 30$, highlighting the individual effect of exponent P on P_D and P_F.

To obtain optimum P using simulations, P_{error} is calculated as the sum of P_F and P_M. Then, the result is plotted with respect to different values of P, keeping γ fixed for one time and then, keeping P_F fixed for the second time. The value of P at which P_{error} shows minimum value, gives optimum

P. The optimum P and corresponding P_{error} for MCD scheme at $\gamma = -8$, -10 and -11 dB have been presented in Table 3.2. Further, P_F is assumed as 0.01. The N is assumed to be 30. At $\gamma = -8$, -10 and -11 dB, the respective values of P_{error} are 0.074, 0.1586 and 0.2648, and the corresponding values of optimum P are obtained as 0.684, 0.642 and 0.602. It can be observed that as average SNR increases, optimum P increases and P_{error} decreases.

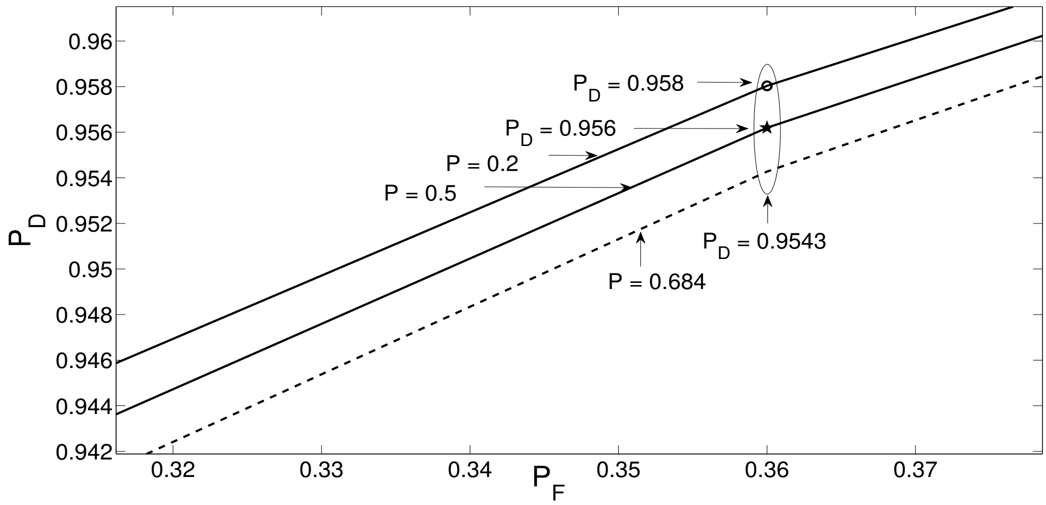

Figure 3.2: ROC (expanded view) for MCD scheme with $P = 0.2$, 0.5 and 0.684 at $\gamma = -8$ dB over a specified P_F range ($0.316 \leq P_F \leq 0.3785$).

Similarly, as average SNR increases, a reverse trend is observed, i.e., optimum P increases and P_{error} decreases.

Further, optimum P at $P_F = 0.01$, 0.05 and 0.1 have been presented keeping γ fixed at -8 dB. Here also, N is assumed as 30.

Table 3.2: The P_o and P_{error} for MCD with varying γ and P_F at $N = 30$.

$P_F = 0.01$			
γ (in dB)	$\gamma = -8$	$\gamma = -10$	$\gamma = -11$
P_o	0.684	0.642	0.602
P_{error}	0.074	0.1586	0.2648
$\gamma = -8$ dB			
P_F	$P_F = 0.01$	$P_F = 0.05$	$P_F = 0.1$
P_o	0.684	0.683	0.680
P_{error}	0.074	0.062	0.005

At P_F= 0.01, 0.05 and 0.1, the respective values of P_{error} are found to be 0.074, 0.062 and 0.005, and the corresponding values of optimum P are obtained as 0.684, 0.683 and 0.680. It can be observed that as P_F increases, optimum P and P_{error} decreases.

Figure 3.1 shows ROC for the MCD scheme at $P = 0.2$, 0.684, 1 and 1.2. The γ is assumed as -8 dB and $N = 30$. It can be seen that the P_D improves as P reduces from 1.2 to 0.2. At an arbitrary value of $P_F = 0.1$, the P_D at $P = 0.2$ and 0.5 are 0.776 and 0.7735, respectively. Similarly, at $P = 0.684$, 1 and 1.2, respective values of P_D are 0.7723, 0.7028 and 0.6138. It can be seen that

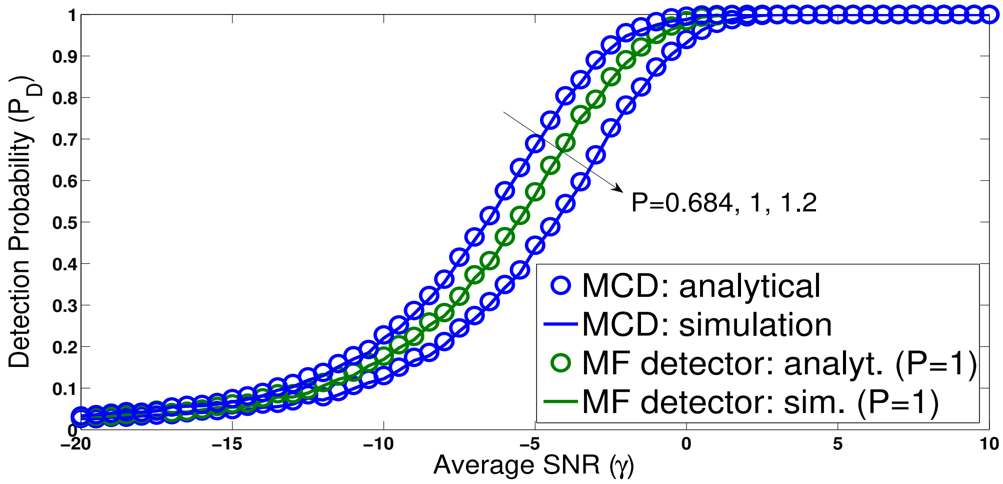

Figure 3.3: P_D vs. γ for MCD scheme with different values of P at $P_F = 0.01$ and $N = 30$.

the performance of the proposed scheme improves marginally if P is decreased below 0.684. Hence, this value of P is denoted as optimum P at $\gamma = -8$ dB. At $P = 1$, the MCD is reduced to the conventional MF detector which is a general correlation detector. Thus, the proposed detector at $P < 1$ outperformed the conventional detectors such as MF detector and TD. In this figure, analytical results have been presented along with simulation results. It can be seen that there is a close match between the two.

Figure 3.2 presents the expanded monochrome view of Figure 3.1 over a range of P_F from 0.316 to 0.3785. The γ is assumed as -8 dB and N is assumed to be 30. At an arbitrary value of $P_F = 0.36$, the values of P_D at $P = 0.684$, 0.5 and 0.2 are 0.9543 and 0.956 and 0.958, respectively. It can be observed that as P increases, P_D decreases and vice versa. It can also be observed that there is a negligible increase of P_D beyond $P = 0.684$. Hence, this value of P is optimum, at the corresponding value of average SNR.

Figure 3.3 shows P_D versus average SNR for the MCD scheme. The assumed values of P are 0.684, 1 and 1.2 over a range of γ from -20 dB to 10 dB. The N is assumed to be 30. Further, P_F is assumed as 0.01. At an arbitrary SNR of -10 dB, the values of P_D at $P = 0.684$, 1 and 1.2 are 0.2284, 0.1693 and 0.1224, respectively. Similarly, at a high SNR of -2 dB, respective values of P_D at $P = 0.684$, 1 and 1.2 are 0.948, 0.891 and 0.7737. Thus, it is observed that as P increases, P_D reduces and performance decreases. The proposed detector outperforms conventional MF detector at $P < 1$. At $P > 1$, the MF detector outperforms the proposed detector. Finally, simulation results have been presented with the analytical counterparts. It can be observed that both match closely.

3.5 Conclusion

In this chapter, a spectrum sensing scheme based on MCD was proposed in additive Laplacian noise environment. The expressions of P_D and P_F for the MCD scheme were derived. The analytical results were presented using ROC for different values of the parameter P. We also presented simulation results and found a close match with their analytical counterparts. The optimum P was found corresponding to different values of average SNR and P_F. Finally, a special case of the proposed scheme was presented by assuming $P = 1$, i.e., conventional correlation detector and compared it with the case available in the literature. We conclude that the detection performance improves if the value of P reduces below 1. However, below a certain value of P, there was no substantial improvement in the performance. We called it optimum P. In the next chapter, we will present a collaborative spectrum sensing scheme known as the CSS scheme where MCD is used as a localized detection scheme.

Chapter 4

Cooperative Spectrum Sensing Based on MCD in ALN

This chapter presents Cooperative Spectrum Sensing (CSS) scheme based on the Modified Correlation Detector (MCD) as a localized detection scheme in additive Laplacian noise environment. Using MCD and MF detectors at the cognitive terminal, all the hard decisions are forwarded to the fusion center (FC). Then, they are combined according to standard fusion rules of the CSS scheme. Subsequently, the FC decides the presence of the PU. The closed-form expressions of detection probability and false alarm probability have been derived and results are presented using ROC. The analytical results are corroborated using a close match between simulation results and analytical findings. Finally, the chapter ends with a brief conclusion.

4.1 Introduction

During spectrum sensing, CR frequently suffers from a well-known HPUN problem [165]. In this case, under the strong effect of shadowing and multipath fading, CR causes undesirable interference to the PU receiver, instead of accurately detecting the PU transmitter [166]. The CSS mitigates the Hidden Primary User Node (HPUN) problem by using multiple CRs, thus achieving diversity gain [167–169]. In CSS, M_o CRs exist which receive the PU signal via sensing channel. Out of these M_o CRs, at least k_o CRs infer the presence of the PU. They perform localized detection using some detection schemes to produce local hard decisions in the form of '0' and '1'. The hard decisions are sent to the FC via reporting channel where they are fused using standard fusion schemes available in the literature such as CSS: OR, CSS: AND, and CSS: majority. Finally, the FC decides the availability of the PU. The majority rule (k_o out of M_o rule, where $k_o < M_o$) has been used to analyze the CSS scheme in the Laplacian noise environment with static behavior of PU [131]. It has been shown that CSS based on Rao detector (CSS-Rao) outperformed CSS based on conventional ED (CSS-ED) in the noise modeled using GGD [128].

This chapter presents the CSS scheme based on MCD in additive Laplacian noise environment. Each M_o CR uses MCD as a localized detection scheme to produce a local hard decision. All the single-bit hard decisions from the CRs are communicated to the FC, where they are fused together using standard CSS fusion schemes. Finally, FC delivers its decision on the presence or absence of the PU. The expressions of detection probability and false alarm probability have been derived at the FC. Besides this, the optimum P is also obtained for several values of average SNR and P_F using simulations.

The rest of the chapter is presented in the following manner. The system model for the CSS scheme is presented in Section 4.2. Section 4.3 presents the performance analysis of CSS scheme using MCD as a localized detection scheme. Further, this section also presents the MF detection scheme. Finally, results are presented in Section 4.4 before presenting a brief conclusion in Section 4.5.

4.2 System Model

Let $\mathbf{y} = [y_1, y_2, \ldots, y_N]$ be an array of N observations of PU signal received at the cognitive terminal. Each received observation y_m at the cognitive terminal can be represented as

$$\begin{aligned} H_o &: y_m = n_m; \\ H_1 &: y_m = \sqrt{\gamma} s_m + n_m, \end{aligned} \tag{4.1}$$

where $m = 1, 2, \ldots, N$. Here, H_o denotes the null hypothesis. In this case, no presence of PU is detected. Similarly, H_1 denotes the alternate hypothesis. It signifies the case when PU signal is present. The γ indicates the average SNR. The BPSK modulated PU signal is denoted as s_m where $s_m \in \{-1, 1\}$. The n_m stands for the Laplacian noise with a mean equal to 0 and variance equal to $2\kappa^2$, i.e., $n_m \sim L(0, \kappa)$. It is assumed that all the received observations at the cognitive terminal are iid.

With reference to Chapter 3, the MCD detection scheme can be represented as

$$\Upsilon(\mathbf{y}) = \sum_{\mathrm{m=1}}^{\mathrm{N}} \left(\sqrt{\gamma}\mathrm{s_m y_m}\right)^{\mathrm{P}} \underset{\mathrm{H_o}}{\overset{\mathrm{H_1}}{\gtrless}} \Psi, \tag{4.2}$$

where $\Upsilon(\mathbf{y})$ is the decision statistic, assuming that the SU has information about PU a priori and Ψ is the detection threshold. The NP test is used to obtain the detection threshold. The received symbol y_m at the cognitive terminal is correlated with the PU signal s_m. Finally, they are raised to the exponent P with $0 < P \leq 2$. In addition to this, a collaborative scenario is considered where M_o CRs are available out of which k_o CRs are active. Each M_o CR uses MCD as its localized detection scheme to detect the PU signal. The localized hard decisions based on MCD, are individually communicated to the FC via reporting channel. Subsequently, the FC uses CSS: OR, CSS: AND, and CSS: majority fusion schemes on the received decisions to make a final decision on the availability of the PU.

4.3 Performance Analysis

In this section, closed-form expressions of P_D and P_F at the FC are presented. In CSS, it is assumed that the surrounding CRs use MCD as a localized detection scheme to obtain local hard decisions about the presence or absence of the PU. All the Single-bit hard decisions from each M_o CR are combined at the centralized FC according to the decision rule expressed as

$$U = \sum_{l=1}^{M_o} U_l \underset{H_o}{\overset{H_1}{\gtrless}} k_o, \tag{4.3}$$

where U_l is the hard decision from each M_o CR. Finally, at the FC, P_F and P_D at the cognitive terminal can be expressed as [109]

$$\begin{aligned} P_F &= \sum_{l=k_o}^{M_o} \binom{M_o}{l} Q_f^l (1-Q_f)^{M_o-l}, \\ P_D &= \sum_{l=k_o}^{M_o} \binom{M_o}{l} Q_d^l (1-Q_d)^{M_o-l}, \end{aligned} \tag{4.4}$$

where Q_f and Q_d denote the false alarm probability and detection probability, respectively, using MCD as a localized detection scheme at each M_o CR. Here, $k_o = 1$ represents CSS: OR rule, while $k_o = M_o$ indicates CSS: AND rule and $k_o < M_o$ signifies CSS: majority rule. The localized detection probability Q_d at each M_o CR can be expressed as

$$Q_d = Prob\Big\{\Upsilon(\mathbf{y}) > \Psi | H_1\Big\} = Q\bigg(\frac{\Psi - \mu_1}{\sigma_1}\bigg). \tag{4.5}$$

Similarly, the localized false alarm probability Q_f at each M_o CR can be expressed as

$$Q_f = Prob\Big\{\Upsilon(\mathbf{y}) > \Psi | H_o\Big\} = Q\bigg(\frac{\Psi - \mu_o}{\sigma_o}\bigg), \tag{4.6}$$

where μ_o and μ_1 denote the mean under hypotheses H_o and H_1, respectively. Similarly, σ_o^2 and σ_1^2 denote the respective variance under hypotheses H_o and H_1. The expressions of μ_o and σ_o^2 are evaluated in (3.12) and (3.13), which can be expressed as

$$\begin{aligned} \mu_o &= \frac{N\kappa^P}{2\sqrt{\gamma}}\Big\{\Gamma\big(P+1\big)\big(\sqrt{\gamma}\big)^{P+1}\Big\}\Big\{1+\big(-1\big)^P\Big\}, \\ \sigma_o^2 &= \frac{N\kappa^{2P}}{2\sqrt{\gamma}}\Big\{\Gamma\big(2P+1\big)\big(\sqrt{\gamma}\big)^{2P+1}\Big\{1+\big(-1\big)^{2P}\Big\}\Big\} - \frac{N\kappa^{2P}}{4\gamma}\Big\{\Gamma\big(P+1\big)\big(\sqrt{\gamma}\big)^{P+1}\Big\{1+\big(-1\big)^P\Big\}\Big\}^2. \end{aligned} \tag{4.7}$$

Similarly, the expressions of μ_1 and σ_1^2 have been derived in (3.21) and (3.22), which can be expressed as

$$\mu_1 = \frac{Nc_o^P}{2}\Bigg\{\Gamma(P+1)\Bigg\{\exp\left(\frac{\alpha_o}{a}\right) + (-1)^P\exp\left(-\frac{\alpha_o}{c_o}\right)\Bigg\}\Bigg\},$$

$$\sigma_1^2 = \frac{Nc_o^{2P}}{2}\Bigg\{\Gamma(2P+1)\Bigg\{\exp\left(\frac{\alpha_o}{c_o}\right) + (-1)^{2P}\exp\left(-\frac{\alpha_o}{c_o}\right)\Bigg\}\Bigg\}$$

$$-\frac{Nc_o^{2P}}{4}\Bigg\{\Gamma(P+1)\Bigg\{\exp\left(\frac{\alpha_o}{c_o}\right) + (-1)^P\exp\left(-\frac{\alpha_o}{c_o}\right)\Bigg\}\Bigg\}^2. \tag{4.8}$$

Finally, P_D and P_F at the FC can be derived by substituting the values of Q_d and Q_f in (4.4). Unless specified otherwise, reporting channel is assumed to be perfect. Besides this, a case of imperfect reporting channel is also considered with M_o cooperative CRs. In this case, the CSS: OR fusion scheme is assumed at the FC, to make decisions about the presence of the PU. The P_F can be expressed as [105]

$$P_F = 1 - \Big\{(1-Q_f)(1-\rho) + \rho Q_f\Big\}^{M_o}. \tag{4.9}$$

Similarly, the P_D can be expressed as

$$P_D = 1 - \Big\{Q_m(1-\rho) + \rho(1-Q_m)\Big\}^{M_o}, \tag{4.10}$$

where $Q_m = 1 - Q_d$, is the missed detection probability at each of the M_o CRs. Here, ρ is the error probability of receiving hard decisions from CRs at the FC with its range between 0 and 1.

The optimum P, denoted as P_o can be derived in a similar way as described in Chapter 3 as

$$P_o = \arg\min_P (P_{error}) = \arg\min_P (P_F + P_M), \tag{4.11}$$

where P_{error} is the total error probability and P_M is the missed detection probability at the FC. The value of P, where P_{error} shows minimum value gives optimum P. The optimum P with varying γ (constant P_F) and with varying P_F (constant γ) has been shown in Table 4.1.

4.4 Simulation Results

In this section, the performance of the CSS at the FC has been presented using different fusion schemes in additive Laplacian noise environment. Here, it is assumed that M_o CRs use detection schemes such as MCD and MF to get localized hard decisions on the availability of the PU.

Finally, the fusion rules are applied to the received observations at the FC. The CSS fusion schemes based on the localized detection schemes such as MCD and MF at the M_o CRs have been compared with conventional schemes. The conventional schemes refer to the MCD and MF detection schemes

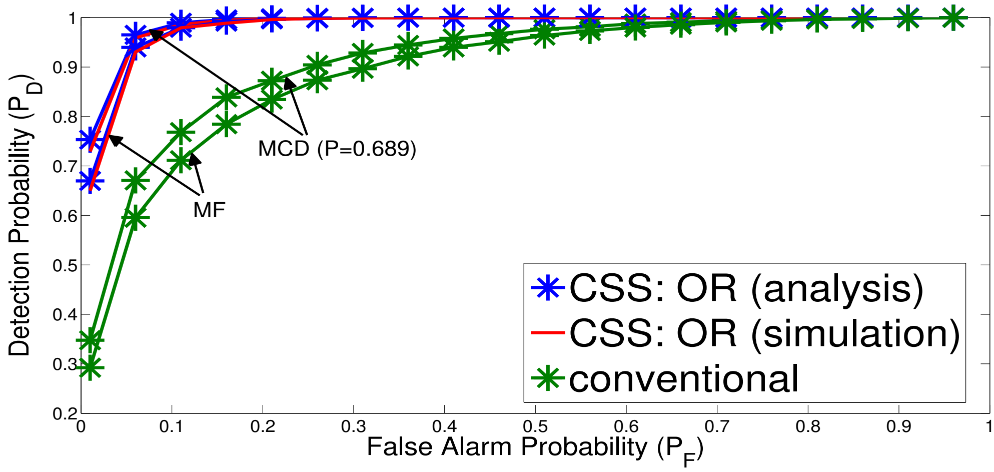

Figure 4.1: ROC for CSS: OR fusion scheme and conventional schemes at $\gamma = -8$ dB and $N = 30$.

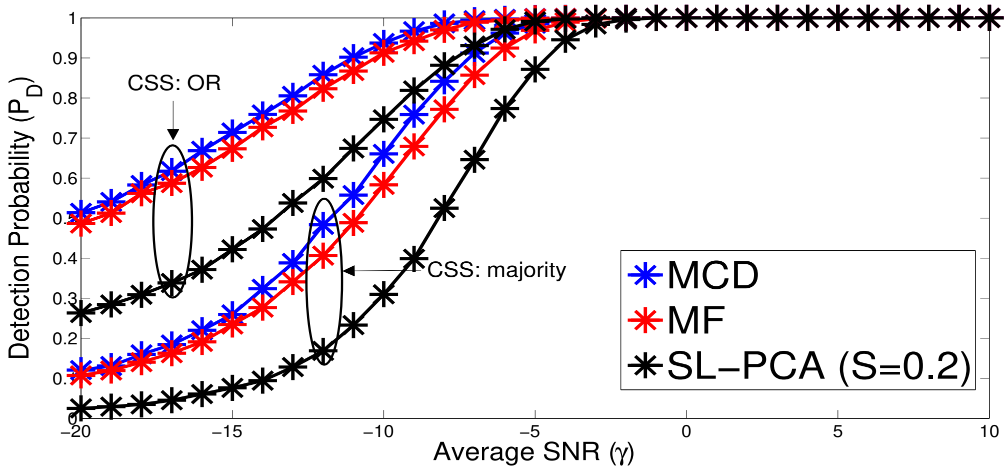

Figure 4.2: P_D vs. γ for CSS: OR and CSS: majority fusion schemes and conventional schemes at $N = 30$ and $P_F = 0.1$.

in a non-cooperative scenario. It means that, in conventional schemes, there exists a single cognitive terminal that uses MCD and MF as detection schemes to give final judgment on the availability of the PU. The performance is shown in terms of the ROC and P_D versus the average SNR. Further, the optimum P for CSS: OR fusion scheme has been obtained for different values of γ and P_F using simulations, as shown in Table 4.1. At fixed P_F of 0.1, the optimum values of P for conventional MCD scheme are 0.680, 0.642 and 0.602 at $\gamma = -8$, -10, and -11 dB, respectively. The values of optimum P are increased marginally for CSS scheme based on MCD, where at $\gamma = -8$, -10, and -11 dB, the respective optimum values of P stand at 0.689, 0.656 and 0.628. Similarly, at fixed γ of -8 dB, the optimum values of P for conventional MCD scheme are 0.684, 0.683 and 0.680 at $P_F = 0.01$, 0.05, and 0.1, respectively. The values of optimum P are increased marginally for the CSS scheme based on MCD, where at $P_F = 0.01$, 0.05, and 0.1 dB, the respective optimum values of P stand at 0.695, 0.692 and 0.689.

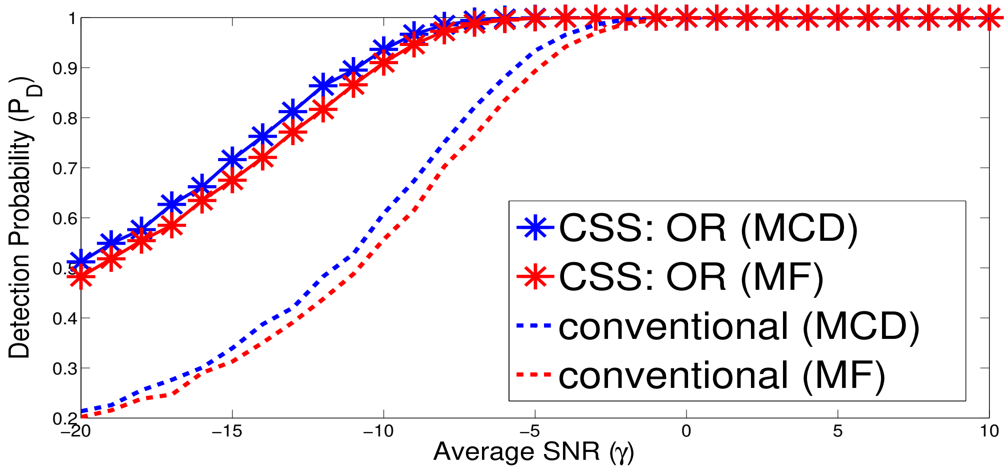

Figure 4.3: P_D vs. γ for CSS: OR fusion scheme and conventional schemes at $N = 30$ and $P_F = 0.1$.

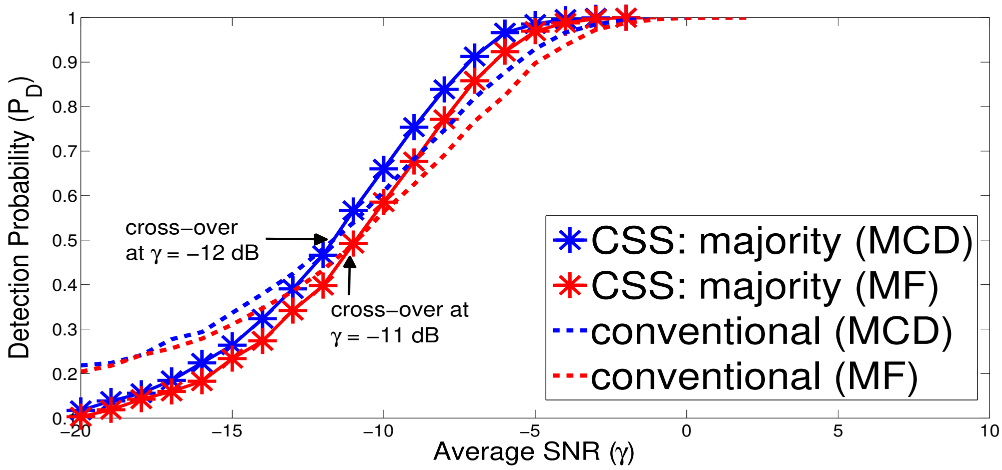

Figure 4.4: P_D vs. γ for the CSS: majority fusion scheme and conventional schemes at $N = 30$ and $P_F = 0.1$.

Further, the performance of the CSS scheme is also presented when reporting channel is imperfect. The κ is assumed to be 1 in simulations. For the plot of P_D versus γ, P_F is assumed as 0.1. For MF detection scheme, P is assumed to be 1. Further, it is assumed that P is equal to 0.689 (optimum P) for CSS: OR scheme based on MCD at $\gamma = -8$ dB.

Figure 4.1 shows the ROC for CSS: OR fusion scheme and conventional detection schemes such as MCD and MF. The optimum value of P is obtained as 0.689 at $\gamma = -8$ dB. The N is assumed to be 30. The values of P_D at $\gamma = -8$ dB and $P_F = 0.1$ for conventional MCD and MF detection schemes are 0.7489 and 0.6901, respectively. With CSS: OR fusion scheme based on MCD and MF, the values of P_D are improved to 0.9852 and 0.9705, respectively. It is observed that the CSS: OR fusion scheme outperforms conventional detection schemes. Apart from this, it is also observed that there exists a close match between analysis and simulations for CSS: OR scheme.

Figure 4.2 shows P_D versus average SNR for CSS: OR and CSS: majority fusion schemes. The

Table 4.1: The optimum P for CSS: OR fusion scheme with varying γ and P_F at $N = 30$.

$P_F = 0.1$			
γ (in dB)	$\gamma = -8$	$\gamma = -10$	$\gamma = -11$
MCD	0.680	0.642	0.602
CSS-MCD	0.689	0.656	0.628
$\gamma = -8$ dB			
P_F	$P_F = 0.01$	$P_F = 0.05$	$P_F = 0.1$
MCD	0.684	0.683	0.680
CSS-MCD	0.695	0.692	0.689

MCD, MF and correlated SL-PCA have been used as localized detection schemes at the M_o CRs over $-20 \leq \gamma \leq 10$ dB. In correlated SL-PCA, the received observations at the cognitive terminal are first correlated with the known PU sequence. Then, the existing SL-PCA scheme [117] is used as a localized detection scheme over the received observations. It is assumed that $k_o = 2$ and $M_o = 3$ for CSS: majority fusion scheme. The N is assumed to be 30. The soft-limiting parameter S in SL-PCA scheme is assumed as 0.2. The values of P_D at $\gamma = -8$ dB and $P_F = 0.1$ for conventional MCD and MF detection schemes are 0.7489 and 0.6901, respectively. With CSS: majority fusion scheme based on MCD and MF, the values of P_D are improved to 0.8387 and 0.7714, respectively. It is also observed that the performance of the CSS: OR and CSS: majority fusion schemes based on MCD and MF at the M_o CRs improves over CSS with correlated SL-PCA detection scheme.

Figure 4.3 shows P_D versus average SNR for CSS: OR fusion scheme and conventional schemes over $-20 \leq \gamma \leq 10$ dB. The N is assumed to be 30 and $P_F = 0.1$. It is clear that CSS: OR fusion scheme based on MCD and MF detectors outperforms conventional schemes.

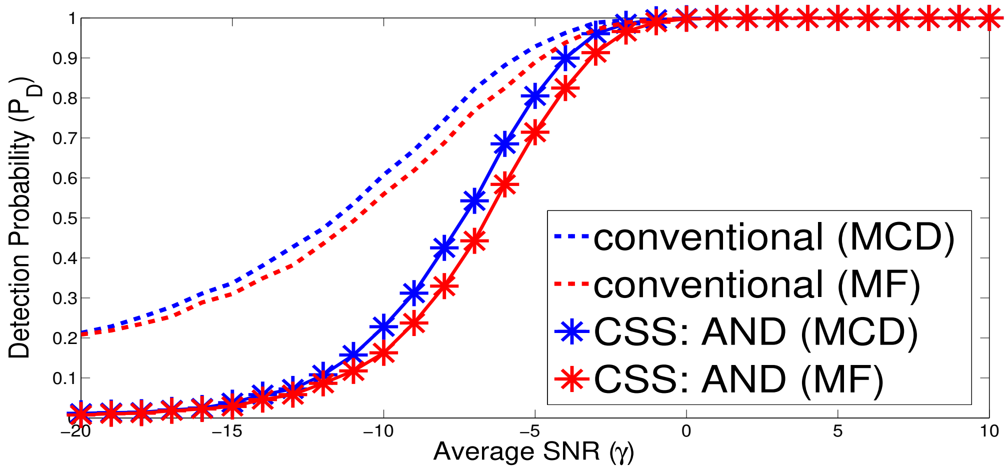

Figure 4.5: P_D vs. γ for CSS: AND fusion scheme and conventional schemes at $N = 30$ and $P_F = 0.1$.

Figure 4.4 shows P_D versus average SNR for CSS: majority fusion scheme and conventional schemes over $-20 \leq \gamma \leq 10$ dB. It is assumed that $k_o = 2$ and $M_o = 3$ for this scheme. The N is assumed to be 30. It can be seen that the CSS: majority fusion scheme outperforms conventional detection schemes such as MCD and MF over a fixed range of γ. It is to be noted that, there exists a cross-

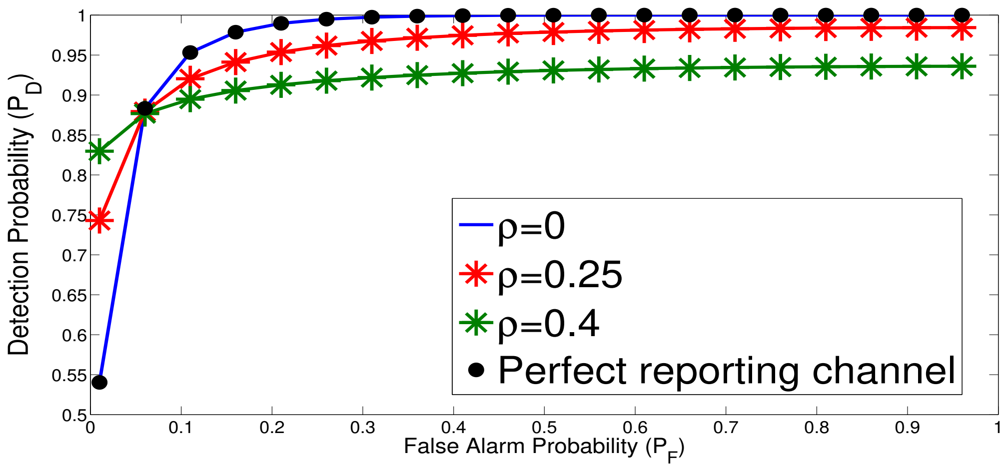

Figure 4.6: ROC for CSS: OR fusion scheme over imperfect reporting channel with varying ρ at $N = 30$, $\gamma = -10$ dB.

over point where the CSS: majority fusion scheme crosses its conventional counterparts. Beyond this cross-over point, CSS: majority fusion scheme outperforms its conventional counterparts. Below the cross-over point, conventional detection schemes perform better. The cross-over points in the case of CSS majority fusion scheme using localized MCD and MF detection schemes are at $\gamma = -12$ dB and -11 dB, respectively.

Figure 4.5 shows P_D versus average SNR for CSS: AND fusion scheme and conventional schemes over $-20 \leq \gamma \leq 10$ dB. The values of P_D at $\gamma = -8$ dB and $P_F = 0.1$ for conventional MCD and MF detection schemes are 0.7489 and 0.6901, respectively. With CSS: AND fusion scheme based on localized MCD and MF detection schemes, the values of P_D are decreased to 0.4253 and 0.3297, respectively. Thus, in this case, conventional schemes outperform CSS: AND fusion scheme.

Figure 4.6 shows ROC comparison of CSS: OR fusion scheme based on localized detection schemes such as MCD and MF over imperfect reporting channel with an error probability ρ. The range of ρ varies from 0 to 1. The γ is assumed to be -10 dB. It is quite clear that at $\rho = 0$, the ROC exactly coincides with the perfect reporting channel. The values of P_D at $\rho = 0$ and 0.25 are 0.9561 and 0.9167, respectively which further decrease to 0.892 and 0 at $\rho = 0.4$ and 1, respectively. As ρ increases, error probability in the reporting channel increases, hence the performance degrades.

4.5 Conclusion

In this chapter, the CSS fusion schemes were presented in additive Laplacian noise environment. Each k_o CR out of M_o CRs used MCD and its special case MF as its localized detection schemes. All single-bit hard decisions from each k_o CR were fused together at the FC according to different fusion schemes to deliver the final judgment on the presence of the PU. The analytical results of CSS: OR scheme were presented with a close match with their simulation counterparts. The CSS fusion schemes ('OR' and 'majority' schemes) which used localized detection schemes such as MCD and MF were compared with conventional detection schemes. The results were presented in terms of ROC and P_D versus average SNR. Besides this, optimum P for different values of P_F and γ was also obtained using simulations. It is concluded that over $-20 \leq \gamma \leq 10$ dB, the detection performance of the conventional schemes was improved using CSS: OR fusion scheme. It is also concluded that the performance of conventional schemes was improved using the CSS: majority fusion scheme, only for a specified range of γ which is -12 dB and -11 dB using MCD and MF detectors, respectively. Further, it is concluded that the CSS: AND fusion scheme could not improve the detection performance of conventional schemes. Hence, the CSS: AND fusion scheme is found to be an inefficient scheme, unlike the case of Gaussian noise, where CSS: AND fusion scheme improves the detection performance. Till now, we have presented the case of static PU with the prior availability of information on PU at the CR. In a practical scenario, neither PU can be always static nor information about the PU is always available at the CR. Hence, in the next chapter, we will present the case of dynamic PU with one transition point within the sensing period. The PU is assumed to be unknown. Further, a non-coherent spectrum sensing scheme is presented in ALN environment.

Chapter 5

Spectrum Sensing Based on Dynamic PU With One Transition in ALN

In this chapter, spectrum sensing schemes with dynamic and unknown PU are presented in the environment of additive Laplacian noise. It means that the PU may not be present or absent during the whole sensing period. A scenario of one transition of the PU is assumed within the sensing time interval, where PU arrives or departs randomly. Further, the random transitions (arrival and departure) of the PU follow the Poisson distribution. The considered detection scheme is improved Absolute Value Cumulation Detection (i-AVCD), with Absolute Value Cumulation Detection (AVCD) and Energy Detection (ED) as its special cases. These schemes are used with dynamic parameters such as the arrival rate and departure rate of the PU. The performance is presented with ROC and P_D versus average SNR using simulations. The chapter finally ends with a brief conclusion.

5.1 Introduction

A majority of the conventional spectrum sensing schemes assumed the static behavior of the PU during the sensing period. It means that the PU remains active or inactive throughout the whole sensing period [170–172]. In this scenario, it is a simple binary hypothesis testing problem, in which the assumed static model of the PU is valid for a slow variation in PU traffic. However, when PU traffic varies fast or in other words, PU follows dynamic behavior as in cellular communication or Wireless LAN, the performance of these conventional schemes degrades. The dynamic behavior of the PU is characterized by single or multiple transitions within the sensing period. The case of single transition has been proposed in [143]. Spectrum sensing based on two transitions of the PU has been proposed in [146]. The case of multiple transitions of the PU based on different applications of the

Markov chain has been presented in [153–157].

In this chapter, the dynamic behavior of the PU in additive Laplacian noise is presented. The i-AVCD scheme has been explored, with AVCD and ED as its special cases. It has been assumed that the PU makes one transition within the sensing period under both hypotheses H_o and H_1. The transition is random in nature. The random arrival and departure of the PU have been modeled using the Poisson distribution. The arrival rate and departure rate of the PU are the dynamic parameters, that denote the rate at which PU arrives and departs, respectively. Besides this, PU is assumed to be unknown.

The rest of the chapter is organized as follows. The system model for the spectrum sensing scheme based on dynamic PU has been presented in Section 5.2. The section presents the received observations within the sensing period and the transition points under both the hypotheses. Section 5.3 presents the performance analysis of the detection schemes in the dynamic PU model. Finally, results are presented in Section 5.4, before a brief conclusion of the work in Section 5.5.

5.2 System Model

In general, with static PU, H_o denotes the null hypothesis when PU is absent and H_1 denotes the alternate hypothesis when PU is present. Here, it is assumed that the PU randomly departs under hypothesis H_o and randomly arrives under hypothesis H_1 during the sensing period. The received signal at the cognitive terminal under the random arrival and departure of the PU can be expressed as [143]

$$\begin{aligned} H_o : y_m &= \begin{cases} s_m + n_m & , m = 1, \ldots, \vartheta_o \\ n_m & , m = \vartheta_o + 1, \vartheta_o + 2, \vartheta_o + 3, \ldots, N; \end{cases} \\ H_1 : y_m &= \begin{cases} n_m & , m = 1, \ldots, \vartheta_1 \\ s_m + n_m & , m = \vartheta_1 + 1, \vartheta_1 + 2, \vartheta_1 + 3, \ldots, N, \end{cases} \end{aligned} \tag{5.1}$$

where m denotes the sensing sample with $1 \leq m \leq N$. The N indicates the total number of samples present during the sensing period. It is assumed that $N = BT$, where B is the bandwidth of the bandpass filter used to filter PU signal and T is the interval at which filtered PU signal is sampled. The s_m is the unknown PU signal while n_m indicates Laplacian noise with mean 0 and variance $2\kappa^2$. The ϑ_o and ϑ_1 indicate the first level transition points of the PU under hypotheses H_o and H_1, respectively. Transition of the PU occurs between samples ϑ_o and $\vartheta_o + 1$ under H_o (when PU randomly departs) and between the samples ϑ_1 and $\vartheta_1 + 1$ under H_1 (when PU randomly arrives). In a nutshell, the arrival and departure of the PU have been assumed under hypothesis H_1 and H_o, respectively.

5.3 Performance Analysis

In this section, two subsections have been presented. In the first subsection, three cases are presented for the i-AVCD scheme. In the first case, the scenario of static PU as a special case of dynamic PU is presented. In the second and third cases, the random arrival and departure of the dynamic PU are presented. The AVCD has been presented as a special case of i-AVCD. Further, P_D is derived in each of the cases of the i-AVCD and the results are corroborated using a close match with simulations. In the second subsection, the same three cases of the PU have been presented for the ED scheme. The first case presents the case of static PU as a special case of dynamic PU, while the second and third cases present the random arrival and departure of the dynamic PU, respectively.

5.3.1 improved Absolute Value Cumulation Detection

In the scenario of Laplacian noise, improved Absolute Value Cumulation Detection (i-AVCD) is one of the prevailing detection schemes available in the literature. In the i-AVCD, received samples at the cognitive terminal are raised to a positive exponent P with $0 < P \leq 2$. Being a special case of i-AVCD at $P = 1$, corresponding parameters of AVCD can be obtained by substituting the value of $P = 1$ in the expressions obtained for i-AVCD. Considering i-AVCD as the detection scheme, the likelihood function under hypothesis H_o can be expressed as [143]

$$f(\mathbf{y}|\mathbf{s}_{co}, H_o) = \frac{1}{(2\kappa)^N} \exp\left\{-\sum_{m=1}^{\vartheta_o} \frac{|y_m - s_m|^P}{\kappa} - \sum_{m=\vartheta_o+1}^{N} \frac{|y_m|^P}{\kappa}\right\}, \tag{5.2}$$

and the likelihood function under hypothesis H_1 can be expressed as

$$f(\mathbf{y}|\mathbf{s}_{c1}, H_1) = \frac{1}{(2\kappa)^N} \exp\left\{-\sum_{m=1}^{\vartheta_1} \frac{|y_m|^P}{\kappa} - \sum_{m=\vartheta_1+1}^{N} \frac{|y_m - s_m|^P}{\kappa}\right\}, \tag{5.3}$$

where $\mathbf{y} = [y_1, y_2, y_3, \ldots, y_N]$, $\mathbf{s}_{co} = [s_1, s_2, s_3, \ldots, s_{\vartheta_o}]$ and $\mathbf{s}_{c1} = [s_{\vartheta_1+1}, s_{\vartheta_1+2}, s_{\vartheta_1+3}, \ldots, s_N]$. As the parameter s_m is unknown, CR is not aware of any information about the PU signal. Hence, it needs to be removed from the likelihood function. This belongs to the composite hypothesis testing problem where some of the parameters in the hypothesis are unknown and can be estimated using various estimation techniques. More specifically, GLRT is used for spectrum sensing and MLE is used to find out the estimate of s_m. This gives

$$\frac{f\left(\mathbf{y}|\hat{\mathbf{s}}_{c1}, H_1\right)}{f\left(\mathbf{y}|\hat{\mathbf{s}}_{co}, H_o\right)} = \frac{\frac{1}{\left(2\kappa\right)^N} \exp\left(\sum_{m=1}^{\vartheta_1} - \frac{|y_m|^P}{\kappa}\right)}{\frac{1}{\left(2\kappa\right)^N} \exp\left(\sum_{m=\vartheta_o+1}^{N} - \frac{|y_m|^P}{\kappa}\right)} \underset{H_o}{\overset{H_1}{\gtrless}} \Psi, \tag{5.4}$$

where $\hat{\mathbf{s}}_{co} = [\hat{s}_1, \hat{s}_2, \hat{s}_3, \ldots, \hat{s_{\vartheta_o}}]$ and $\hat{\mathbf{s}}_{c1} = [\hat{s}_{\vartheta_1+1}, \hat{s}_{\vartheta_1+2}, \ldots, \hat{s}_N]$. The $\hat{s}_m$ is the Maximum Likelihood (ML) estimate of s_m which is calculated manually and found to be y_m, i.e., $\hat{s}_m = y_m$. Simplifying (5.4), the detection scheme can be represented as

$$\Upsilon(\mathbf{y}) = \sum_{m=\vartheta_o+1}^{N} |\mathrm{y_m}|^{\mathrm{P}} - \sum_{\mathrm{m}=1}^{\vartheta_1} |\mathrm{y_m}|^{\mathrm{P}} \underset{\mathrm{H_o}}{\overset{\mathrm{H_1}}{\gtrless}} \Psi', \tag{5.5}$$

where Ψ' is the detection threshold which is equal to $\kappa \cdot ln(\Psi)$. It is obtained using the NP test. The ϑ_o and ϑ_1 are averaged out in (5.5) over their distributions. Finally, the P_D can be expressed as

$$P_D = Prob\Big\{\Upsilon(\mathbf{y}) > \Psi'|\mathrm{H_1}\Big\}. \tag{5.6}$$

Similarly, P_F can be expressed as

$$P_F = Prob\Big\{\Upsilon(\mathbf{y}) > \Psi'|\mathrm{H_o}\Big\}. \tag{5.7}$$

If X denotes a random variable signifying non-arrival of the PU, then its Probability Mass Function (PMF) can be expressed as

$$\begin{aligned} f(g; \theta_A T) &= Prob(X = g) \\ &= \frac{\exp\big(-\theta_A T\big) \cdot \big(\theta_A T\big)^g}{g!}, \end{aligned} \tag{5.8}$$

where θ_A denotes the arrival rate of the PU. The T is the time interval at which the PU signal is sampled. The g denotes the number of occurrences of events (arrivals) within the time interval T. Here, for simplicity, it is assumed that $g = 0$. The same case applies when PU randomly departs. The θ_D which represents the departure rate of the PU. Hence, the probability with which the PU arrives or departs during sample interval T is given by $1 - \exp\big(-\theta_A T\big)$ and $1 - \exp\big(-\theta_D T\big)$, respectively. The probability of the random transitions of the PU in the ϑ_o^{th} and ϑ_1^{th} sample can be expressed as [143]

$$\begin{aligned} Prob\Big\{\vartheta_o\Big\} &= \Big\{1 - \exp\big(-\theta_D T\big)\Big\}\Big\{\exp\big(-\theta_D T\big)\Big\}^{\vartheta_o}, \\ Prob\Big\{\vartheta_1\Big\} &= \Big\{1 - \exp\big(-\theta_A T\big)\Big\}\Big\{\exp\big(-\theta_A T\big)\Big\}^{\vartheta_1}, \end{aligned} \tag{5.9}$$

where $Prob\{\vartheta_o\}$ and $Prob\{\vartheta_1\}$ are the probabilities of random departure and arrival of the PU, respectively. The three cases of the PU are presented in the following sections.

(1) Static PU:

Static PU signifies a low traffic scenario case when $\vartheta_o = 0$ and $\vartheta_1 = 0$. The i-AVCD scheme in the static scenario can be represented as

$$\Upsilon(\mathbf{y}) = \sum_{m=1}^{N} |\mathrm{y_m}|^{\mathrm{P}} \underset{\mathrm{H_o}}{\overset{\mathrm{H_1}}{\gtrless}} \Psi', \tag{5.10}$$

where Ψ' is the detection threshold obtained using the NP test. For large values of N, CLT is invoked to approximate the PDF of $\Upsilon(\mathbf{y})$ as Gaussian with mean μ_s and variance σ_s^2 as

$$\Upsilon(\mathbf{y}) \sim N(\mu_s, \sigma_s^2), \tag{5.11}$$

where μ_s and σ_s^2 can be expressed as [97]

$$\begin{aligned} \mu_s &= \kappa^P \Gamma(P+1), \\ \sigma_s^2 &= \kappa^{2P} \Big\{ \Gamma(2P+1) - \Gamma^2(P+1) \Big\}, \end{aligned} \tag{5.12}$$

where $\Gamma(v) = \int_0^{+\infty} e^{-t} t^{v-1} dt$ [77]. Using (5.11), Ψ' is expressed as

$$\Psi' = Q^{-1}(P_F)\sigma_s + \mu_s, \tag{5.13}$$

where $Q(.)$ represents the Q-function given by $Q(l) = \frac{1}{\sqrt{2\pi}} \int_l^{+\infty} \exp\left(-\frac{t^2}{2}\right) dt$. The P_F can be derived from (5.13) and P_D can be obtained using simulations.

(2) Random Transition in Dynamic PU (Arrival case):

The case of $\vartheta_o = 0$ signifies the absence of the PU during the complete duration of the sensing period. However, it also marks the beginning of transmission of the PU. Here, if it is assumed that ϑ_1 follows exponential distribution, then using (5.5) and (5.9), detection scheme under this scenario can be represented as [143]

$$\begin{aligned} \Upsilon(\mathbf{y}) &= \sum_{\vartheta_1=0}^{N-1} \Big\{ 1 - \exp\big(-\theta_A T\big) \Big\} \Big\{ \exp\big(-\theta_A T\big) \Big\}^{\vartheta_1} \left\{ \sum_{m=1}^{N} |y_m|^P - \sum_{m=1}^{\vartheta_1} |y_m|^P \right\} \underset{H_o}{\overset{H_1}{\gtrless}} \Psi' \\ &= \sum_{m=1}^{N} \Big\{ 1 - \exp\big(-\theta_A T m\big) \Big\} |y_m|^P \underset{H_o}{\overset{H_1}{\gtrless}} \Psi', \end{aligned} \tag{5.14}$$

where Ψ' is the detection threshold obtained using the NP test. For large values of N, CLT can be invoked so that $\Upsilon(\mathbf{y})$ tends to be Gaussian with mean μ_{a_o} and variance $\sigma_{a_o}^2$. Thus, Ψ' can be expressed as

$$\Psi' = Q^{-1}\big(P_F\big)\sigma_{a_o} + \mu_{a_o}, \tag{5.15}$$

where μ_{a_o} denotes the mean and $\sigma^2_{a_o}$ denotes the variance of the decision statistic $\Upsilon(\mathbf{y})$ obtained in (5.14) under hypothesis H_o. The expression of μ_{a_o} can be derived as

$$\mu_{a_o} = \mu_s\Bigg\{N - \Bigg\{\frac{\exp\big(-\theta_A T\big)\Big\{1-\exp\big(-\theta_A TN\big)\Big\}}{1-\exp\big(-\theta_A T\big)}\Bigg\}\Bigg\}, \tag{5.16}$$

while the expression of $\sigma^2_{a_o}$ can be derived as

$$\sigma^2_{a_o} = \sigma^2_s\Bigg\{N - \Bigg\{\frac{\exp\big(-2(\theta_A T+1)\big)\Big\{1-\exp\big(1-N\big)\Big\}}{1-\exp\big(-1\big)} + \exp\big(-2\theta_A T\big)\Bigg\}\Bigg\}. \tag{5.17}$$

Using the value of Ψ' in (5.15), P_F can be derived. Subsequently, P_D can be obtained using simulations.

(3) Random Transition in Dynamic PU (Departure case):

The case of $\vartheta_1 = 0$ signifies the presence of the PU during the whole sensing period. However, it also marks the beginning of the last phase of the active transmission of the PU. Here, if it is assumed that ϑ_o follows exponential distribution, then using (5.5) and (5.9), detection scheme under this scenario can be expressed as

$$\begin{aligned}\Upsilon(\mathbf{y}) &= \sum_{\vartheta_o=0}^{N-1}\Big\{1-\exp\big(-\theta_D T\big)\Big\}\Big\{\exp\big(-\theta_D T\big)\Big\}^{\vartheta_o}\Bigg\{\sum_{m=1}^{N}|y_m|^P - \sum_{m=1}^{\vartheta_o}|y_m|^P\Bigg\} \underset{H_o}{\overset{H_1}{\gtrless}} \Psi' \\ &= \sum_{m=1}^{N}\Big\{1-\exp\big(-\theta_D Tm\big)\Big\}|y_m|^P \underset{H_o}{\overset{H_1}{\gtrless}} \Psi',\end{aligned} \tag{5.18}$$

where Ψ' is the detection threshold obtained using the NP test. For large values of N, CLT is used, which approximates $\Upsilon(\mathbf{y})$ to be Gaussian with mean μ_{d_o} and variance $\sigma^2_{d_o}$. Thus, Ψ' can be expressed as

$$\Psi' = Q^{-1}\big(P_F\big)\sigma_{d_o} + \mu_{d_o}, \tag{5.19}$$

where μ_{d_o} denotes the mean and $\sigma^2_{d_o}$ denotes the variance of the decision statistic $\Upsilon(\mathbf{y})$ obtained in (5.18) under hypothesis H_o. The expression of μ_{d_o} can be derived and expressed as

$$\mu_{d_o} = \mu_s\Bigg\{N - \Bigg\{\frac{\exp\big(-\theta_D T\big)\Big\{1-\exp\big(-\theta_D TN\big)\Big\}}{1-\exp\big(-\theta_D T\big)}\Bigg\}\Bigg\}, \tag{5.20}$$

and the expression of $\sigma^2_{d_o}$ can be expressed as

$$\sigma^2_{d_o} = \sigma^2_s \Bigg\{ N - \Bigg\{ \frac{\exp\big(-2(\theta_D T + 1)\big)\Big\{1 - \exp\big(1 - N\big)\Big\}}{1 - \exp\big(-1\big)} + \exp\big(-2\theta_D T\big) \Bigg\} \Bigg\}. \tag{5.21}$$

Using the value of Ψ' in (5.19), P_F can be derived. Subsequently, P_D can be obtained using simulations.

5.3.2 Energy Detection

The Energy Detection (ED) is one of the classical detection schemes used for spectrum sensing. It is a special case of i-AVCD at $P = 2$. Considering ED as a detection scheme, the likelihood function under hypothesis H_o can be expressed as [143]

$$f(\mathbf{y}|\mathbf{s}_{co}, H_o) = \frac{1}{(2\kappa)^N} \exp\left\{ -\sum_{m=1}^{\vartheta_o} \frac{|y_m - s_m|^2}{\kappa} - \sum_{m=\vartheta_o+1}^{N} \frac{|y_m|^2}{\kappa} \right\}. \tag{5.22}$$

Similarly, the likelihood function under hypothesis H_1 can be expressed as

$$f(\mathbf{y}|\mathbf{s}_{c1}, H_1) = \frac{1}{(2\kappa)^N} \exp\left\{ -\sum_{m=1}^{\vartheta_1} \frac{|y_m|^2}{\kappa} - \sum_{m=\vartheta_1+1}^{N} \frac{|y_m - s_m|^2}{\kappa} \right\}, \tag{5.23}$$

where $\mathbf{y} = [y_1, y_2, y_3, \ldots, y_N]$, $\mathbf{s}_{co} = [s_1, s_2, s_3, \ldots, s_{\vartheta_o}]$ and $\mathbf{s}_{c1} = [s_{\vartheta_1+1}, s_{\vartheta_1+2}, s_{\vartheta_1+3}, \ldots, s_N]$. As the parameter s_m is unknown, CR is not aware of any information about the PU signal. Hence, it needs to be removed from the likelihood function. This belongs to the composite hypothesis testing problem where some of the parameters in the hypotheses are unknown and can be estimated using various estimation techniques. More specifically, GLRT is used for spectrum sensing and MLE is used to find out the estimate of s_m. This gives

$$\frac{f\big(\mathbf{y}|\hat{\mathbf{s}}_{c1}, H_1\big)}{f\big(\mathbf{y}|\hat{\mathbf{s}}_{co}, H_o\big)} = \frac{\frac{1}{\left(2\kappa\right)^N} \exp\left(\sum_{m=1}^{\vartheta_1} - \frac{|y_m|^2}{\kappa} \right)}{\frac{1}{\left(2\kappa\right)^N} \exp\left(\sum_{m=\vartheta_o+1}^{N} - \frac{|y_m|^2}{\kappa} \right)} \underset{H_o}{\overset{H_1}{\gtrless}} \Psi, \tag{5.24}$$

where $\hat{\mathbf{s}}_{co} = [\hat{s}_1, \hat{s}_2, \hat{s}_3, \ldots, \hat{s}_{\vartheta o}]$ and $\hat{\mathbf{s}}_{c1} = [\hat{s}_{\vartheta_1+1}, \hat{s}_{\vartheta_1+2}, \ldots, \hat{s}_N]$. The $\hat{s}_m$ is the ML estimate of s_m which is calculated manually and found to be y_m, i.e., $\hat{s}_m = y_m$. Simplifying (5.24), detection scheme can be represented as

$$\Upsilon(\mathbf{y}) = \sum_{m=\vartheta_o+1}^{N} |\mathrm{y_m}|^2 - \sum_{\mathrm{m}=1}^{\vartheta_1} |\mathrm{y_m}|^2 \underset{\mathrm{H_o}}{\overset{\mathrm{H_1}}{\gtrless}} \Psi', \tag{5.25}$$

where Ψ' is the detection threshold which is equal to $\kappa \cdot ln(\Psi)$. It is obtained using the NP test.

The ϑ_o and ϑ_1 are averaged out in (5.25) over their distributions. The P_D can be expressed as

$$P_D = Prob\Big\{\Upsilon(\mathbf{y}) > \Psi'|\mathrm{H}_1\Big\}, \tag{5.26}$$

and P_F can be expressed as

$$P_F = Prob\Big\{\Upsilon(\mathbf{y}) > \Psi'|\mathrm{H}_\mathrm{o}\Big\}. \tag{5.27}$$

Here also, using (5.8), the probabilites of the random transition of the PU in the ϑ_o^{th} and ϑ_1^{th} sample are expressed as [143]

$$\begin{aligned} Prob\Big\{\vartheta_o\Big\} &= \Big\{1-\exp\big(-\theta_D T\big)\Big\}.\Big\{\exp\big(-\theta_D T\big)\Big\}^{\vartheta_o}, \\ Prob\Big\{\vartheta_1\Big\} &= \Big\{1-\exp\big(-\theta_A T\big)\Big\}.\Big\{\exp\big(-\theta_A T\big)\Big\}^{\vartheta_1}, \end{aligned} \tag{5.28}$$

where $Prob\{\vartheta_o\}$ and $Prob\{\vartheta_1\}$ are the probability of random departure and arrival of the PU, respectively. The three cases of the PU are presented in the following sections.

(1) Static PU:

Static PU signifies a low traffic scenario case when $\vartheta_o = 0$ and $\vartheta_1 = 0$. Finally, the detection scheme in the static scenario can be expressed as

$$\Upsilon(\mathbf{y}) = \sum_{m=1}^{N} |\mathrm{y_m}|^2 \underset{\mathrm{H_o}}{\overset{\mathrm{H_1}}{\gtrless}} \Psi', \tag{5.29}$$

where Ψ' is the detection threshold obtained using the NP test. For large values of N, using CLT, the PDF of $\Upsilon(\mathbf{y})$ can be approximated as Gaussian with mean μ_s and variance σ_s^2 as

$$\Upsilon(\mathbf{y}) \sim \mathrm{N}(\mu_\mathrm{s}, \sigma_\mathrm{s}^2), \tag{5.30}$$

where μ_s and σ_s^2 can be expressed as [98]

$$\begin{aligned} \mu_s &= 2N\kappa^2, \\ \sigma_s^2 &= 2\sqrt{5N}\kappa^2. \end{aligned} \tag{5.31}$$

Using (5.30), Ψ' is expressed as

$$\Psi' = Q^{-1}\big(P_F\big)\sigma_s + \mu_s. \tag{5.32}$$

Using the value of Ψ' in (5.32), P_F can be derived and P_D can be obtained using simulations.

(2) Random Transition in Dynamic PU (Arrival case):

The case of $\vartheta_o = 0$ signifies the absence of the PU during the complete duration of the sensing period. However, it also marks the beginning of transmission of the PU. Here, if it is assumed that ϑ_1 follows exponential distribution, then using (5.25) and 5.28, detection scheme under this scenario can be represented as [143]

$$\begin{aligned}\Upsilon(\mathbf{y}) &= \sum_{\vartheta_1=0}^{N-1}\Big\{1-\exp\big(-\theta_a T\big)\Big\}\Big\{\exp\big(-\theta_A T\big)\Big\}^{\vartheta_1}\left\{\sum_{m=1}^{N}|y_m|^2-\sum_{m=1}^{\vartheta_1}|y_m|^2\right\}\underset{H_o}{\overset{H_1}{\gtrless}}\Psi' \\ &= \sum_{m=1}^{N}\Big\{1-\exp\big(-\theta_A Tm\big)\Big\}|y_m|^2\underset{H_o}{\overset{H_1}{\gtrless}}\Psi', \end{aligned} \tag{5.33}$$

where Ψ' is the detection threshold obtained using the NP test. For large values of N, using CLT, $\Upsilon(\mathbf{y})$ tends to be Gaussian with mean μ_{a_o} and variance $\sigma^2_{a_o}$. Thus, Ψ' can be expressed as

$$\Psi' = Q^{-1}(P_F)\sigma_{a_o} + \mu_{a_o}, \tag{5.34}$$

where μ_{a_o} denotes the mean and $\sigma^2_{a_o}$ denotes the variance of the decision statistic $\Upsilon(\mathbf{y})$ obtained in (5.33) under hypothesis H_o. The expression of μ_{a_o} can be derived as

$$\mu_{a_o} = \mu_s\left\{N-\left\{\frac{\exp\big(-\theta_A T\big)\Big\{1-\exp\big(-\theta_A TN\big)\Big\}}{1-\exp\big(-\theta_A T\big)}\right\}\right\}. \tag{5.35}$$

Similarly, the expression of $\sigma^2_{a_o}$ can be derived as

$$\sigma^2_{a_o} = \sigma^2_s\left\{N-\left\{\frac{\exp\big(-2(\theta_A T+1)\big)\Big\{1-\exp\big(1-N\big)\Big\}}{1-\exp\big(-1\big)}+\exp\big(-2\theta_A T\big)\right\}\right\}. \tag{5.36}$$

Using the value of Ψ' in (5.34), P_F can be derived and P_D can be obtained using simulations.

(3) Random Transition in Dynamic PU (Departure case):

The case of $\vartheta_1 = 0$ signifies the presence of the PU during the whole sensing period. However, it also marks the beginning of the last phase of the PU active transmission. Here, if it is assumed that ϑ_o follows exponential distribution, then using (5.25) and 5.28, detection scheme under this scenario can be expressed as

$$\begin{aligned}\Upsilon(\mathbf{y}) &= \sum_{\vartheta_o=0}^{N-1}\Big\{1-\exp\big(-\theta_D T\big)\Big\}\Big\{\exp\big(-\theta_D T\big)\Big\}^{\vartheta_o}\left\{\sum_{m=1}^{N}|y_m|^2-\sum_{m=1}^{\vartheta_o}|y_m|^2\right\}\underset{H_o}{\overset{H_1}{\gtrless}}\Psi' \\ &= \sum_{m=1}^{N}\Big\{1-\exp\big(-\theta_D Tm\big)\Big\}|y_m|^2\underset{H_o}{\overset{H_1}{\gtrless}}\Psi', \end{aligned} \tag{5.37}$$

where Ψ' is the detection threshold obtained using the NP test. For large values of N, using CLT, the PDF of $\Upsilon(\mathbf{y})$ can be approximated as Gaussian with mean μ_{d_o} and variance $\sigma^2_{d_o}$. Thus, Ψ' can be expressed as

$$\Psi' = Q^{-1}(P_F)\sigma_{d_o} + \mu_{d_o}, \tag{5.38}$$

where μ_{d_o} denotes the mean and $\sigma^2_{d_o}$ denotes the variance of the decision statistic $\Upsilon(\mathbf{y})$ obtained in (5.37) under hypothesis H_o. The expression of μ_{d_o} can be derived and expressed as

$$\mu_{d_o} = \mu_s\left\{N - \left\{\frac{\exp\left(-\theta_D T\right)\left\{1-\exp\left(-\theta_D TN\right)\right\}}{1-\exp\left(-\theta_D T\right)}\right\}\right\}. \tag{5.39}$$

Similarly, the expression of $\sigma^2_{d_o}$ can be expressed as

$$\sigma^2_{d_o} = \sigma^2_s\left\{N - \left\{\frac{\exp\left(-2(\theta_D T+1)\right)\left\{1-\exp\left(1-N\right)\right\}}{1-\exp\left(-1\right)} + \exp\left(-2\theta_D T\right)\right\}\right\}. \tag{5.40}$$

Using the value of Ψ' in (5.38), P_F can be derived and P_D can be obtained using simulations. The optimum P, also denoted as P_o can be obtained in a similar way as described in Chapter 3 as

$$P_o = \arg\min_P\left(P_{error}\right) = \arg\min_P\left(P_F + P_M\right), \tag{5.41}$$

where P_{error} is the total error probability. The value of P where P_{error} shows minimum value gives optimum P. The optimum P with varying γ (constant P_F) and with varying P_F (constant γ) has been shown in Table 5.1 for i-AVCD scheme. Here, γ denotes the average SNR, which is defined as $\gamma = (1/N)\sum_{m=1}^{N}(s^2_m)/(2\kappa^2)$.

5.4 Simulation Results

In this section, the performance of the i-AVCD scheme and its two special cases AVCD and ED in dynamic PU environment with additive Laplacian noise is presented in terms of the ROC and P_D versus average SNR using Monte Carlo simulations. For simulations, the ϑ_o and ϑ_1 are assumed to be 10 and 15, respectively. For static PU environment, $\vartheta_o = 0$ and $\vartheta_1 = 0$, whereas for dynamic PU environment both are less than N.

Table 5.1 shows optimum P, i.e., P_o for $\gamma = -2, -5$ and -10 dB at $P_F = 0.1$ using i-AVCD scheme. For static PU, the values of P_o at $\gamma = -2, -5$ and -10 dB are 0.126, 0.105 and 0.102, respectively. For dynamic PU with $\theta_A T/\,\theta_D T = 1$, the values of P_o respectively decrease to 0.118, 0.101 and 0.10 at $\gamma = -2, -5$ and -10 dB. Similarly, at a fixed SNR of -5 dB, optimum P has been shown for $P_F = 0.01$, 0.05 and 0.1. For static PU, the values of P_o at $P_F = 0.01$, 0.05 and 0.1 are 0.251, 0.151 and 0.105, respectively. For dynamic PU with $\theta_A T/\,\theta_D T = 1$, the values of P_o respectively decrease

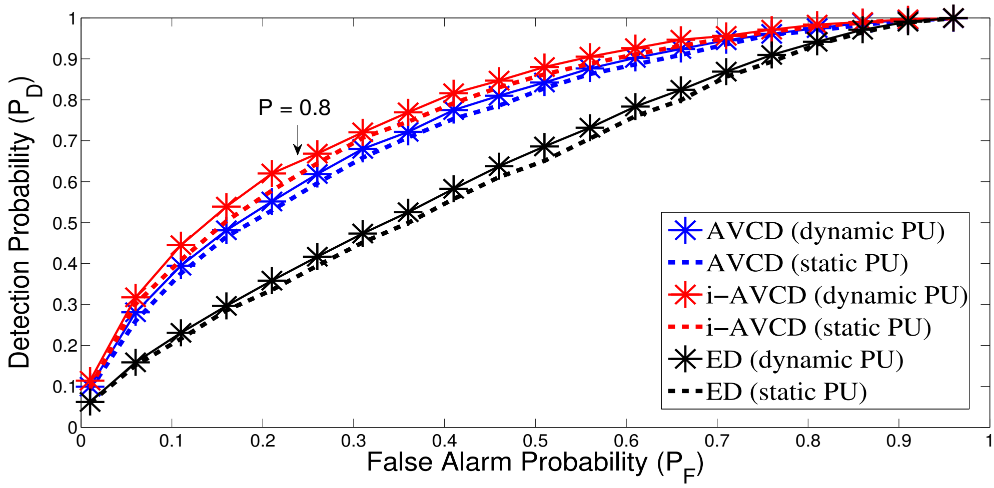

Figure 5.1: ROC for i-AVCD, AVCD and ED schemes with static and dynamic PU at $N = 50$, $\gamma = -5$ dB, $\theta_A T = 1$ and $\theta_D T = 1$.

Table 5.1: The optimum P for i-AVCD scheme with varying γ and P_F at $N = 50$ for static and dynamic PU.

$P_F = 0.1$			
γ (in dB)	$\gamma = -2$	$\gamma = -5$	$\gamma = -10$
Static PU	0.126	0.105	0.102
Dynamic PU ($\theta_A T/\ \theta_D T = 1$)	0.118	0.101	0.10
$\gamma = -5$ dB			
P_F	$P_F = 0.01$	$P_F = 0.05$	$P_F = 0.1$
Static PU	0.251	0.151	0.105
Dynamic PU ($\theta_A T/\ \theta_D T = 1$)	0.201	0.149	0.101

to 0.201, 0.149 and 0.101 at $P_F = 0.01$, 0.05 and 0.1. It is observed that optimum P for i-AVCD remains around 0.1 for all the assumed values of γ and P_F. Thus, optimum P for i-AVCD can be assumed as 0.1 for all the assumed values of average SNR and P_F.

Figure 5.1 shows the ROC for i-AVCD, AVCD and ED schemes. The P for i-AVCD is arbitrarily assumed as 0.8. For AVCD and ED, the values of P are 1 and 2, respectively. The γ is assumed as -5 dB, while $\theta_A T$ and $\theta_D T$ are assumed to be 1. Further, N is assumed as 50. At $P_F = 0.1$, the values of P_D for i-AVCD, AVCD and ED schemes in dynamic PU scenario are 0.4219, 0.389 and 0.2176, respectively. In the case of static PU, the values of P_D for i-AVCD, AVCD and ED are 0.3941, 0.354 and 0.2039, respectively. It is clear that the performance of the detection schemes in the dynamic PU scenario is better than the performance of the schemes in static PU scenario. Further, it is also clear that with an increase in P, detection performance decreases and vice-versa. The detection performance of i-AVCD can be improved further, by choosing optimum P corresponding to the values of P_F and γ. The values of P_D for i-AVCD scheme in both static and dynamic scenarios are given in Table 5.2. In the table, the values of detection probabilities are presented at optimum P of 0.1 and arbitrarily chosen P of 0.8 for different values of $\theta_A T/\ \theta_D T$.

Figure 5.2 presents P_D versus average SNR for all the three detection schemes, i.e., i-AVCD, AVCD

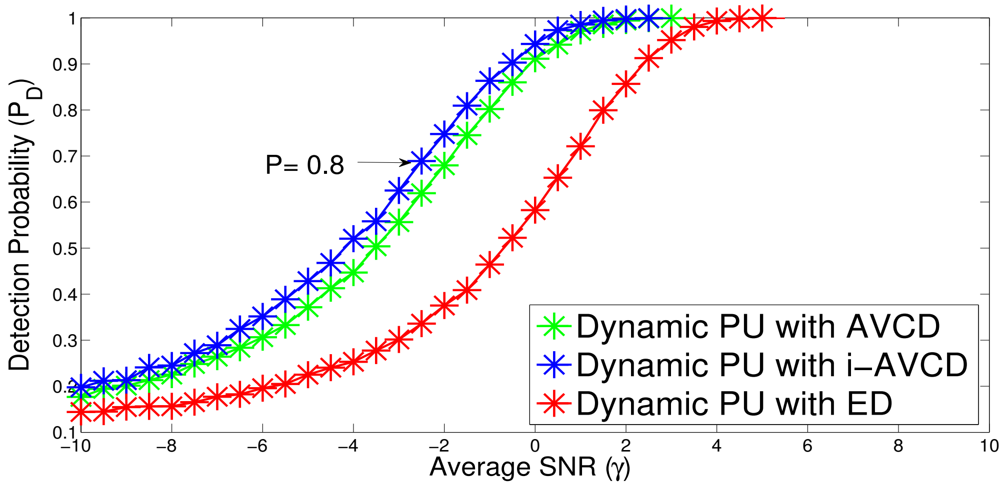

Figure 5.2: P_D vs. γ for randomly arriving and/or departing PU with i-AVCD, AVCD, ED schemes at $N = 50$, $P_F = 0.1$, $\theta_A T = 1$ and $\theta_D T = 1$.

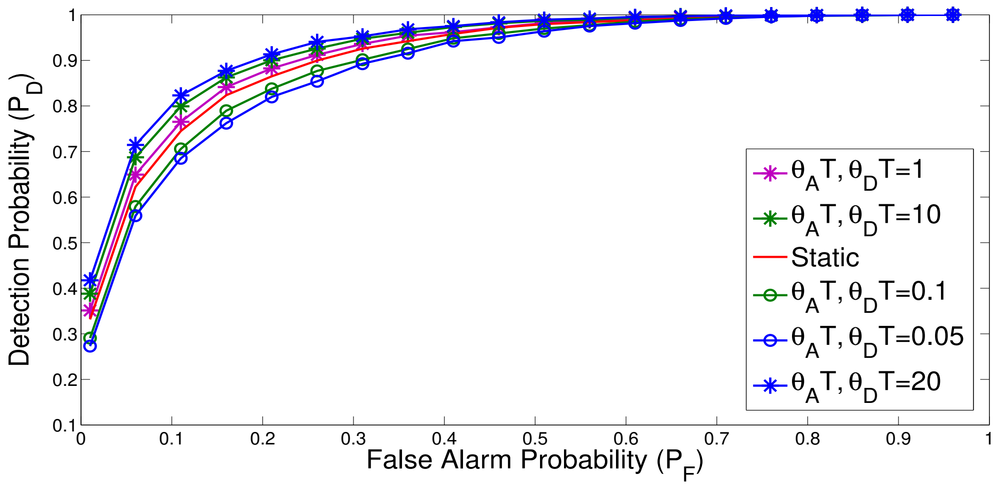

Figure 5.3: ROC for the i-AVCD scheme with random arrival and/or departure of the PU at $N = 50$, $P = 0.8$ and $\gamma = -2$ dB.

and ED in dynamic PU scenario. It is assumed that $P_F = 0.1$, $\theta_A T = 1$, $\theta_D T = 1$ and $N = 50$. For i-AVCD, P is assumed as 0.8. Here also, i-AVCD outperforms the other two schemes over $-10 \leq \gamma \leq 10$ dB.

In Figure 5.3, detection performance of i-AVCD scheme is presented for different values of $\theta_A T$ and $\theta_D T$. The range of $\theta_A T$ and $\theta_D T$ varies from 0.05 to 20 with $P = 0.8$, $\gamma = -2$ dB and $N = 50$. For static PU, the P_D at $P_F = 0.1$ is 0.7207. For dynamic PU, the values of P_D for $\theta_A T$ and $\theta_D T$= 0.05 and 0.1 are 0.6619 and 0.6779, respectively. Similarly for $\theta_A T$ and $\theta_D T$= 1, 10 and 20, the values of P_D are increased to 0.7441, 0.78 and 0.8015, respectively. It can be observed that the performance of i-AVCD with $\theta_A T$ and $\theta_D T$= 1, 10 and 20 is better than the performance of the scheme in the static PU scenario. However, the performance of the scheme with $\theta_A T$ and $\theta_D T = 0.05$ and 0.1 is worse than the performance of the scheme in static PU scenario. The values of P_D for different values

Table 5.2: The P_D for i-AVCD, AVCD and ED in static and dynamic PU scenarios with different values of $\theta_A T/\ \theta_D T$ at $\gamma = -2$ dB, $N = 50$, $P = 0.8$, $P_o = 0.1$ and $P_F = 0.1$.

Dynamic PU				
$\theta_A T/\ \theta_D T$	**i-AVCD** $P = 0.8$	**i-AVCD** $P_o = 0.1$	**AVCD**	**ED**
	Detection Probability (P_D)			
0.05	0.6619	0.78	0.582	0.327
0.1	0.6779	0.8	0.6173	0.3466
1	0.7441	0.85	0.6761	0.382
10	0.78	0.898	0.7292	0.40095
20	0.8015	0.997	0.7305	0.52
Static PU				
	0.7207	0.88	0.6523	0.372

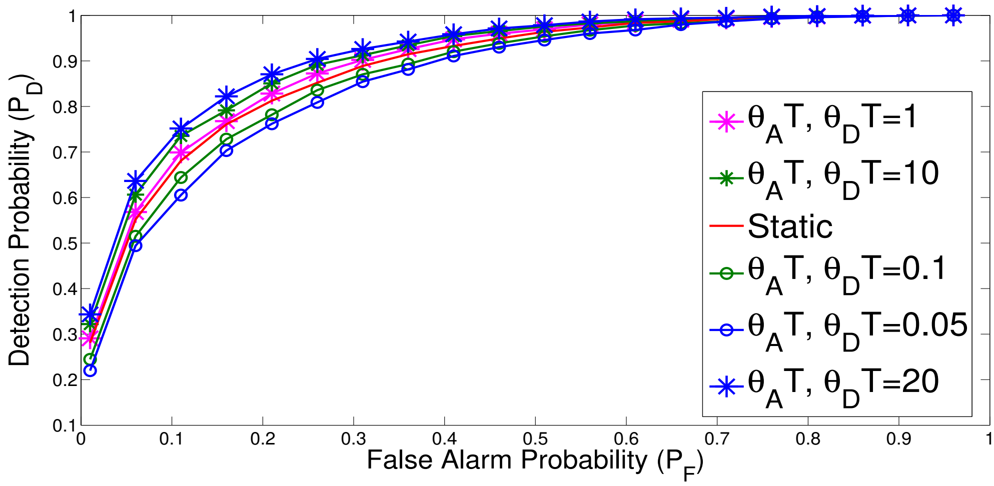

Figure 5.4: ROC for AVCD scheme with random arrival and/or departure of the PU at $N = 50$ and $\gamma = -2$ dB.

of $\theta_A T$ and $\theta_D T$ are given in Table 5.2. It can be observed that the performance of i-AVCD in the dynamic PU scenario is better than its performance in the static PU scenario beyond $\theta_A T$ and/or $\theta_D T = 1$.

Figure 5.4 shows the ROC for AVCD scheme with different values of $\theta_A T$ and $\theta_D T$ at $\gamma = -2$ dB and $N = 50$. With reference to Table 5.2, for $\theta_A T$ and/or $\theta_D T = 0.05$ and 0.1, the values of P_D are 0.582 and 0.6173, respectively. The values of P_D further increase to 0.6761, 0.7292 and 0.7305 for $\theta_A T$ and $\theta_D T$= 1, 10 and 20, respectively. The performance of the scheme with the static scenario is also presented. It can be seen that the performance improves as $\theta_A T$ and $\theta_D T$ are increased from 0.05 to 20. However, the performance of the scheme for $\theta_A T$ and $\theta_D T$ below 1 is worse than the performance with static PU scenario.

Similar to the the above figures, Figure 5.5 shows the ROC for ED scheme in both dynamic and static PU scenarios with different values of $\theta_A T$ and $\theta_D T$. Further, it is assumed that $\gamma = -2$ dB and $N = 50$. With reference to Table 5.2, for $\theta_A T$ and $\theta_D T$= 0.05, 0.1 and 1, the values of P_D are 0.327,

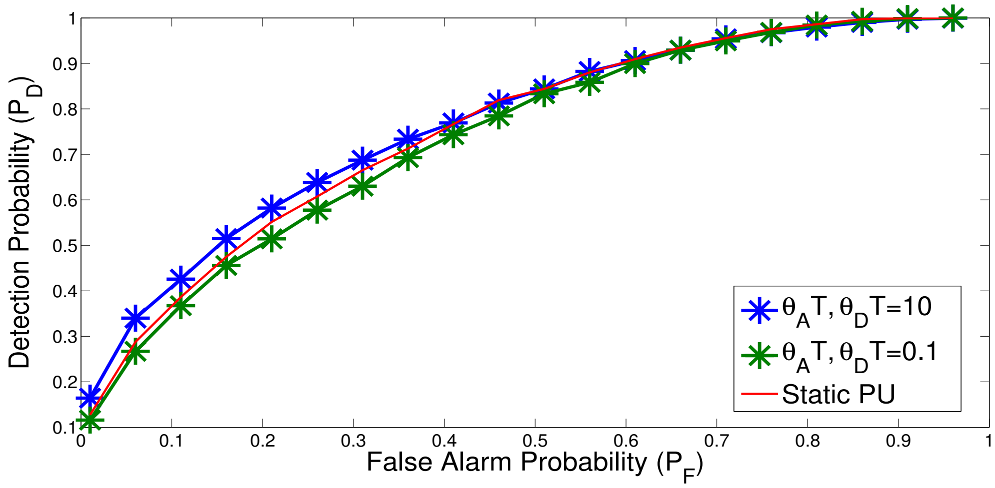

Figure 5.5: ROC for ED scheme with random arrival and/or departure of the PU at $N = 50$ and $\gamma = -2$ dB.

0.3466 and 0.382, respectively. Similarly for $\theta_A T$ and $\theta_D T=$ 10 and 20, the respective values of P_D are 0.40095 and 0.52. Again, a similar trend is observed. Further, it is observed that the i-AVCD and AVCD outperform the ED scheme.

5.5 Conclusion

In this chapter, spectrum sensing schemes such as ED, AVCD and i-AVCD were presented. Dynamic parameters such as $\theta_A T$ and/or $\theta_D T$ were used with these schemes in additive Laplacian noise environment. Further, the dynamic behavior of the PU was explored by assuming its random arrival and/or departure (in terms of $\theta_A T$ and/or $\theta_D T$) in the sensing interval. We presented the performance using simulations in term of the ROC. Besides this, we also obtained the optimum P for i-AVCD in the scenarios of static PU and dynamic PU. It is concluded that the performance of the schemes with the dynamic scenario, for $\theta_A T$ and/or $\theta_D T$ beyond 1 is better than their performance with the static scenario. Further, it is also concluded that the optimum P for i-AVCD at different values of P_F and γ did not show significant deviation in their values. Hence, optimum P can be assumed to be 0.1, irrespective of the variations in the P_F and γ. In the next chapter, we will present the performance of the CSS scheme in a dynamic PU scenario where i-AVCD is used as a localized detection scheme.

Chapter 6

Cooperative Spectrum Sensing for Dynamic PU in ALN

In this chapter, cooperative spectrum sensing (CSS) for dynamic PU is presented in the Laplacian noise environment. The dynamic PU is characterized by its transitions from the ON (present) state to the OFF (absent) state and vice-versa. It means that the PU appears or disappears intermittently during the entire sensing duration. A collaborative scenario of M_o CRs has been assumed, where each CR uses the conventional detection scheme such as i-AVCD and its special cases such as AVCD and ED. These schemes are used with dynamic parameters such as the arrival rate and departure rate of the PU to produce local hard decisions. Conventional scheme refers to the detection scheme in a non-cooperative scenario. All single-bit hard decisions received from M_o CRs fuse at the FC according to fusion schemes such as CSS: OR, CSS: AND, and CSS: majority to make a final decision on the appearance or disappearance of the PU. Further, the dynamic nature of PU in terms of its arrival rate (θ_A) and departure rate (θ_D) has been analyzed. We present the performance of the CSS for dynamic PU using ROC and P_D versus average SNR using Monte Carlo simulations. Finally, a brief conclusion is presented at the end of the chapter.

6.1 Introduction

The CSS scheme, presented in Chapter 3, possesses sensing diversity gain by employing a collaborative scenario of multiple CRs. Local decisions from each surrounding CRs are fused at the FC using standard fusion schemes. Finally, the FC makes a final decision on the presence or absence of the PU.

The CSS based on Dynamic Double Threshold Energy Detection (DDTHED) has been proposed in circularly symmetric Gaussian noise [110]. It was shown that CSS based on DDTHED outperformed CSS based on ED. It has been shown that the CSS based on the Rao detector outperformed CSS based on ED in Generalized Gaussian Noise (GGN) [128]. The CSS: majority rule (k_o out of M_o

rule, where $k_o \leq M_o$) has been addressed in the Laplacian noise environment [131]. The performance of CSS scheme, based on Modified Correlation Detector (MCD) as a localized detection scheme in additive Laplacian noise, has been evaluated in Chapter 3. However, the PU possesses static behavior and the localized detection scheme was coherent in nature. Further, the CSS schemes presented in [110, 128, 131] assumed static PU scenario.

In this chapter, the CSS scheme is presented for dynamic PU in additive Laplacian noise environment. It is assumed that there exists M_o number of CRs and out of which k_o CRs are active. These M_o CRs independently sense the presence of the PU using non-coherent localized detection scheme such as the i-AVCD with its special cases such as AVCD and ED. The FC uses standard fusion schemes to make a final judgment on the availability of the PU. The detection probability and false alarm probability at each CR are denoted as Q_d and Q_f, respectively. The detection probability and false alarm probability at the FC are denoted as P_D and P_F, respectively. Further, it is assumed that the random transition of the PU is modeled using Poisson distribution [143].

The rest of the chapter is organized as follows. Section 6.2 presents the system model. Section 6.3 presents performance analysis of the CSS scheme for dynamic PU. Section 6.4 presents simulation results. Finally, a brief conclusion is presented in Section 6.5.

6.2 System Model

In the assumed dynamic scenario, H_o denotes the hypothesis when PU is present up to a specified sample ϑ_o and thereafter PU is absent. In a similar way, H_1 denotes the alternate hypothesis when PU is absent up to a specified sample ϑ_1 and thereafter PU is present. Thus, the received signal at each of the M_o cognitive terminals can be expressed as

$$\begin{aligned} H_o : y_m &= \begin{cases} s_m + n_m & , m = 1, \ldots, \vartheta_o \\ n_m & , m = \vartheta_o + 1, \vartheta_o + 2, \vartheta_o + 3 \ldots, N; \end{cases} \\ H_1 : y_m &= \begin{cases} n_m & , m = 1, \ldots, \vartheta_1 \\ s_m + n_m & , m = \vartheta_1 + 1, \vartheta_1 + 2, \vartheta_1 + 3 \ldots, N, \end{cases} \end{aligned} \tag{6.1}$$

where m denotes the sensing sample with $1 \leq m \leq N$. The N indicates the total number of samples present during the sensing period. The s_m is the unknown PU signal, while the n_m indicates Laplacian noise with mean 0 and variance $2\kappa^2$, where κ is the scale parameter of the Laplacian noise. The ϑ_o and ϑ_1 indicate the first level transition points of the PU under hypotheses H_o and H_1 respectively. Transition of the PU occurs between the samples ϑ_o and $\vartheta_o + 1$ under H_o (when PU randomly departs) and between the samples ϑ_1 and $\vartheta_1 + 1$ under H_1 (when PU randomly arrives).

A collaborative scenario of CRs is considered, where each of the M_o cognitive terminals uses i-AVCD, AVCD and ED as localized detection schemes to decide the presence or absence of PU. The local hard decisions are individually communicated to the FC via reporting channel. After collecting hard decisions in the form of '0' and '1', the FC uses standard fusion schemes such as the CSS: OR, CSS: AND and CSS: majority, respectively.

6.3 Performance Analysis

In this section, two subsections have been presented. In the first subsection, three different cases of PU using the CSS-i-AVCD scheme are presented. Besides this, the case of AVCD is also discussed as a special case of i-AVCD. The first case presents the case of static PU as a special case of dynamic PU, while the second and third cases present the scenarios of random arrival and random departure of the dynamic PU, respectively. In the second subsection, all the three cases of PU in CSS-ED are presented. Further, P_D and P_F in each of the cases for CSS-ED and CSS-i-AVCD schemes have been derived.

6.3.1 CSS based on i-AVCD

In the scenario of Laplacian noise, i-AVCD and AVCD are the two actively used detection schemes. In i-AVCD, received samples at the cognitive terminal are raised to a positive exponent P in the range $0 < P \leq 2$. Being a special case of i-AVCD at $P = 1$, corresponding parameters for the AVCD scheme can be obtained by substituting the value of $P = 1$ in the expressions obtained for i-AVCD. Simplifying (5.4), the detection scheme can be represented as

$$\Upsilon(\mathbf{y}) = \sum_{m=\vartheta_o+1}^{N} |y_m|^P - \sum_{m=1}^{\vartheta_1} |y_m|^P \underset{H_o}{\overset{H_1}{\gtrless}} \Psi', \tag{6.2}$$

where Ψ' is the detection threshold which is equal to $\kappa \cdot ln(\Psi)$. It is obtained using the NP test. The values of ϑ_o and ϑ_1 are averaged out over their distributions, as they are unknown and random. All the single bit hard decisions from each M_o CRs are combined at the centralized FC according to a decision rule expressed as

$$U = \sum_{l=1}^{M_o} U_l \underset{H_o}{\overset{H_1}{\gtrless}} k_o, \tag{6.3}$$

where U_l is the hard decision from each CR. Finally, at the FC, P_F and P_D can be expressed as [109]

$$\begin{aligned} P_F &= \sum_{l=k_o}^{M_o} \binom{M_o}{l} Q_f^l (1 - Q_f)^{M_o - l}, \\ P_D &= \sum_{l=k_o}^{M_o} \binom{M_o}{l} Q_d^l (1 - Q_d)^{M_o - l}. \end{aligned} \tag{6.4}$$

Here, $k_o = 1$ represents CSS: OR rule, while $k_o = M_o$ indicates CSS: AND rule and $k_o < M_o$ signifies CSS: majority rule. The localized detection probability Q_d at each M_o CR can be expressed as

$$Q_d = Prob\Big\{\Upsilon(\mathbf{y}) > \Psi'|H_1\Big\}, \tag{6.5}$$

and the localized false alarm probability Q_f at each M_o CR can be expressed as

$$Q_f = Prob\Big\{\Upsilon(\mathbf{y}) > \Psi'|H_o\Big\}. \tag{6.6}$$

The three cases of the PU are presented in the following sections.

(1) Static PU:

Static PU signifies a case of low traffic scenario when $\vartheta_o = 0$ and $\vartheta_1 = 0$. The i-AVCD scheme is used at each M_o CR which can be expressed as

$$\Upsilon(\mathbf{y}) = \sum_{m=1}^{N} |y_m|^P \underset{H_o}{\overset{H_1}{\gtrless}} \Psi', \tag{6.7}$$

where Ψ' is the detection threshold obtained using the NP test. For large values of N, CLT is invoked to approximate the PDF of decision statistics $\Upsilon(\mathbf{y})$ as Gaussian with mean μ_s and variance σ_s^2 as

$$\Upsilon(\mathbf{y}) \sim N(\mu_s, \sigma_s^2), \tag{6.8}$$

where μ_s and σ_s^2 can be obtained from (5.12). Using (6.8), Ψ' can be expressed as

$$\Psi' = Q^{-1}(Q_f)\sigma_s + \mu_s, \tag{6.9}$$

where $Q(.)$ denotes the Q-function expressed as $Q(l) = \frac{1}{\sqrt{2\pi}} \int_l^{+\infty} \exp\left(-\frac{t^2}{2}\right) dt$.

Further, Q_f can be derived from (6.9). This value is substituted in (6.4) to get P_F at the FC. Finally, P_D can be obtained using simulations.

(2) Random Transition in Dynamic PU (Arrival case):

The case of $\vartheta_o = 0$ signifies the absence of the PU during the complete duration of the sensing period. However, it also marks the beginning of transmission of the PU. Here, if it is assumed that ϑ_1 follows an exponential distribution, then using (5.5) and (5.9), the detection scheme in this scenario can be expressed as

$$\Upsilon(\mathbf{y}) = \sum_{\vartheta_1=0}^{N-1}\Big\{1-\exp\big(-\theta_A T\big)\Big\}\Big\{\exp\big(-\theta_A T\big)\Big\}^{\vartheta_1}\left\{\sum_{m=1}^{N}|y_m|^P - \sum_{m=1}^{\vartheta_1}|y_m|^P\right\} \underset{H_o}{\overset{H_1}{\gtrless}} \Psi'$$
$$= \sum_{m=1}^{N}\Big\{1-\exp\big(-\theta_A Tm\big)\Big\}|y_m|^P \underset{H_o}{\overset{H_1}{\gtrless}} \Psi'. \tag{6.10}$$

For large values of N, CLT can be applied so that $\Upsilon(\mathbf{y})$ tends to be Gaussian with mean μ_{a_o} and variance $\sigma^2_{a_o}$. Thus, Ψ' is expressed as

$$\Psi' = Q^{-1}(Q_f)\sigma_{a_o} + \mu_{a_o}, \tag{6.11}$$

where μ_{a_o} denotes the mean and $\sigma^2_{a_o}$ denotes the variance of the decision statistic $\Upsilon(\mathbf{y})$. They have been derived in (5.16) and (5.17), respectively. The Q_f can be derived from (6.11). This value is substituted in (6.4) to get P_F at the FC. Finally, P_D can be obtained using simulations.

(3) Random Transition in Dynamic PU (Departure case):

The case of $\vartheta_1 = 0$ signifies the presence of the PU during the whole sensing period. However, it also marks the beginning of the last phase of the active transmission of the PU. Here, if it is assumed that ϑ_o follows exponential distribution, then using (5.5) and (5.9), detection scheme in this scenario can be expressed as

$$\Upsilon(\mathbf{y}) = \sum_{\vartheta_o=0}^{N-1}\Big\{1-\exp\big(-\theta_D T\big)\Big\}\Big\{\exp\big(-\theta_D T\big)\Big\}^{\vartheta_o}\left\{\sum_{m=1}^{N}|y_m|^P - \sum_{m=1}^{\vartheta_o}|y_m|^P\right\} \underset{H_o}{\overset{H_1}{\gtrless}} \Psi'$$
$$= \sum_{m=1}^{N}\Big\{1-\exp\big(-\theta_D Tm\big)\Big\}|y_m|^P \underset{H_o}{\overset{H_1}{\gtrless}} \Psi', \tag{6.12}$$

where Ψ' is the detection threshold when PU randomly departs. For large values of N, CLT can be applied so that $\Upsilon(\mathbf{y})$ tends to be Gaussian with mean μ_{d_o} and variance $\sigma^2_{d_o}$. Thus, Ψ' is expressed as

$$\Psi' = Q^{-1}(Q_f)\sigma_{d_o} + \mu_{d_o}, \tag{6.13}$$

where μ_{d_o} denotes the mean and $\sigma^2_{d_o}$ denotes the variance of the decision statistic $\Upsilon(\mathbf{y})$. They have been derived in (5.20) and (5.21), respectively. The Q_f can be derived from (6.13). This value is substituted in (6.4) to get P_F at the FC. Finally, P_D can be obtained using simulations.

6.3.2 CSS based on ED

The ED is one of the classical detection schemes used for spectrum sensing. It is a special case of i-AVCD at $P = 2$. Simplifying (5.24), detection scheme can be represented as

$$\Upsilon(\mathbf{y}) = \sum_{m=\vartheta_o+1}^{N} |y_m|^2 - \sum_{m=1}^{\vartheta_1} |y_m|^2 \underset{H_o}{\overset{H_1}{\gtrless}} \Psi', \tag{6.14}$$

where Ψ' is the detection threshold which is equal to $\kappa \cdot ln(\Psi)$. It is obtained using NP test. The Q_d at each M_o CR can be expressed as

$$Q_d = Prob\Big\{\Upsilon(\mathbf{y}) > \Psi'|H_1\Big\}, \tag{6.15}$$

and Q_f at each M_o CR can be expressed as

$$Q_f = Prob\Big\{\Upsilon(\mathbf{y}) > \Psi'|H_o\Big\}. \tag{6.16}$$

The hard decision from each CR using (6.15) and (6.16), is then forwarded to the FC. The P_D and P_F at the FC are derived from (6.4). The three cases of the PU are presented in the following sections.

(1) Static PU:

Static PU signifies a case of low traffic scenario when $\vartheta_o = 0$ and $\vartheta_1 = 0$. The ED scheme is used at each M_o CR which can be expressed as

$$\Upsilon(\mathbf{y}) = \sum_{m=1}^{N} |y_m|^2 \underset{H_o}{\overset{H_1}{\gtrless}} \Psi', \tag{6.17}$$

where Ψ' is the detection threshold obtained using the NP test. For large values of N, CLT is used to approximate the PDF of $\Upsilon(\mathbf{y})$ as

$$\Upsilon(\mathbf{y}) \sim N(\mu_s, \sigma_s^2), \tag{6.18}$$

where μ_s and σ_s^2 can be obtained from (5.31). Using (6.18), Ψ' is expressed as

$$\Psi' = Q^{-1}(Q_f)\sigma_s + \mu_s, \tag{6.19}$$

where $Q(.)$ represents the Q-function. The Q_f can be derived from (6.19). This value is substituted in (6.4) to get P_F at the FC. Finally, P_D can be obtained using simulations.

(2) Random Transition in Dynamic PU (Arrival case):

The case of $\vartheta_o = 0$ signifies the absence of the PU during the complete duration of the sensing period. However, it also marks the beginning of transmission of the PU. Here, if it is assumed that ϑ_1 follows exponential distribution, then using (5.25) and 5.28, detection scheme in this scenario can be expressed as

$$\begin{aligned} \Upsilon(\mathbf{y}) &= \sum_{\vartheta_1=0}^{N-1}\Big\{1-\exp\big(-\theta_a T\big)\Big\}\Big\{\exp\big(-\theta_A T\big)\Big\}^{\vartheta_1}\left\{\sum_{m=1}^{N}|y_m|^2-\sum_{m=1}^{\vartheta_1}|y_m|^2\right\}\underset{H_o}{\overset{H_1}{\gtrless}}\Psi' \\ &= \sum_{m=1}^{N}\Big\{1-\exp\big(-\theta_A Tm\big)\Big\}|y_m|^2\underset{H_o}{\overset{H_1}{\gtrless}}\Psi', \end{aligned} \tag{6.20}$$

where Ψ' is the detection threshold during the random arrival of the PU. For large values of N, CLT can be applied so that $\Upsilon(\mathbf{y})$ tends to be Gaussian with mean μ_{a_o} and variance $\sigma^2_{a_o}$. Thus, Ψ' is expressed as

$$\Psi' = Q^{-1}(Q_f)\sigma_{a_o} + \mu_{a_o}, \tag{6.21}$$

where μ_{a_o} denotes the mean and $\sigma^2_{a_o}$ denotes the variance of the decision statistic $\Upsilon(\mathbf{y})$ obtained in (6.20) under hypothesis H_o. The expressions of μ_{a_o} and $\sigma^2_{a_o}$ can be obtained from (5.35) and (5.36), respectively. Finally, Q_f can be derived from (6.21). This value is substituted in (6.4) to get P_F at the FC. Finally, P_D can be obtained using simulations.

(3) Random Transition in Dynamic PU (Departure case):

If it is assumed that ϑ_o follows an exponential distribution, then using (5.25) and 5.28, detection scheme in this scenario can be expressed as

$$\begin{aligned} \Upsilon(\mathbf{y}) &= \sum_{\vartheta_o=0}^{N-1}\Big\{1-\exp\big(-\theta_D T\big)\Big\}\Big\{\exp\big(-\theta_D T\big)\Big\}^{\vartheta_o}\left\{\sum_{m=1}^{N}|y_m|^2-\sum_{m=1}^{\vartheta_o}|y_m|^2\right\}\underset{H_o}{\overset{H_1}{\gtrless}}\Psi' \\ &= \sum_{m=1}^{N}\Big\{1-\exp\big(-\theta_D Tm\big)\Big\}|y_m|^2\underset{H_o}{\overset{H_1}{\gtrless}}\Psi', \end{aligned} \tag{6.22}$$

where Ψ' is the detection threshold when PU randomly departs. Applying CLT for large values of N, $\Upsilon(\mathbf{y})$ tends to be Gaussian with mean μ_{d_o} and variance $\sigma^2_{d_o}$. Thus, Ψ' can be expressed as

$$\Psi' = Q^{-1}(Q_f)\sigma_{d_o} + \mu_{d_o}, \tag{6.23}$$

where μ_{d_o} denotes the mean and $\sigma^2_{d_o}$ denotes the variance of the decision statistic $\Upsilon(\mathbf{y})$ obtained in (6.22) under hypothesis H_o. The expressions of μ_{d_o} and $\sigma^2_{d_o}$ can be obtained from (5.39) and (5.40), respectively. The Q_f can be derived from (6.23). This value is substituted in (6.4) to get P_F at the

FC. Finally, P_D can be obtained using simulations.

6.4 Simulation Results

In this section, the performance of the CSS scheme in dynamic PU environment with additive Laplacian noise is presented in terms of ROC and P_D versus average SNR using Monte Carlo simulations. The average SNR is defined as $\gamma = (1/N) \sum_{m=1}^{N} (s_m^2)/(2\kappa^2)$. The ϑ_o and ϑ_1 are assumed to be 10 and 15, respectively. For static PU environment, $\vartheta_o = 0$ and $\vartheta_1 = 0$. Similarly, for random transitions of the PU, i.e., in the dynamic environment, both are less than N. The P and κ are assumed to be 0.8 and 1, respectively, throughout the simulations. Further, the value of N is also assumed as 50.

Table 6.1: The P_D for dynamic PU with conventional detection schemes and CSS fusion schemes at $\gamma = -5$ dB, $N = 50$, $P = 0.8$ and $P_F = 0.1$.

Dynamic PU ($\theta_A T/\theta_D T = 1$)				
Detection Scheme	**Conventional Scheme**	**CSS Fusion Scheme**		
		CSS: OR	CSS:majority	CSS: AND
i-AVCD	0.42196	0.852	0.450	0.1
AVCD	0.389	0.79	0.389	0.069
ED	0.2176	0.53	0.123	0.01
Static PU				
i-AVCD	0.3941	0.824	0.429	0.08
AVCD	0.354	0.682	0.245	0.04
ED	0.2039	0.496	0.119	0.008

Figure 6.1 shows the ROC for conventional i-AVCD scheme and CSS: OR fusion scheme in dynamic PU scenario. Here, conventional i-AVCD refers to the i-AVCD scheme used by CR in a non-cooperative scenario. The CSS: OR scheme uses localized detection scheme i-AVCD at each M_o cognitive terminals. The $\theta_A T$, $\theta_D T$ are assumed to be 10 and 0.1, respectively. The N is assumed to be 50 and $\gamma = -2$ dB. For static PU, the P_D at $P_F = 0.1$ is 0.7207 which is improved to 0.9771 using CSS: OR scheme. For dynamic PU, the values of P_D at $\theta_A T$, $\theta_D T = 0.1$ and 10 are 0.6779 and 0.78, respectively. These values of P_D are improved to 0.9659 and 0.9885, respectively, using CSS: OR fusion scheme. Thus, it is observed that the performance of CSS: OR based on localized i-AVCD scheme in the dynamic scenario is better than the performance in static scenario for $\theta_A T = 10$, while the same is not true for $\theta_A T = 0.1$. Further, it is observed that the performance of CSS: OR with localized i-AVCD is better than the performance with conventional i-AVCD. The performance can be further improved with an increase in the N and a decrease in the P.

Figure 6.2 shows the ROC for conventional AVCD and CSS: OR fusion scheme. Here, CSS: OR uses localized detection scheme such as AVCD at each M_o cognitive terminal. The values of $\theta_A T$, $\theta_D T$ are assumed to be 10 and 0.1. The N is assumed to be 50 and $\gamma = -2$ dB. For static PU, the P_D at $P_F = 0.1$ is 0.6523, which is improved to 0.9596 using CSS: OR scheme. For dynamic PU, the values of P_D at $\theta_A T$, $\theta_D T = 0.1$ and 10 are 0.6173 and 0.7292, respectively. These values of P_D

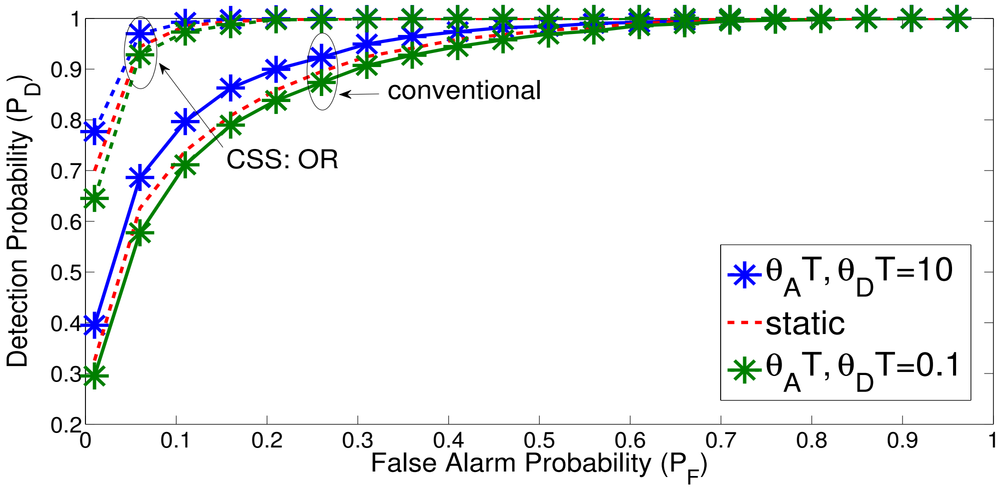

Figure 6.1: ROC for CSS: OR fusion scheme and conventional i-AVCD scheme at $N = 50$, $\gamma = -2$ dB, $\theta_A T$ and/or $\theta_D T$ =0.1 and 10.

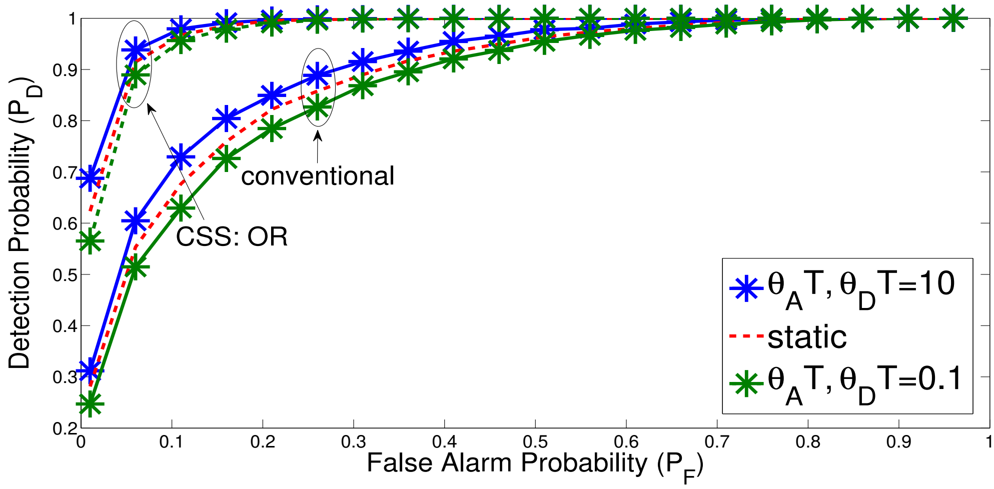

Figure 6.2: ROC for CSS: OR fusion scheme and conventional AVCD scheme at $N = 50$, $\gamma = -2$ dB, $\theta_A T$ and/or $\theta_D T$ =0.1 and 10.

are respectively improved to 0.9486 and 0.9715 using CSS: OR fusion scheme. It can be seen that the dynamic PU outperforms the static PU at $\theta_A T = 10$. Further, it is observed that the CSS: OR scheme outperforms conventional AVCD.

Similarly, Figure 6.3 shows the ROC for conventional ED and CSS: OR fusion scheme. Here, CSS: OR uses localized detection scheme such as ED at each M_o cognitive terminal. The values of $\theta_A T$, $\theta_D T$ are assumed to be 10 and 0.1. The N is assumed to be 50 and $\gamma = -2$ dB. For static PU, the P_D at $P_F = 0.1$ is 0.372, which is improved to 0.7482 using CSS scheme. For dynamic PU, the values of P_D at $\theta_A T$, $\theta_D T = 0.1$ and 10 are 0.3466 and 0.40095, respectively. These values of P_D are respectively improved to 0.7246 and 0.8008 using CSS: OR fusion scheme. It is observed that the performance of the schemes in the dynamic scenario is better than the performance in the static PU scenario. Further, it is observed that the CSS: OR outperforms the conventional ED.

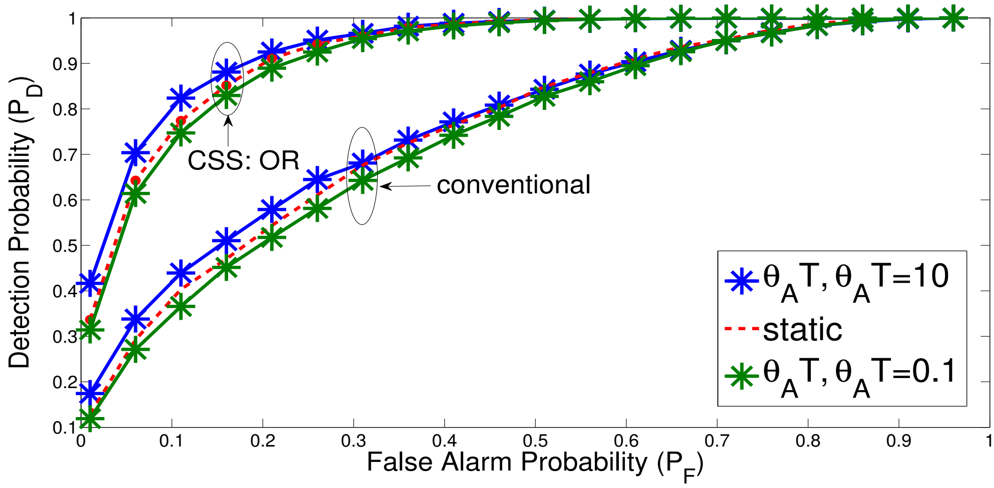

Figure 6.3: ROC for CSS: OR fusion scheme and conventional ED scheme at $N = 50$, $\gamma = -2$ dB, $\theta_A T$ and/or $\theta_D T$ =0.1 and 10.

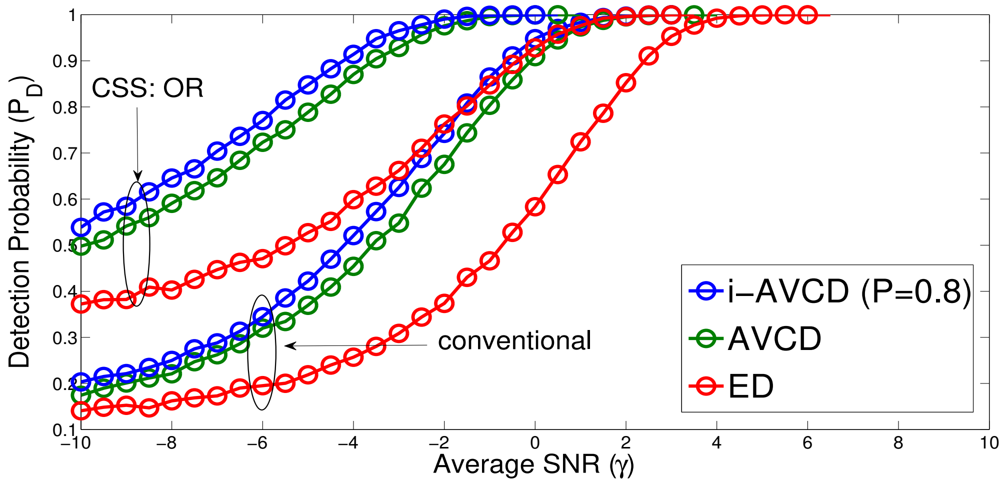

Figure 6.4: P_D vs. γ for conventional detection schemes and CSS: OR fusion scheme at $N = 50$, $P = 0.8$ and $P_F = 0.1$ when PU randomly arrives or departs.

In Figure 6.4, P_D versus average SNR is presented for conventional detection schemes such as i-AVCD, AVCD, ED and CSS: OR fusion scheme. It is assumed that $\theta_A T$, $\theta_D T = 1$ with $P = 0.8$, $N = 50$. Further, γ ranges from -10 to 10 dB with an interval of 0.5 dB. It is observed that the CSS: OR scheme outperforms the conventional schemes.

Figure 6.5 presents P_D versus average SNR for CSS: majority ($k_o = 2$ out of $M_o = 3$ CRs) scheme and conventional schemes such as i-AVCD, AVCD and ED. It is assumed that $\theta_A T$, $\theta_D T = 1$ with $P = 0.8$, $N = 50$. Further, γ ranges from -10 to 10 dB with an interval of 0.5 dB. Here, it is observed that for a specified low range of SNR, conventional scheme performs better, while for a specified high range of SNR, CSS: majority fusion scheme performs better. The CSS: majority scheme outperforms conventional schemes such as ED, AVCD and i-AVCD beyond -1,-5 and -6 dB, respectively.

In Figure 6.6, P_D versus average SNR for CSS: AND fusion scheme and conventional schemes such

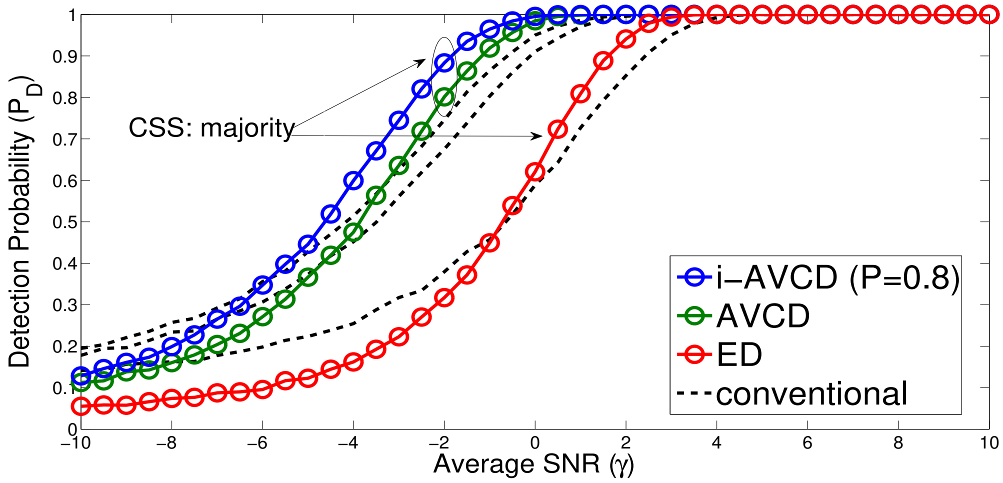

Figure 6.5: P_D vs. γ for conventional detection schemes and CSS: majority fusion scheme at $N = 50$, $P = 0.8$, $P_F = 0.1$, $k_o = 2$, $M_o = 3$ when PU randomly arrives or departs.

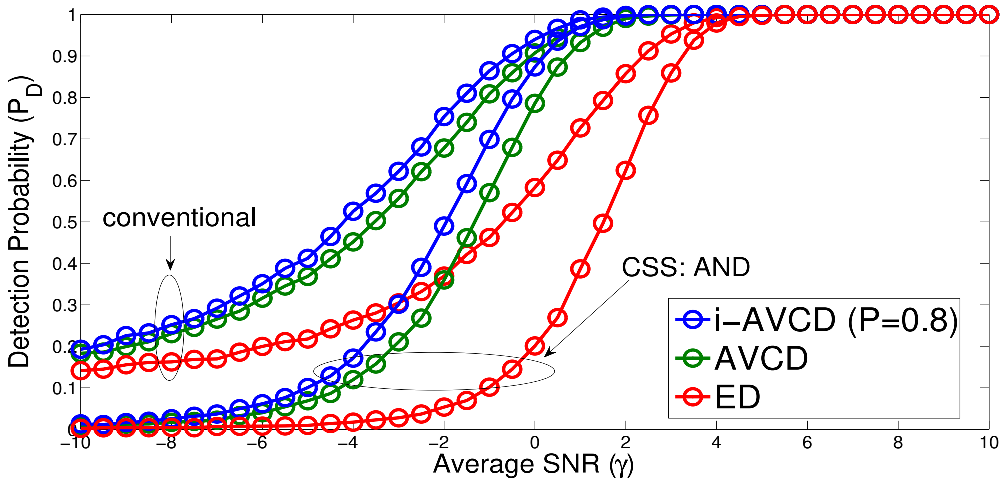

Figure 6.6: P_D vs. γ for conventional detection schemes and CSS: AND fusion scheme at $N = 50$, $P = 0.8$ and $P_F = 0.1$ when PU randomly arrives or departs.

as i-AVCD, AVCD and ED is presented. It is assumed that $\theta_A T$, $\theta_D T = 1$ with $P = 0.8$, $N = 50$ and γ ranges from -10 to 10 dB with an interval of 0.5 dB. Here, it is observed that the conventional scheme performs better than CSS: AND scheme.

For better analysis, the performance of different CSS fusion schemes is compared with conventional detection schemes for both static and dynamic PU scenario in Table 6.1. The assumed parameters are $\gamma = -5$ dB, $P = 0.8$, $P_F = 0.1$ and $\theta_A T$, $\theta_D T = 1$. It is observed that the performance of CSS: OR scheme is substantially improved as compared to the performance achieved with other fusion schemes.

6.5 Conclusion

In this chapter, the CSS scheme was presented along with conventional sensing schemes such as ED, AVCD, and i-AVCD in additive Laplacian noise environment. These schemes were used with dynamic parameters such as $\theta_A T$ and/or $\theta_D T$, assuming random transition of the PU within the sensing interval. The detection performance of the spectrum sensing schemes was presented using simulations in terms of the ROC and P_D versus average SNR. It is concluded that the CSS: OR scheme outperforms conventional spectrum sensing schemes over $-10 \leq \gamma \leq 10$ dB. It is because, in CSS: OR rule, there exists at least one CR which has a local decision based on hypothesis H_1. Hence, CSS: OR rule is much reserved to let CRs access the licensed band. Also, interference caused to the PU is minimized drastically. It is also concluded that the conventional schemes outperform CSS: AND scheme. Hence, CSS: AND scheme is unsuitable for enhancing the detection probability, unlike that in the case of Gaussian noise. Further, it is also concluded that CSS: majority scheme outperforms the conventional schemes beyond specified values of SNR which is $-1, -5, -6$ dB, respectively, for ED, AVCD and i-AVCD schemes. In the next chapter, we will present the performance of detection schemes for dynamic PU with two transition points within the sensing period.

Chapter 7

Spectrum Sensing for Dynamic PU With Two Transitions in ALN

This chapter presents a real-time scenario of dynamic PU in additive Laplacian noise. Two transitions or status changes of the PU in the fixed sensing time are assumed. The Last Status Change Point (LSCP) is estimated with Maximum Likelihood (ML) estimation. The Cumulative Sum (CuSum) based weighted samples are used in the three detection schemes, such as Sample Mean Detector (SMD), ED and i-AVCD. Closed-form expressions of P_D and P_F for all the three schemes are derived and results are presented with ROC. Besides this, simulation results are also presented which closely match with their analytical counterparts. The ROC of the considered system is compared with the conventional schemes. In the conventional schemes, all samples in the sensing time are used for detection without LSCP estimation and weight. Finally, the conclusion is presented at the end of this chapter.

7.1 Introduction

The dynamic behavior of the PU has been modeled in several ways in the literature. In [143], this randomness was modeled by the Poisson process. In the case of dynamic PU, Cumulative Sum (CuSum) based detection scheme has been explored in [30]. This CuSum has been adopted to various spectrum sensing schemes such as SMD [30], ED [100, 101] and Improved ED (iED) [102].

The dynamic behavior of the PU has been further explored at the cognitive terminal by estimating the status change points or transitions of PU in the specified sensing interval. The LSCP of the PU has been estimated, and then sensing was done in the interval from LSCP to the end of the sensing time, using CuSum based weighted samples in ED and cyclostationarity based detectors [146, 173]. It was found that the performance of these detectors was better with LSCP estimation compared to the performance without LSCP estimation. Further, the background noise was assumed as Gaussian.

In this chapter, dynamic PU with a maximum of two status changes is assumed during the sensing period. However, the additive noise is modeled by Laplacian distribution. Using dynamic programming, ML estimation of the LSCP is determined. Then, the samples in the interval from the LSCP to the end of the sensing time are used for detection of PU. Subsequently, the weighted samples are used in CuSum based detectors. The considered detectors are SMD, ED, and i-AVCD. The closed-form expressions of P_D and P_F are derived. The ROC is presented using the analytical expressions and the same is validated by comparing with simulations. It is observed that the considered detection schemes outperform the conventional detection schemes, wherein the full sensing time is used for detection without weighted samples. Further, the ROC of the considered system is compared with the ROC of the system by taking one status change of PU. In one status change of PU, the LSCP is estimated and sensing is done from the LSCP to the end of the sensing interval. It is found that the one status change of the PU outperforms the considered system for the same LSCP in the same sensing interval. The reason is less estimation error occurred in LSCP for the case of one status change of the PU.

The rest of the chapter is organized as follows: Section 7.2 deals with the system model. Section 7.3 presents the detailed performance analysis. In this section, LSCP along with CuSum based weighing scheme is presented in additive Laplacian noise. Section 7.4 presents the results with ROC, followed by a brief conclusion of the work in Section 7.5.

7.2 System Model

The null and alternate hypotheses are denoted as H_o and H_1, respectively. The received symbol at the cognitive terminal under the random arrival and departure of the PU can be expressed as

$$\begin{aligned} H_o : y_m &= \begin{cases} n_{m,} & m = 1, \ldots, \vartheta_o \\ s_m + n_m, & m = \vartheta_o + 1, \vartheta_o + 2, \ldots, \vartheta_o' \\ n_m, & m = \vartheta_o' + 1, \vartheta_o' + 2, \ldots, N; \end{cases} \\ H_1 : y_m &= \begin{cases} s_m + n_{m,} & m = 1, \ldots, \vartheta_1 \\ n_{m,} & m = \vartheta_1 + 1, \vartheta_1 + 2, \ldots, \vartheta_1' \\ s_m + n_{m,} & m = \vartheta_1' + 1, \vartheta_1' + 2, \ldots, N, \end{cases} \end{aligned} \tag{7.1}$$

where $1 < \vartheta_o < \vartheta_o' < N$ and $1 < \vartheta_1 < \vartheta_1' < N$. Here, ϑ_o and ϑ_1 are first transitions of the PU and ϑ_o' and ϑ_1' are the second ones. The N indicates the total number of samples present during the sensing period. The s_m is the unknown PU signal and n_m denotes sample of the Laplacian noise with mean 0 and variance $2\kappa^2$, where κ is the scale parameter of the Laplacian noise. Similarly, for one PU change, the system model can be expressed as

$$\begin{aligned} H_o : y_m &= \begin{cases} s_m + n_m, & m = 1, \ldots, \vartheta_o \\ n_m, & m = \vartheta_o + 1, \vartheta_o + 2, \ldots, N; \end{cases} \\ H_1 : y_m &= \begin{cases} n_m, & m = 1, \ldots, \vartheta_1 \\ s_m + n_m, & m = \vartheta_1 + 1, \vartheta_1 + 2, \ldots, N. \end{cases} \end{aligned} \tag{7.2}$$

7.3 Performance Analysis

In this section, the LSCP estimation is presented along with CuSum based weighing scheme [146]. Then, the expressions of P_D and P_F are derived.

The LSCP estimation is obtained using Maximum Likelihood Estimation (MLE). The PU signal s_m is assumed to be unknown constant C. The joint MLE of C, ϑ_o and ϑ'_o under hypothesis H_o is determined by minimizing the following cost function [146]

$$J_{H_o}(C, \vartheta_o, \vartheta'_o) = \sum_{m=1}^{\vartheta_o} |y_m| + \sum_{m=\vartheta_o+1}^{\vartheta'_o} |y_m - C| + \sum_{m=\vartheta'_o+1}^{N} |y_m| \, . \tag{7.3}$$

Similarly, under H_1, the cost function to be minimized can be expressed as

$$J_{H_1}(C, \vartheta_1, \vartheta'_1) = \sum_{m=1}^{\vartheta_1} |y_m - C| + \sum_{m=\vartheta_1+1}^{\vartheta'_1} |y_m| + \sum_{m=\vartheta'_1+1}^{N} |y_m - C| \, . \tag{7.4}$$

Here, the estimated values of ϑ'_o and ϑ'_1 are denoted as $\hat{\vartheta}'_o$ and $\hat{\vartheta}'_1$, respectively. Dynamic programming is used for the same [30].

Now, with $\hat{\vartheta}'_o$ and $\hat{\vartheta}'_1$, the effective hypotheses H'_o and H'_1 can be expressed as

$$\begin{aligned} &H'_o : y_m = n_m; & m &= \hat{\vartheta}'_o + 1, \hat{\vartheta}'_o + 2, \ldots, N \\ &H'_1 : y_m = s_m + n_m; & m &= \hat{\vartheta}'_1 + 1, \hat{\vartheta}'_1 + 2, \ldots, N. \end{aligned} \tag{7.5}$$

After LSCP estimation, the CuSum based weighted samples are used in the following three detectors.

7.3.1 Sample Mean Detector

The decision statistic can be expressed as [146]

$$\Upsilon(\mathbf{y}) = \frac{1}{N - l_{scp}} \left(\sum_{m=1}^{N-l_{scp}} (N - l_{scp} - m + 1) y_{N-m+1} \right), \tag{7.6}$$

where l_{scp} denotes the last status change point of the PU, i.e., $l_{scp} \in \{\hat{\vartheta}'_o, \hat{\vartheta}'_1\}$. Now, using the CLT [63], the PDF of $\Upsilon(\mathbf{y})$ can be expressed as Gaussian under both the hypotheses. Under hypothesis H'_o, the mean of $\Upsilon(\mathbf{y})$ can be expressed as

$$E\Big[\Upsilon(\mathbf{y})\Big] = 0, \tag{7.7}$$

and the variance of $\Upsilon(\mathbf{y})$ can be expressed as

$$var\Big[\Upsilon(\mathbf{y})\Big] = \frac{2\kappa^2}{6}\left\{\frac{(N-\hat{\vartheta}'_o+1)\{2(N-\hat{\vartheta}'_o)+1\}}{(N-\hat{\vartheta}'_o)}\right\}. \tag{7.8}$$

Similarly, under hypothesis H'_1, the mean of $\Upsilon(\mathbf{y})$ can be expressed as

$$E\Big[\Upsilon(\mathbf{y})\Big] = \frac{C}{2}\Big\{N-\hat{\vartheta}'_1-1\Big\}, \tag{7.9}$$

while, the variance of $\Upsilon(\mathbf{y})$ can be expressed as

$$var\Big[\Upsilon(\mathbf{y})\Big] = \frac{2\kappa^2}{6}\left\{\frac{(N-\hat{\vartheta}'_1+1)\{2(N-\hat{\vartheta}'_1)+1\}}{(N-\hat{\vartheta}'_1)}\right\}, \tag{7.10}$$

where $E[\cdot]$ and $var[\cdot]$ denote mean and variance, respectively. Derivation of (7.7) and (7.8) are given in Appendix II.1 and Appendix II.2, respectively. Derivations of (7.9) and (7.10) are given in Appendix II.3 and Appendix II.4, respectively. It should be noted here that similar steps as given in the Appendices to calculate mean and variance for SMD are followed in case of ED as well as i-AVCD.

7.3.2 improved-Absolute Value Cumulation Detection

The decision statistic can be expressed as

$$\Upsilon(\mathbf{y}) = \frac{1}{N-l_{scp}}\left(\sum_{m=1}^{N-l_{scp}}(N-l_{scp}-m+1)\left|y_{N-m+1}\right|^P\right). \tag{7.11}$$

Now, using the CLT, the PDF of $\Upsilon(\mathbf{y})$ can be expressed as Gaussian under both the hypotheses. Under hypothesis H'_o, the mean of $\Upsilon(\mathbf{y})$ can be expressed as

$$E\Big[\Upsilon(\mathbf{y})\Big] = \frac{\kappa^P\Gamma(P+1)\big(N-\hat{\vartheta}'_o+1\big)}{2}. \tag{7.12}$$

Similarly, variance of $\Upsilon(\mathbf{y})$ can be expressed as

$$var\Big[\Upsilon(\mathbf{y})\Big] = \frac{\kappa^{2P}\Big\{\Gamma(2P+1)-\Gamma^2(P+1)\Big\}}{6} \times \left\{\frac{(N-\hat{\vartheta}'_o+1)\{2(N-\hat{\vartheta}'_o)+1\}}{(N-\hat{\vartheta}'_o)}\right\}, \tag{7.13}$$

where $\Gamma(v) = \int_0^{+\infty} e^{-t} t^{v-1} dt$ is the complete Gamma function [77]. Similarly, under hypothesis H_1', the mean of $\Upsilon(\mathbf{y})$ can be expressed as

$$E\Big[\Upsilon(\mathbf{y})\Big] = \frac{u_o(P) \times (N - \hat{\vartheta}_1' + 1)}{2}, \tag{7.14}$$

and variance of $\Upsilon(\mathbf{y})$ can be expressed as

$$var\Big[\Upsilon(\mathbf{y})\Big] = \frac{v_o(P)}{6} \times \Bigg\{ \frac{(N - \hat{\vartheta}_1' + 1)\{2(N - \hat{\vartheta}_1') + 1\}}{(N - \hat{\vartheta}_1')} \Bigg\}, \tag{7.15}$$

where

$$u_o(P) = \frac{\kappa^P}{2} \exp\left(\frac{|C|}{\sqrt{2}\kappa^2}\right) \Gamma\left(P + 1, \frac{|C|}{\sqrt{2}\kappa^2}\right) + \frac{\kappa^P}{2} \exp\left(\frac{-|C|}{\sqrt{2}\kappa^2}\right) \Gamma\Big(P + 1\Big) \\ + \frac{\kappa^P}{2} \exp\left(\frac{-|C|}{\sqrt{2}\kappa^2}\right) M_o\left(P, \frac{|C|}{\sqrt{2}\kappa^2}\right). \tag{7.16}$$

Here, $M_o(w, x) = \int_0^x e^t t^w dt$, $\Gamma(w, x) = \int_x^\infty e^{-t} t^{w-1} dt$ is the upper incomplete Gamma function [77], and

$$v_o(P) = u_o(2P) \times u_o^2(P). \tag{7.17}$$

7.3.3 Energy Detection

The decision statistic can be expressed as

$$\Upsilon(\mathbf{y}) = \frac{1}{N - l_{scp}} \left(\sum_{m=1}^{N - l_{scp}} (N - l_{scp} - m + 1) y_{N-m+1}^2 \right). \tag{7.18}$$

Now, using the CLT, the PDF of $\Upsilon(\mathbf{y})$ can be expressed as Gaussian under both the hypotheses. Under hypothesis H_o', the mean of $\Upsilon(\mathbf{y})$ can be expressed as

$$E\Big[\Upsilon(\mathbf{y})\Big] = \kappa^2 \big(N - \hat{\vartheta}_o' + 1\big), \tag{7.19}$$

while, the variance of $\Upsilon(\mathbf{y})$ can be expressed as

$$var\Big[\Upsilon(\mathbf{y})\Big] = \frac{20\kappa^4}{6} \Bigg\{ \frac{(N - \hat{\vartheta}_o' + 1)\{2(N - \hat{\vartheta}_o') + 1\}}{(N - \hat{\vartheta}_o')} \Bigg\}. \tag{7.20}$$

Similarly, under hypothesis H_1', the mean of $\Upsilon(\mathbf{y})$ can be expressed as

$$E\Big[\Upsilon(\mathbf{y})\Big] = \frac{N - \hat{\vartheta}_1' + 1}{2} \Big\{ 2\kappa^2 + C^2 \Big\}, \tag{7.21}$$

and the variance of $\Upsilon(\mathbf{y})$ can be expressed as

$$var\Big[\Upsilon(\mathbf{y})\Big] = \frac{1}{6}\left\{\frac{(N-\hat{\vartheta}_1'+1)\{2(N-\hat{\vartheta}_1')+1\}}{(N-\hat{\vartheta}_1')}\right\} \times \Big\{20\kappa^4 + C^4 + 8\kappa^2 C^2\Big\}. \tag{7.22}$$

Finally, the P_F and P_D in each case can be expressed as

$$P_F = Prob\Big\{\Upsilon(\mathbf{y}) > \Psi|H_o'\Big\} = Q\left(\frac{\Psi - E[\Upsilon(\mathbf{y})|_o]}{\sqrt{var\Big[\Upsilon(\mathbf{y})|H_o'\Big]}}\right). \tag{7.23}$$

Similarly,

$$P_D = Prob\Big\{\Upsilon(\mathbf{y}) > \Psi|H_1'\Big\} = Q\left(\frac{\Psi - E\Big[\Upsilon(\mathbf{y})|H_1'\Big]}{\sqrt{var\Big[\Upsilon(\mathbf{y})|H_1'\Big]}}\right). \tag{7.24}$$

Here, Ψ is the detection threshold obtained using the NP test.

7.4 Simulation Results

In this section, the performance of the considered schemes is presented with ROC. After estimating the LSCP, CuSum based weighted samples are applied for the detection schemes such as SMD, ED and i-AVCD. Using the NP test, detection threshold Ψ is determined from (7.23) and subsequently, P_D is obtained using (7.24). It can be observed from Table 5.1 that optimum P for i-AVCD remains around 0.1 with varying P_F and γ. Hence, $P = 0.1$ is chosen for simulations in the case of i-AVCD scheme. Here, γ denotes the average SNR defined as $\gamma = (1/N)\sum_{m=1}^{N}(s_m^2)/(2\kappa^2)$. The ROC for the considered schemes is presented for i-AVCD, SMD and ED.

Table 7.1: P_D for dynamic PU with one transition within sensing period at $\gamma = -5$ dB, $N = 100$, $P = 0.1$ and $P_F = 0.1$.

	Dynamic PU with one transition					
Detection Schemes	**LSCP with CuSum** (*Ch.* 7)	**Random arrival and departure of the PU** (*Ch.* 6)		**Random arrival/ departure of the PU based on CSS** (*Ch.* 5)		
		$\theta_A T/\theta_D T = 1$	$\theta_A T/\theta_D T = 20$	OR	Majority	AND
i-AVCD	**0.985**	0.721	0.8	0.9	0.58	0.2
AVCD	**0.95**	0.65	0.72	0.88	0.52	0.18
SMD	**0.9311**	NA	NA	NA	NA	NA
ED	**0.51**	0.36	0.48	0.61	0.36	0.1

Figure 7.1 shows the ROC for the considered schemes at $\gamma = -5$ dB, $\vartheta_o = 30$ and $\vartheta_o' = 40$. Further, it is assumed that $\vartheta_1 = 10$, $\vartheta_1' = 40$ and $N = 50$. At $P_F = 0.1$, the values of P_D for LSCP

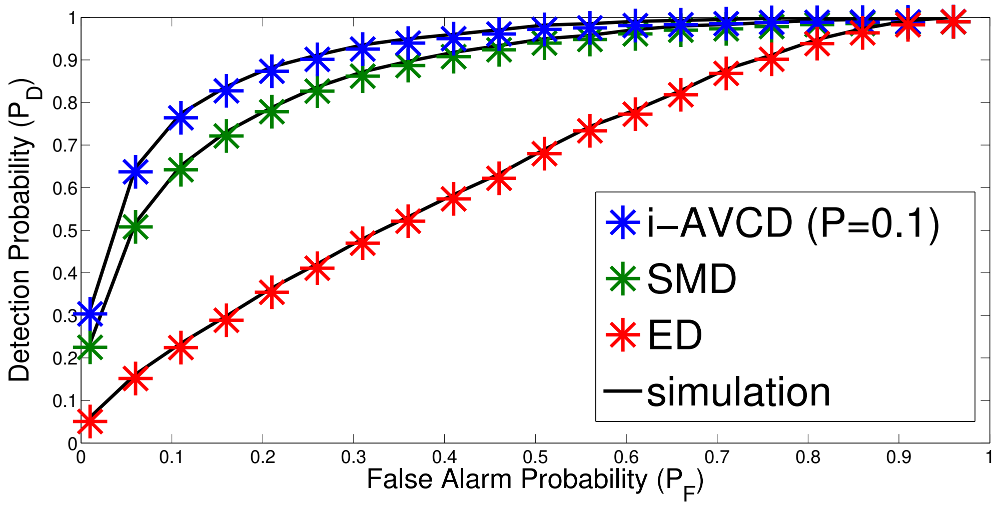

Figure 7.1: ROC for LSCP estimation based CuSum to SMD, ED and i-AVCD at $N = 50$ and $\gamma = -5$ dB.

estimation based CuSum to SMD, i-AVCD and ED are 0.6252, 0.7488 and 0.22, respectively. It can be seen that the i-AVCD outperforms the remaining two schemes. Besides this, the simulation results are also presented for all three schemes. The close matching of the simulation results with analytical counterpart validates our analysis.

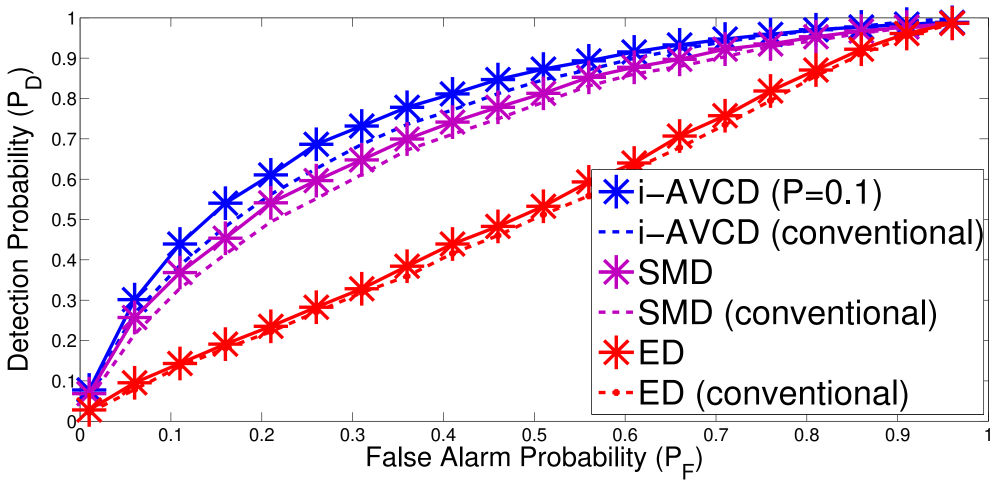

Figure 7.2: ROC for the LSCP estimation based CuSum to SMD, ED and i-AVCD and conventional schemes at $N = 50$ and $\gamma = -10$ dB.

Figure 7.2 shows the ROC for the considered schemes at $\gamma = -10$ dB, $\vartheta_o = 30$ and $\vartheta'_o = 40$. Further, it is assumed that $\vartheta_1 = 10$, $\vartheta'_1 = 50$ and $N = 50$. The performance of the three schemes is shown without the LSCP and CuSum based decision statistics. They are referred to as conventional schemes. At $P_F = 0.1$, the values of P_D for LSCP estimation based CuSum to SMD, i-AVCD and ED are 0.3497, 0.4138 and 0.1361, respectively. For conventional sensing schemes such as SMD, i-AVCD and ED, the values of P_D are 0.307, 0.3659 and 0.1352, respectively. It can be seen that the considered schemes outperform the conventional schemes.

Figure 7.3 shows the ROC for the SMD scheme with 'two PU changes' at $\gamma = -20$ dB. It is assumed that $\vartheta_o = 10$ and $\vartheta'_o = 30$. Further, it is assumed that $\vartheta_1 = 10$, $\vartheta'_1 = 30$ and $N = 100$. Besides this, the performance of 'one PU change' is also presented in which only one transition of PU is there at ϑ_o and ϑ_1 under H_o and H_1, respectively, with total samples of N in the sensing time. After applying LSCP estimation using dynamic programming, the $\hat{\vartheta}_o$ and $\hat{\vartheta}_1$ have been obtained. Then, CuSum based SMD scheme is used using $\hat{\vartheta}_o$ and $\hat{\vartheta}_1$. It is assumed that $N = 100$, $\vartheta_o = 30$, $\vartheta_1 = 30$, and $\gamma = -20$ dB. For a fair comparison between the two, the effective sensing time is kept at 30 samples and total samples in sensing time at 100. At $P_F = 0.1$ and $\gamma = -5$ dB, the values of

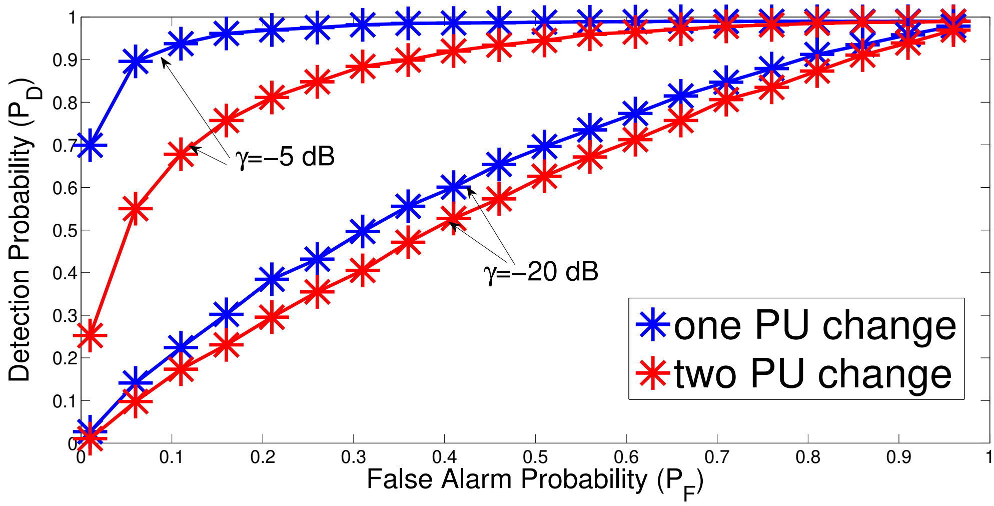

Figure 7.3: ROC of the LSCP estimation based CuSum to SMD for one PU status change and two PU status changes at $\gamma = -5$, -20 dB and $N = 100$.

P_D for LSCP estimation based CuSum to SMD with one PU change and two PU changes are 0.9311 and 0.681, respectively, which subsequently reduce to 0.2091 and 0.1671 at $\gamma = -20$ dB. It can be seen that the SMD scheme with one PU change outperforms the scheme with two PU changes. The reason behind this is less error in estimating LSCP in case of one PU change.

Finally, in Table 7.1, the performance of dynamic PU with one transition, presented in this chapter, has been compared with the performance achieved in the previous two chapters in term of detection probability P_D. The ϑ_o and ϑ_1 are assumed to be 30. We have assumed $\gamma = -5$ dB and $N = 100$. Further, it is assumed that $P = 0.1$ for i-AVCD and $P_F = 0.1$. In this chapter, we have presented the i-AVCD, AVCD and ED schemes modified with CuSum. In Chapter 5, the Poisson process modeled the random transitions of the PU. The performance of dynamic PU was dependent on the dynamic parameters such as $\theta_A T$ and $\theta_D T$. Similarly, Chapter 6 presented the CSS scheme under the random arrival and departure of the PU where each M_o CR used localized detection schemes such as i-AVCD, AVCD and ED modified with dynamic parameters such as $\theta_A T$ and $\theta_D T$. Finally, different CSS fusion schemes were used at the FC to deliver the final decision on the availability of the PU. It is observed that the detection schemes used in this chapter outperform the schemes used in Chapters 5 and 6.

7.5 Conclusion

In this Chapter, the effect of the dynamic behavior of the PU was observed on the ROC in the additive Laplacian noise channel. The dynamic behavior of the PU was assumed using two status changes of the PU in the fixed sensing time. The LSCP was estimated by dynamic programming and then PU was detected using the samples available from the LSCP to the end of sensing time by ignoring the samples before LSCP and boosting the samples after LSCP. Then, CuSum based weighted samples were used in the detection schemes such as i-AVCD, SMD and ED. The expressions of P_D and P_F were derived for all three schemes. The ROC for the considered schemes was presented and it was found that the i-AVCD outperforms the remaining two schemes. The simulation results were also presented and found to be in a close match with their analytical counterparts. The performance of the considered schemes was compared with the conventional schemes, where no LSCP or CuSum based weighted samples were used. In this case, the considered schemes outperform the conventional schemes. Next, the considered schemes with two PU status changes were compared with one PU status change. It is concluded that detection schemes with one PU status change outperform the schemes with two PU status changes due to less estimation error in LSCP. Finally, the performance of the detection schemes used in the previous two chapters has been compared with the schemes used in this chapter. It is observed that LSCP estimation when applied with CuSum based weighted samples in the considered detection schemes outperform the schemes used in the previous two chapters. In the next chapter, we will present the performance of the spectrum sensing schemes for dynamic PU with multiple transitions.

Chapter 8

Spectrum Sensing for Dynamic PU With Multiple Transitions in ALN

In this chapter, spectrum sensing for dynamic PU is presented in additive Laplacian noise. Further, the dynamic behavior of PU is assumed, where their transitions in both the null and the alternate hypotheses are modeled by two state Discrete Time Markov Chain (DTMC). The PU signal is assumed to be quadrature amplitude modulated (M-QAM) with 'M' modulation order. The Markov parameters are τ_s and τ_d, which represent an average number of samples present during the active (ON) state and idle (OFF) state of the PU, respectively. Further, the τ_d and τ_s are functions of the Transition Probability Matrix (TPM) in DTMC. For spectrum sensing, perfect information of the TPM or in other words, τ_d and τ_s has been assumed at the cognitive terminal. Then, the detection scheme such as i-AVCD is used with the TPM. We refer to this scheme as a modified i-AVCD and derive the resulting detection variable along with the threshold. In the detection variable, the received samples at the cognitive terminal are raised to a positive exponent P with $0 < P \leq 2$. The analytical expressions of the P_D and P_F have been derived and the results are presented using ROC for the modified scheme. Besides this, simulation results are also presented and found to be in a close match with their analytical counterparts. The effect of increasing modulation order M on the detection performance has been explored. A special case of M-QAM at $M = 2$, which refers to the BPSK modulation scheme for PU is also presented. Further, special cases of the i-AVCD scheme at $P = 1$ and $P = 2$, i.e., modified AVCD and modified ED, respectively, have been presented. Finally, the performance of the modified i-AVCD scheme is compared with the conventional i-AVCD scheme, where information on DTMC or in other words TPM, is not available at the cognitive terminal. It is found that the modified scheme outperforms the conventional scheme. The conclusion is presented at the end of this chapter.

8.1 Introduction

The case of dynamic PU with one and two transitions has been presented in the previous chapters. However, in such cases of dynamic PU, a limited number of transitions were assumed. In a real-time scenario, there may not be any limitations on the number of transitions [138–142]. The case of multiple transitions of the PU has been proposed in [148], where PU changed its status multiple times. In this case, the performance of the spectrum sensing schemes has been analyzed in term of throughput versus sensing period. It has been shown in [149] that multiple PU changes caused significant degradation in the detection performance using the ED scheme. The principle of the Markov chain based spectrum sensing lies in the fact that the transition from one state to another depends on the current state occupied [30]. The Markov chain has been evaluated in different ways to model the scenario of dynamic PU in the Gaussian noise [153–157].

In this chapter, a modified detection scheme is proposed using i-AVCD and the underlying Markov parameters, where Markov parameters are used to model the dynamic PU based spectrum sensing. This modified detection scheme has been referred to as modified i-AVCD. The M-QAM modulation scheme is assumed for PU. Similar to [97, 116], a non-fading channel has been assumed in additive Laplacian noise environment. It is assumed that Markov parameters τ_s and τ_d are known at the SU, where τ_s and τ_d represent average number of samples present during active period and idle period, respectively. The ON-state (active-state) to OFF-state (inactive-state) transitions and vice-versa are determined by the TPM. The transition probabilities, which correspond to the ON-state to OFF-state transitions of the PU are derived from the TPM. The analytical expressions of P_D and P_F have been derived. A special case of M-QAM at $M = 2$ has been presented, which means BPSK modulation scheme for the PU. Two special cases of modified i-AVCD at $P = 1$ and $P = 2$, referred to as modified AVCD and modified ED, respectively, are also presented. Simulation results are presented for the modified scheme and a close match between simulations and their analytical counterparts validates our analysis.

The rest of the chapter is organized as follows: Section 8.2 presents the proposed system model in dynamic PU scenario using i-AVCD as a detection scheme. In this section, the random appearance and disappearance of the PU are modeled in term of two-state DTMC. The principle of the Markov chain is also explained which models dynamic PU activities. Section 8.3 presents the performance analysis of dynamic PU with modified i-AVCD and two special cases of it. Section 8.4 presents the simulation results with ROC, followed by a brief conclusion in Section 8.5.

8.2 System Model

In this section, the dynamic scenario of PU is presented. The active or inactive state of the PU happens in a random fashion. In this case, it is assumed that there can be multiple random transitions of the PU from ON-state to OFF-state and vice-versa under hypotheses H_o and H_1.

Figure 8.1 shows the random behavior of the PU in ON and OFF states within the sensing interval N.

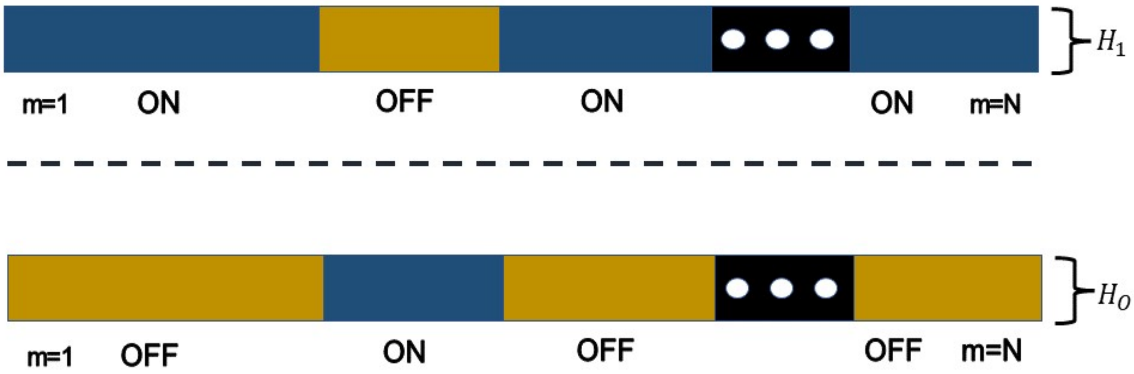

Figure 8.1: Dynamic PU activity under the null-hypothesis and alternate hypothesis within the sensing period N showing multiple transitions.

The active state of the PU has a certain duration, which is exponentially distributed with mean τ_s. The PDF of the exponentially distributed active period is represented as $\frac{1}{\tau_s}\exp(-\frac{x}{\tau_s})$. Similarly, the idle period of the PU is exponentially distributed with mean τ_d, and its PDF represented as $\frac{1}{\tau_d}\exp(-\frac{x}{\tau_d})$. When these periods are sampled at some specified sampling frequency, τ_s and τ_d represent average number of samples present during the active and idle periods, respectively. The received symbol at the cognitive terminal under the random appearance (ON-state) and disappearance (OFF-state) of the PU can be expressed as

$$\begin{aligned} H_o : y_m &= g_{00}^{(N-m)} n_m \Big|_{m=1,2,3,\ldots,N_{00}} + g_{01}^{(N-m)} s_m \Big|_{m=1,2,3,\ldots,N_{01};} \\ H_1 : y_m &= g_{10}^{(N-m)} n_m \Big|_{m=1,2,3,\ldots,N_{10}} + g_{11}^{(N-m)} s_m \Big|_{m=1,2,3,\ldots,N_{11},} \end{aligned} \tag{8.1}$$

where m denotes the number of sensing samples. Here, N is the aggregate sensing samples present during the sensing period. The s_m is the M-QAM (Quadrature amplitude modulation) PU signal where 'M' denotes modulation order. The n_m represents the Laplacian noise with mean 0 and variance $2\kappa^2$.

Now, g_{00}, g_{01}, g_{10}, g_{11} represent one step transition probabilities, which are determined using (8.2). The corresponding sensing samples are denoted as l_{00}, l_{01}, l_{10}, l_{11}, which can be obtained using (8.4). Further, the N_{00}, N_{01}, N_{10}, N_{11} represent sensing samples corresponding to $(N-m)$ step transition probabilities, which are obtained using (8.5). These transition probabilities and corresponding sensing samples indeed depend on the values of Markov parameters τ_s and τ_d.

It is assumed that the active period and inactive period of the PU are mutually exclusive. Hence, they can be modeled by two state DTMC. In DTMC modeling of the PU, the transition from the

ON-state to the OFF-state and vice-versa is represented using transition probabilities present in the TPM. One step TPM is represented as [30]

$$\mathbf{T}_{\text{matrix}} = \begin{bmatrix} g_{00} & g_{01} \\ g_{10} & g_{11} \end{bmatrix} = \frac{\tau_d \tau_s}{\tau_d + \tau_s} \begin{bmatrix} \frac{1}{\tau_s} + \frac{1}{\tau_d} e^{-\left(\frac{1}{\tau_s}+\frac{1}{\tau_d}\right)} & \frac{1}{\tau_d} - \frac{1}{\tau_d} e^{-\left(\frac{1}{\tau_s}+\frac{1}{\tau_d}\right)} \\ \frac{1}{\tau_s} - \frac{1}{\tau_s} e^{-\left(\frac{1}{\tau_s}+\frac{1}{\tau_d}\right)} & \frac{1}{\tau_d} + \frac{1}{\tau_s} e^{-\left(\frac{1}{\tau_s}+\frac{1}{\tau_d}\right)} \end{bmatrix}, \tag{8.2}$$

where g_{ij} represents transition of the PU from the i_{th} state to the j_{th} state. Both i and j have two states, i.e., i, j$\in \{0, 1\}$. At the end of the sensing interval, a total of N samples are collected. Transition probabilities are determined when PU makes transition from i_{th} state to the j_{th} state at any sampling instant $m = 1, 2, 3, \ldots, N$. Hence, one step transition probability must be modified to $(N - m)$ step transition probability as

$$\mathbf{T}_{matrix}^{(N-m)} = \begin{bmatrix} g_{00}^{(N-m)} & g_{01}^{(N-m)} \\ g_{10}^{(N-m)} & g_{11}^{(N-m)} \end{bmatrix}. \tag{8.3}$$

Corresponding to the PU to be in state $j \in \{0, 1\}$, given the PU is in state $i \in \{0, 1\}$ at sampling instant $m = 1, 2, \ldots, N$, modified number of sensing samples can be expressed as [153]

$$l_{ij} = g_{ij} \times N. \tag{8.4}$$

The expression of l_{ij} consists of g_{ij} as one of its constituent terms. As explained earlier, τ_d and τ_s denote average number of sensing samples present during the idle and active periods, respectively. As g_{ij} depends on τ_d and τ_s, l_{ij} also depends on τ_d and τ_s. Hence, l_{ij} denotes average number of sensing samples. From (8.4), average number of sensing samples during PU transitions from i_{th} state to j_{th} state can be represented in term of $(N - m)$ step transition probability as

$$N_{ij} = l_{ij}^{(N-m)} = g_{ij}^{(N-m)} \times N. \tag{8.5}$$

With reference to the hypotheses shown in (8.1), the modified i-AVCD scheme is represented as [97]

$$\Upsilon(\mathbf{y}) \underset{H_o}{\overset{H_1}{\gtrless}} \Psi, \tag{8.6}$$

where under H_o, $\Upsilon(\mathbf{y})$ can be expressed as

$$\Upsilon(\mathbf{y}) = \sum_{m=1}^{N_{00}} g_{00}^{(N-m)} |y_m|^P + \sum_{m=1}^{N_{01}} g_{01}^{(N-m)} |y_m|^P; \tag{8.7}$$

while under H_1, $\Upsilon(\mathbf{y})$ can be expressed as

$$\Upsilon(\mathbf{y}) = \sum_{m=1}^{N_{10}} g_{10}^{(N-m)} |y_m|^P + \sum_{m=1}^{N_{11}} g_{11}^{(N-m)} |y_m|^P. \tag{8.8}$$

Here, $\mathbf{y} = [y_1, y_2, \ldots, y_{N_{ij}}]$ and $i, j \in \{0, 1\}$ and Ψ is the detection threshold which is obtained by performing NP test.

8.3 Performance Analysis

In this section, the analytical expressions of P_F and P_D have been derived. For this, the PDF of $\Upsilon(\mathbf{y})$ is required for both hypotheses. Now, using Generalized CLT, the PDF of $\Upsilon(\mathbf{y})$ can be approximated as Gaussian with specified mean and variance under both the hypotheses [64]. Hence, the expressions of P_F and P_D can be determined in the form of Q-function as

$$P_F = Prob\Big\{\Upsilon(\mathbf{y}) > \Psi | H_o\Big\} = Q\left(\frac{\Psi - E\Big[\Upsilon(\mathbf{y})|H_o\Big]}{\sqrt{var\Big[\Upsilon(\mathbf{y})|H_o\Big]}}\right) \tag{8.9}$$

and

$$P_D = Prob\Big\{\Upsilon(\mathbf{y}) > \Psi | H_1\Big\} = Q\left(\frac{\Psi - E\Big[\Upsilon(\mathbf{y})|H_1\Big]}{\sqrt{var\Big[\Upsilon(\mathbf{y})|H_1\Big]}}\right), \tag{8.10}$$

where $E\Big[\Upsilon(\mathbf{y})|H_o\Big]$ and $var\Big[\Upsilon(\mathbf{y})|H_o\Big]$ represent mean and variance under hypothesis H_o, while $E\Big[\Upsilon(\mathbf{y})|H_1\Big]$ and $var\Big[\Upsilon(\mathbf{y})|H_1\Big]$ represent mean and variance under hypothesis H_1. The detection threshold Ψ can be determined corresponding to P_F as shown in (8.9). The NP test is used for the same. Subsequently,P_D is determined from 8.10.

8.3.1 Average SNR (γ) under both the hypotheses H_o and H_1

With reference to the expressions of H_o and H_1 given in (8.1), noise power P_n and signal power P_s under hypothesis H_o can be represented as

$$\begin{aligned} H_o: P_n &= \sum_{m=1}^{N_{00}} E\left[\left\{{g_{00}}^{N-m} n_m\right\}^2\right] \\ &= 2\kappa^2\left\{{g_{00}}^{2(N-1)} + {g_{00}}^{2(N-2)} + \cdots + {g_{00}}^{2(N-m_{00})}\right\}; \\ P_s &= \sum_{m=1}^{N_{01}} E\left[\left\{{g_{01}}^{N-m} s_m\right\}^2\right]; \\ &= \frac{f_o^2 E_s}{M}\left\{{g_{01}}^{2(N-1)} + {g_{01}}^{2(N-2)} + \cdots + {g_{01}}^{2(N-m_{01})}\right\}, \end{aligned} \tag{8.11}$$

where E_s denotes the energy of the PU signal. The M denotes modulation order of M-QAM PU signal which equals to 2, 4, 16 and 64. The f_o represents normalizing factor of M-QAM PU signal which can be expressed as [174]

$$f_o = \begin{cases} \sqrt{\frac{3}{2(M-1)}}, & \text{for} \quad M = 4, 16, 64; \\ 1, & \text{for} \quad M = 2. \end{cases} \tag{8.12}$$

Here $M = 2$ is a special case of M-QAM which represents BPSK modulation scheme. The modulation order $M = 4$ denotes QPSK.

Similarly, P_n and P_s under hypothesis H_1 can be represented as

$$\begin{aligned} H_1: P_n &= \sum_{m=1}^{N_{10}} E\left[\left\{{g_{10}}^{(N-m)} n_m\right\}^2\right] \\ &= 2\kappa^2\left\{{g_{10}}^{2(N-1)} + {g_{10}}^{2(N-2)} + \cdots + {g_{10}}^{2(N-m_{10})}\right\}; \\ P_s &= \sum_{m=1}^{N_{11}} E\left[\left\{{g_{11}}^{(N-m)} s_m\right\}^2\right] \\ &= \frac{f_o^2 E_s}{M}\left\{{g_{11}}^{2(N-1)} + {g_{11}}^{2(N-2)} + \cdots + {g_{11}}^{2(N-m_{11})}\right\}. \end{aligned} \tag{8.13}$$

Now, the resulting average SNR γ can be represented as

$$\gamma = P_s/P_n. \tag{8.14}$$

8.3.2 Mean and variance of $\Upsilon(\mathbf{y})$ under H_o and H_1

Now, mean $E\Big[\Upsilon(\mathbf{y})\Big]$ under hypothesis H_o can be expressed as

$$E\Big[\Upsilon(\mathbf{y})\Big] = \zeta_o \sum_{m=1}^{N_{00}} g_{00}^{(N-m)} + \zeta_1 \sum_{m=1}^{N_{01}} g_{01}^{(N-m)}, \tag{8.15}$$

where ζ_o can be derived as [97]

$$\zeta_o = \kappa^P \Gamma(P+1), \tag{8.16}$$

and ζ_1 can be derived as [97]

$$\begin{aligned}\zeta_1 = {} & \frac{\kappa^P}{M} \exp\left(\frac{\phi_o\sqrt{\gamma}}{\kappa}\right) \Gamma\left(P+1, \frac{\phi_o\sqrt{\gamma}}{\kappa}\right) + \frac{\kappa^P}{M} \exp\left(-\frac{\phi_o\sqrt{\gamma}}{\kappa}\right) \Gamma\left(P+1\right) \\ & + \frac{\kappa^P}{M} \exp\left(-\frac{\phi_o\sqrt{\gamma}}{\kappa}\right) M_o\left(P, \frac{\phi_o\sqrt{\gamma}}{b_l}\right).\end{aligned} \tag{8.17}$$

Here, $\phi_o = \sum_{m=1}^{\frac{\sqrt{M}}{2}} b_o f_o(2m-1)$, $b_o = log_2(M)$, $M_o(u,v) = \int_0^v e^t t^u dt$ and $\Gamma(u,v) = \int_v^\infty e^{-t} t^{u-1} dt$ is the upper incomplete Gamma function [77].

Similarly, under H_o, variance can be expressed as

$$var\Big[\Upsilon(\mathbf{y})\Big] = \sigma_o^2 \sum_{m=1}^{N_{00}} \left\{g_{00}^{(N-m)}\right\}^2 + \sigma_1^2 \sum_{m=1}^{N_{01}} \left\{g_{01}^{(N-m)}\right\}^2, \tag{8.18}$$

where σ_o^2 can be derived as

$$\sigma_o^2 = \kappa^{2P} \left(\Gamma(2P+1) - \Gamma^2(P+1)\right), \tag{8.19}$$

and σ_1^2 can be derived as

$$\begin{aligned}\sigma_1^2 = {} & \frac{\kappa^{2P}}{M} \exp\left(\frac{\phi_o\sqrt{\gamma}}{\kappa}\right) \Gamma\left(2P+1, \frac{\phi_o\sqrt{\gamma}}{\kappa}\right) + \frac{\kappa^{2P}}{M} \exp\left(-\frac{\phi_o\sqrt{\gamma}}{\kappa}\right) \Gamma\left(2P+1\right) \\ & + \frac{\kappa^{2P}}{M} \exp\left(-\frac{\phi_o\sqrt{\gamma}}{\kappa}\right) M_o\left(2P, \frac{\phi_o\sqrt{\gamma}}{\kappa}\right) - \zeta_1^2.\end{aligned} \tag{8.20}$$

The derivations of (8.15) and (8.18) are shown in Appendix III.1 and Appendix III.2, respectively. Similarly, the mean of $\Upsilon(\mathbf{y})$ under hypothesis H_1 can be determined as

$$E\Big[\Upsilon(\mathbf{y})\Big] = \zeta_o \sum_{m=1}^{N_{10}} g_{10}^{(N-m)} + \zeta_1 \sum_{m=1}^{N_{11}} g_{11}^{(N-m)}, \tag{8.21}$$

and the variance of $\Upsilon(\mathbf{y})$ under hypothesis H_1 can be determined as

$$var\Big[\Upsilon(\mathbf{y})\Big] = \sigma_o^2 \sum_{m=1}^{N_{10}} \Big\{g_{10}^{(N-m)}\Big\}^2 + \sigma_1^2 \sum_{m=1}^{N_{11}} \Big\{g_{11}^{(N-m)}\Big\}^2. \tag{8.22}$$

Special case of M-QAM at $M = 2$: BPSK PU

In this section, the mean and variance of $\Upsilon(\mathbf{y})$ under hypotheses H_o and H_1 are presented for BPSK PU signal. Substituting the value of $M = 2$ in the expressions (8.11) – (8.20) obtained for M-QAM modulation scheme, the signal power and noise power can be expressed as

$$\begin{aligned}
H_o : P_n &= \sum_{m=1}^{N_{00}} E\bigg[\Big\{{g_{00}}^{N-m} n_m\Big\}^2\bigg] \\
&= 2\kappa^2 \bigg\{{g_{00}}^{2(N-1)} + {g_{00}}^{2(N-2)} + \cdots + {g_{00}}^{2(N-m_{00})}\bigg\}; \\
P_s &= \sum_{m=1}^{N_{01}} E\bigg[\Big\{{g_{01}}^{N-m} s_m\Big\}^2\bigg] \\
&= \frac{E_s}{2} \bigg\{{g_{01}}^{2(N-1)} + {g_{01}}^{2(N-2)} + \cdots + {g_{01}}^{2(N-m_{01})}\bigg\}.
\end{aligned} \tag{8.23}$$

Similarly,

$$\begin{aligned}
H_1 : P_n &= \sum_{m=1}^{N_{10}} E\bigg[\Big\{{g_{10}}^{N-m} n_m\Big\}^2\bigg] \\
&= 2\kappa^2 \bigg\{{g_{10}}^{2(N-1)} + {g_{10}}^{2(N-2)} + \cdots + {g_{10}}^{2(N-m_{10})}\bigg\}; \\
P_s &= \sum_{m=1}^{N_{11}} E\bigg[\Big\{{g_{11}}^{N-m} s_m\Big\}^2\bigg] \\
&= \frac{E_s}{2} \bigg\{{g_{11}}^{2(N-1)} + {g_{11}}^{2(N-2)} + \cdots + {g_{11}}^{2(N-m_{11})}\bigg\}.
\end{aligned} \tag{8.24}$$

The average SNR γ can be represented as

$$\gamma = P_s/P_n. \tag{8.25}$$

Now, under hypothesis H_o, mean $E\Big[\Upsilon(\mathbf{y})\Big]$ can be expressed as

$$E\Big[\Upsilon(\mathbf{y})\Big] = \zeta_o \sum_{m=1}^{N_{00}} g_{00}^{(N-m)} + \zeta_1 \sum_{m=1}^{N_{01}} g_{01}^{(N-m)}, \tag{8.26}$$

where ζ_o can be derived as

$$\zeta_o = \kappa^P \Gamma(P+1), \tag{8.27}$$

and ζ_1 can be derived as

$$\zeta_1 = \frac{\kappa^P}{2} \exp\left(\frac{|\sqrt{\gamma}|}{\kappa}\right) \Gamma\left(P+1, \frac{|\sqrt{\gamma}|}{\kappa}\right) + \frac{\kappa^P}{2} \exp\left(-\frac{|\sqrt{\gamma}|}{\kappa}\right) \Gamma\left(P+1\right)$$
$$+ \frac{\kappa^p}{2} \exp\left(-\frac{|\sqrt{\gamma}|}{\kappa}\right) M_o\left(P, \frac{|\sqrt{\gamma}|}{b_l}\right). \tag{8.28}$$

Similarly, variance under H_o can be expressed as

$$var\Big[\Upsilon(\mathbf{y})\Big] = \sigma_o^2 \sum_{m=1}^{N_{00}} \left\{g_{00}^{(N-m)}\right\}^2 + \sigma_1^2 \sum_{m=1}^{N_{01}} \left\{g_{01}^{(N-m)}\right\}^2, \tag{8.29}$$

where σ_o^2 can be derived as

$$\sigma_o^2 = \kappa^{2P}\left(\Gamma(2P+1) - \Gamma^2(P+1)\right), \tag{8.30}$$

and σ_1^2 can be derived as

$$\sigma_1^2 = \frac{\kappa^{2P}}{2} \exp\left(\frac{|\sqrt{\gamma}|}{\kappa}\right) \Gamma\left(2P+1, \frac{|\sqrt{\gamma}|}{\kappa}\right) + \frac{\kappa^{2p}}{2} \exp\left(-\frac{|\sqrt{\gamma}|}{\kappa}\right) \Gamma\left(2P+1\right)$$
$$+ \frac{\kappa^{2P}}{2} \exp\left(-\frac{|\sqrt{\gamma}|}{\kappa}\right) M_o\left(2P, \frac{|\sqrt{\gamma}|}{\kappa}\right) - \zeta_1^2. \tag{8.31}$$

Similarly, the mean and variance of $\Upsilon(\mathbf{y})$ under hypothesis H_1 can be determined as

$$E\Big[\Upsilon(\mathbf{y})\Big] = \zeta_o \sum_{m=1}^{N_{10}} g_{10}^{(N-m)} + \zeta_1 \sum_{m=1}^{N_{11}} g_{11}^{(N-m)},$$
$$var\Big[\Upsilon(\mathbf{y})\Big] = \sigma_o^2 \sum_{m=1}^{N_{10}} \left\{g_{10}^{(N-m)}\right\}^2 + \sigma_1^2 \sum_{m=1}^{N_{11}} \left\{g_{11}^{(N-m)}\right\}^2. \tag{8.32}$$

Next, two special cases of the proposed system are presented by assuming $P = 1$ and $P = 2$.

8.3.3 Special case I: modified AVCD

Modified AVCD is a special case of modified i-AVCD at $P = 1$. The decision statistic under hypothesis H_o can be represented as

$$\Upsilon(\mathbf{y}) = \sum_{m=1}^{N_{00}} g_{00}^{(N-m)}|y_m| + \sum_{m=1}^{N_{01}} g_{01}^{(N-m)}|y_m|; \tag{8.33}$$

while under H_1, $\Upsilon(\mathbf{y})$ can be expressed as

$$\Upsilon(\mathbf{y}) = \sum_{m=1}^{N_{10}} g_{10}^{(N-m)}|y_m| + \sum_{m=1}^{N_{11}} g_{11}^{(N-m)}|y_m|. \tag{8.34}$$

The expressions of P_F and P_D in this case can be derived by substituting $P = 1$ in (8.9) and (8.10) respectively.

8.3.4 Special case II: modified ED

Modified ED is a special case of modified i-AVCD at $P = 2$. The decision statistic under hypothesis H_o in this case can be represented as

$$\Upsilon(\mathbf{y}) = \sum_{m=1}^{N_{00}} g_{00}^{(N-m)} |y_m|^2 + \sum_{m=1}^{N_{01}} g_{01}^{(N-m)} |y_m|^2; \tag{8.35}$$

while under H_1, $\Upsilon(\mathbf{y})$ can be expressed as

$$\Upsilon(\mathbf{y}) = \sum_{m=1}^{N_{10}} g_{10}^{(N-m)} |y_m|^2 + \sum_{m=1}^{N_{11}} g_{11}^{(N-m)} |y_m|^2. \tag{8.36}$$

The expressions of P_F and P_D in this case can be derived by substituting $P = 2$ in (8.9) and (8.10) respectively.

8.4 Simulation Results

In this section, the performance of the proposed scheme is presented using ROC. Without loss of generality, the value of κ is assumed to be 1 throughout the simulations. The detection threshold Ψ is obtained using (8.9) for certain values of P_F and then P_D using (8.10). Subsequently, the effect of higher order modulation schemes is compared by increasing the modulation order M in M-QAM modulated PU.

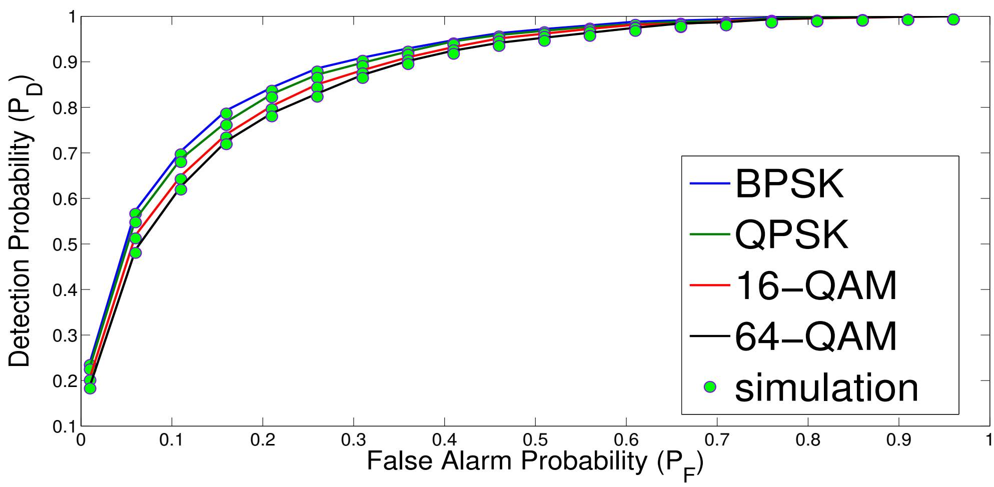

Figure 8.2: ROC for higher order M-QAM modulation schemes using modified i-AVCD at $N = 30$, $\gamma = -2$ dB, $P = 0.1$, $\tau_s = 50$ and $\tau_d = 100$.

Figure 8.2 presents the ROC for modified i-AVCD scheme with BPSK, QPSK, 16-QAM and 64-

QAM modulation schemes. Here, it is assumed that $N = 30$, $P = 0.1$ and $\gamma = -2$ dB. Further, it is assumed that $\tau_s = 50$ and $\tau_d = 100$. Corresponding to the values of τ_s and τ_d, the values of one step transition probabilities g_{00}, g_{01}, g_{10} and g_{11} are obtained as 0.0297, 0.0003, 0.0006 and 0.0294, respectively. The corresponding analytical results are also presented. It can be seen that the simulation results closely match with their analytical counterparts. It can be seen that the detection performance degrades, as we move from BPSK to 64 QAM. The reason is that a higher number of constellation points varies the mean and variance of the decision statistic of Modified i-AVCD. Further, a significant variation in the mean and variance results in an adverse influence on the P_D.

Table 8.1: Average SNR (γ) for modified i-AVCD corresponding to τ_d and τ_s at $N = 30$, $P = 0.1$, M=2 and $E_s = 1$.

Modified-i-AVCD			
$\tau_d = 100$			
	$\tau_s = 50$	$\tau_s = 100$	$\tau_s = 500$
g_{00}	0.0297	0.0198	0.119
g_{01}	0.0003	0.0002	0.0001
g_{10}	0.0006	0.0002	0.0000
g_{11}	0.0294	0.0198	0.0120
$\gamma\|H_o$ (in dB)	-5.4	-4.5	-4
$\gamma\|H_1$ (in dB)	-3	-1.9	-0.4
$\tau_d = 200$			
	$\tau_s = 50$	$\tau_s = 100$	$\tau_s = 500$
g_{00}	0.0249	0.0149	0.0070
g_{01}	0.0001	0.0001	0.000
g_{10}	0.0005	0.0001	0.0000
g_{11}	0.0245	0.0149	0.0070
$\gamma\|H_o$ (in dB)	-7.21	-5.1	-4.5
$\gamma\|H_1$ (in dB)	-7.19	-4.5	-3.8

The ROC for modified i-AVCD at a value of $P = 0.1$, modified AVCD at $P = 1$, and modified ED at $P = 2$ are presented in Figure 8.3. It shows ROC at $\gamma = -2$ dB, $N = 50$, $\tau_s = 50$, and $\tau_d = 100$. Here, BPSK modulation scheme is assumed for the PU. At $P_F = 0.1$, the values of P_D for modified i-AVCD, modified AVCD and modified ED are 0.85, 0.6498 and 0.356, respectively. It can be observed that the modified i-AVCD outperforms its special cases of modified AVCD and modified ED. Analytical expressions of P_D and P_F have been derived. A close match between simulations and the corresponding analytical counterparts validates our assumption of CLT.

Next, the effect of Markov parameters τ_d and τ_s on the ROC is observed. Figure 8.4 shows the ROC for modified i-AVCD at $\tau_s = 50$, 100 and 500. Further, it is assumed that $\tau_d = 100$ and 200 for BPSK modulated PU. Here, P and N are assumed to be 0.1 and 30, respectively. At $P_F = 0.1$, $\tau_s = 50$ and $\tau_d = 100$, the values of P_D for modified i-AVCD, modified AVCD and modified ED schemes are 0.6248, 0.4351 and 0.3237, respectively. These values respectively decrease to 0.2209, 0.1654 and 0.1417 at $\tau_d = 200$. Thus, the detection performance improves as τ_s increases. Contrary to this, the performance degrades, as τ_d is increased.

The reason for the same is as follows. If τ_s is increased, the SNR in (8.14) increases due to

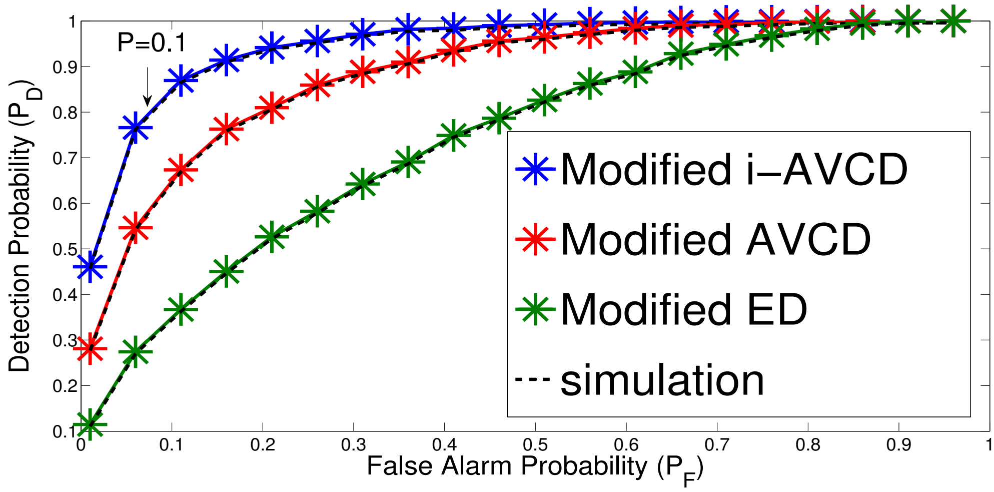

Figure 8.3: ROC for the modified schemes at $N = 50$, $\gamma = -2$ dB, $\tau_s = 50$, $\tau_d = 100$ and $M = 2$, i.e, BPSK modulation scheme for PU.

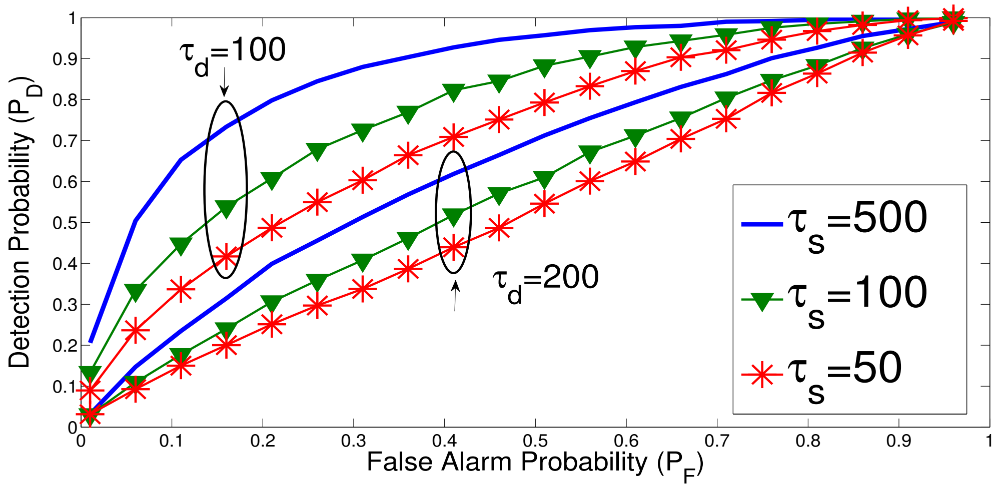

Figure 8.4: ROC for the modified i-AVCD at $N = 30$, $M = 2$, $P = 0.1$ $\tau_s = 50, 100, 500$ and $\tau_d = 100, 200$.

corresponding values of TPM. In fact, the TPM is a function of τ_s and τ_d as shown in (8.2). The variation in γ, conditioned on hypotheses H_o and H_1 for different values of τ_s and τ_d has been shown in Table 8.1. It can be seen that as τ_s in increased from 50 to 500 at $\tau_d = 100$, the γ increases from -3 dB to -0.4 dB, conditioned on hypothesis H_1. The same variation in SNR is also visible conditioned on hypothesis H_o.

In the case of $\tau_d = 200$, the same trend can be noticed. Further, the adverse effect of increasing the value of τ_d from 100 to 200 at a fixed value of $\tau_s = 50$ can also be seen as the γ reduces from -3.8 dB to -7.19 dB, which deteriorates the performance in ROC for the higher value of τ_s. Finally, the positive effect of increasing τ_s from 50 to 500 is more for the lower value of $\tau_d = 100$ compared to the higher value of $\tau_d = 200$.

Finally, the ROC for the conventional detection schemes such as i-AVCD, AVCD and ED is pre-

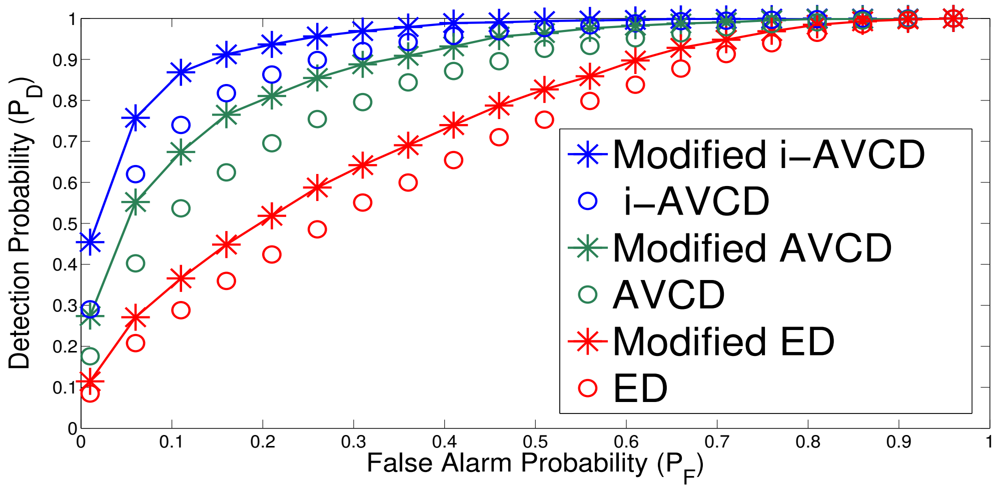

Figure 8.5: ROC for the modified schemes and their conventional counterparts at $N = 50$, $M = 2$, $\gamma = -2$ dB, $\tau_d = 100$ and $\tau_s = 50$.

sented in the same dynamic scenario of the PU. In the case of the conventional detection schemes, Markov parameters τ_d and τ_s are not available for detection of the PU at the cognitive terminal. Figure 8.5 presents the ROC for the modified i-AVCD, modified AVCD and modified ED along with their conventional counterparts of i-AVCD, AVCD and ED. Here, N is assumed to be 50, $M = 2$ and $\gamma = -2$ dB. Further, τ_d and τ_s are assumed to be 100 and 50, respectively. The P is assumed as 0.1. At $P_F = 0.1$, the values of P_D for modified i-AVCD, modified AVCD and modified ED schemes are 0.85, 0.6498 and 0.356, respectively. These values respectively decrease to 0.72, 0.5106 and 0.275 for conventional i-AVCD, AVCD and ED. It can be observed that modified i-AVCD outperforms the conventional i-AVCD. Similar trend is observed for the other two special cases also. It is due to the fact that Markov parameters are assumed to be known at the cognitive terminal, which results in higher average SNR available for the modified i-AVCD scheme compared to the conventional i-AVCD scheme.

8.5 Conclusion

The i-AVCD scheme was presented for multiple transitions of the PU in the sensing interval, assuming additive Laplacian noise environment. Apart from this, the M-QAM modulation scheme was assumed for the PU. The multiple transitions of the PU were modeled by DTMC with underlying parameters of τ_d and τ_s, considered for the idle and active periods of the PU, respectively. The detection scheme i-AVCD was modified by assuming τ_d and τ_s at the detection. For this system, analytical expressions of P_D and P_F were derived. The performance of this system was shown with ROC using simulations. A close match between simulations and their analytical counterparts validated our mathematical analysis. The effect of increasing the modulation order M on the detection performance was explored. Then, a special case of M-QAM was presented at $M = 2$, i.e., BPSK modulation scheme.

Further, special cases of the proposed system were presented by taking exponent $P = 1$ and $P = 2$, corresponding to modified AVCD and modified ED. Conventional detection technique i-AVCD has been used without having any knowledge of parameters τ_d and τ_s at the detection. It is concluded that in the modified i-AVCD scheme, the performance decreases with increasing modulation order M. It is also concluded that the modified i-AVCD scheme outperforms the conventional i-AVCD scheme, wherein the Markov parameters are not known. In the next chapter, we will present modified detection schemes for multiple PU transitions when the channel attenuation possesses Rayleigh distribution.

Chapter 9

Spectrum Sensing for Dynamic PU With Rayleigh Distributed Channel Attenuation in ALN

We propose a real-time scenario of dynamic behavior of the PU with multiple transitions under the Rayleigh Distributed Channel Attenuation (RDCA) for spectrum sensing. We assume MAI as an additive noise which is modeled using Laplacian noise model. Apart from this, we consider higher order modulation scheme such as Quadrature Amplitude Modulation (QAM) with its modulation order M. The Markov chain models the transitions of the PU using transition probabilities (TPs) which are functions of the Markov Chain Parameters (MCPs) τ_s and τ_d. The MCPs are assumed to be known at the receiver. The TPs are used with i-AVCD to get a modified detection scheme, referred to as $\mathcal{M}_r$: i-AVCD. The $\mathcal{M}_r$ refers to the term 'modified' under the effect of MCPs. Special cases, referred to as $\mathcal{M}_r$: AVCD and $\mathcal{M}_r$: ED are formed for the $\mathcal{M}_r$: i-AVCD scheme at $P = 1$ and $P = 2$, respectively. Further, we consider the case of a multiple antenna system at the receiver. We derive closed-form expressions of P_D and P_F. Finally, we present the results using ROC and P_D vs. γ. Our analytical findings are corroborated using a close match between simulations and analytical results. Besides this, the modified schemes have been compared with the conventional schemes. In conventional schemes, no information on MCPs is available at the receiver a priori. We find that the Modified Detection Schemes (MDS) outperform conventional schemes. Further, we observe that performance of MDS degrades as we increase the value of M. We also observe that the spatial diversity improves the performance of the MDS.

9.1 Introduction

Dynamic PU with multiple transitions in the Laplacian noise environment has been presented in Chapter 8, where attenuation was not considered. However, in a practical scenario, it is important to consider channel attenuation in the system. Channel attenuation is a combination of path loss, fading loss and shadowing [175,176]. Time varying attenuation is caused in wideband or frequency selective fading channel [177]. In contrary to this, attenuation is almost constant and possesses the Rayleigh distribution in the narrowband fading or flat-fading channel [178,179].

In this thesis, a modified detection scheme is considered that uses MCPs such as τ_s and τ_d with the i-AVCD scheme to model dynamic behavior of the PU in RDCA. This modified scheme is referred to as $\mathcal{M}_r$: i-AVCD. The $\mathcal{M}_r$ refers to the term 'modified' under the effect of MCPs. It is assumed that PU follows QAM scheme. The modulation order of the QAM is denoted as M and it effects the performance of the scheme. We discuss BPSK as one of the special cases of QAM at a fixed value of $M = 2$. Further, ALN environment is considered. Apart from this, it is assumed that the information on MCPs is available at the SU a priori. The closed-form expressions of P_D and P_F have been derived. Two special cases of $\mathcal{M}_r$: i-AVCD are also discussed at $P = 1$ which corresponds to $\mathcal{M}_r$: AVCD scheme, and $P = 2$ which corresponds to $\mathcal{M}_r$: ED scheme. For the proposed system, simulation results are presented that closely follows their analytical counterparts.

The remaining sections are organized as follows: Section 9.2 presents the system model for dynamic PU with multiple transitions with RDCA. Section 9.3 presents the performance analysis of the MDS. In Section 9.4, we evaluate the performance of the $\mathcal{M}_r$: i-AVCD with a diversity scheme such as EGC. Section 9.5 presents the modified version of the SL-PCA scheme, denoted as $\mathcal{M}_r$: SL-PCA. Section 9.6 presents simulation results before concluding briefly in Section 9.7.

9.2 System Model

In this section, we present dynamic behavior of the PU with multiple random transitions within the sensing period. It is not feasible to have complete absence or presence of PU during hypotheses H_o and H_1. In hypothesis H_o, we assume that for first N_{00} samples, PU is in OFF state. Thereafter, PU transits from OFF state to ON state as shown in (9.1). Similarly, in hypothesis H_1, we assume that for first N_{11} samples, PU is in ON state. Thereafter, PU transits from ON state to OFF state. The ON and OFF states of PU have exponential distribution with respective means as τ_s and τ_d and their corresponding probability density functions of $\frac{1}{\tau_s}\exp(-\frac{x}{\tau_s})$ and $\frac{1}{\tau_d}\exp(-\frac{x}{\tau_d})$ [147].

After sampling of these periods, MCPs such as τ_s and τ_d represent an average of aggregate samples present when PU is in ON and OFF states, respectively. The received symbol at the CR terminal can be represented as

$$
\begin{aligned}
H_o : y_m &= g_{00}^{(L)} n_m \Big|_{m=1,2,\ldots,N_{00}} + g_{01}^{(L)} u_m \Big|_{m=N_{00}+1,N_{00}+2\ldots,N_{00}+N_{01};} \\
H_1 : y_m &= g_{10}^{(L)} n_m \Big|_{m=1,2,\ldots,N10} + g_{11}^{(L)} u_m \Big|_{m=N10+1,N10+2,\ldots,N10+N_{11},}
\end{aligned}
\tag{9.1}
$$

where $u_m = h_m s_m + n_m$, $m = 1, 2, 3, \ldots, N_{\{ij\}}$. Here, $N_{\{ij\}}$ denotes the modified sensing samples with transition probabilities. Further, N denotes the initial aggregate sensing samples such that $N > N_{\{ij\}}$. The s_m represents PU signal with QAM modulation. The h_m denotes the channel attenuation which is static for $N_{\{ij\}}$ samples. Further, it possesses Rayleigh distribution [177]. The n_m denotes the Laplacian noise with its mean and variance of 0 and $2\kappa^2$, respectively. The κ represents the scale parameter of the ALN. Here, n_m models MAI. The respective PDFs of the Laplacian noise and channel attenuation are expressed as

$$
\begin{aligned}
f_{n_m}(x) &= \frac{1}{2\kappa} \exp\left(-\frac{|x|}{\kappa}\right), \\
f_{h_m}(x) &= \frac{x}{\alpha^2} \exp\left(-\frac{x^2}{2\alpha^2}\right),
\end{aligned}
\tag{9.2}
$$

where α is the scale parameter of the RDCA. The $m_{\{ij\}}$ denotes one-step transition probability of the PU from i^{th} state to j^{th} state with $i, j \in \{0, 1\}$ at any value of sampling instant m. The corresponding sensing samples are denoted as $I_{\{ij\}}$. An aggregate of N samples are present initially. Thereafter, PU may randomly transit from i^{th} state to j^{th} state at any instant of $m = N, N-1, N-2 \cdots, N - I_{\{ij\}}$. Hence, one-step transition probability (OSTP) needs to be modified to 'L'-step transition probability (LSTP), where $L = N - m$. The random transitions of PU from one state to another state can be represented in terms of TPs. The OSTPs can be obtained using (8.2). During one step transition, PU transits to state $j \in \{0, 1\}$ conditioned on $i \in \{0, 1\}$ at any two consecutive instants of n. Hence, sensing samples are modified as

$$
I_{ij} = m_{ij} \times N. \tag{9.3}
$$

Further, $I_{00} + I_{01} = N$ and $I_{10} + I_{11} = N$. Similarly, LSTPs can be represented using transition matrix obtained in 8.3. During L step transition, PU transits to state $j \in \{0, 1\}$ conditioned on $i \in \{0, 1\}$ at any instant of sampling $m = 1$ to $I_{\{ij\}}$. Average sensing samples are now modified as

$$
N_{\{ij\}} = I_{\{ij\}}^{(L)} = m_{\{ij\}}^{(L)} \times N. \tag{9.4}
$$

Using (9.4), an aggregate number of modified samples

$$0 < N_{00} + N_{01} < N;$$
$$0 < N10 + N_{11} < N. \tag{9.5}$$

With reference to the hypotheses shown in (9.1), the $\mathcal{M}_r$: i-AVCD scheme can be represented as [97]

$$\Upsilon(\mathbf{y}) \underset{H_o}{\overset{H_1}{\gtrless}} \Psi, \tag{9.6}$$

where

$$\Upsilon(\mathbf{y}) = \sum_{n} m_{\{ij\}}^{(L)} |y_m|^P. \tag{9.7}$$

Under hypothesis H_o, $\Upsilon(\mathbf{y})$ can be represented as

$$\Upsilon(\mathbf{y}) = \sum_{m=1}^{N_{00}} g_{00}^{(L)} |y_m|^P + \sum_{n=N_{00}+1}^{N_{00}+N_{01}} g_{01}^{(L)} |y_m|^P. \tag{9.8}$$

Similarly, under hypothesis H_1, we have

$$\Upsilon(\mathbf{y}) = \sum_{m=1}^{N10} g_{10}^{(L)} |y_m|^P + \sum_{m=N10+1}^{N10+N_{11}} g_{11}^{(L)} |y_m|^P. \tag{9.9}$$

Here, $\mathbf{y} = \left[y_1, y_2, \dots y_{I'_{\{ij\}}}\right]$ and Ψ is the detection threshold obtained using NP approach.

9.3 Performance Analysis

In this section, we derive closed-form expressions of P_F and P_D. The CLT approximates the PDF of $\Upsilon(\mathbf{y})$ to Gaussian distribution [63]. Hence, P_F can be represented as

$$P_F = Pr\Big\{\Upsilon(\mathbf{y}) > \Psi | H_o\Big\} = Q\left(\frac{\Psi - E[\Upsilon(\mathbf{y})|H_o]}{\sqrt{var[\Upsilon(\mathbf{y})|H_o]}}\right). \tag{9.10}$$

Similarly, P_D can be represented as

$$P_D = Pr\Big\{\Upsilon(\mathbf{y}) > \Psi | H_1\Big\} = Q\left(\frac{\Psi - E[\Upsilon(\mathbf{y})|H_1]}{\sqrt{var[\Upsilon(\mathbf{y})|H_1]}}\right), \tag{9.11}$$

where $Q(\cdot)$ represents the Q-function with $Q(v) = \frac{1}{\sqrt{2\pi}} \int_v^{+\infty} \exp\left(-\frac{t^2}{2}\right) dt$. The $E[\Upsilon(\mathbf{y})|H_o]$ and $var[\Upsilon(\mathbf{y})|H_o]$ denote the mean and variance under hypothesis H_o. Similarly, mean and variance under hypothesis H_1 are denoted as $E[\Upsilon(\mathbf{y})|H_1]$ and $var[\Upsilon(\mathbf{y})|H_1]$, respectively. The detection threshold Ψ

corresponding to P_F can be obtained from (9.10). Subsequently, we derive the expression of P_D.

9.3.1 Average SNR under H_o and H_1

Under hypothesis H_o, noise power P_n can be represented as

$$\begin{aligned} P_n = 2\kappa^2 \bigg\{ & {g_{00}}^{2\left(N-1\right)} + {g_{00}}^{2\left(N-2\right)} + \cdots + {g_{00}}^{2\left(N-N_{00}\right)} + {g_{01}}^{2\left(N-N_{00}\right)} \\ & + {g_{01}}^{2\left(N-N_{00}-1\right)} + \cdots + {g_{01}}^{2\left(N-N_{00}-N_{01}\right)} \bigg\}. \end{aligned} \tag{9.12}$$

Similarly, signal power P_s can be represented as

$$\begin{aligned} P_s &= \sum_{m=N_{00}+1}^{N_{00}+N_{01}} E\left[\left\{ {g_{01}}^{(L)} s_m \right\}^2\right] \\ &= \frac{2\alpha^2 f_o^2 E_s}{M} \left\{ {g_{01}}^{2\left(N-N_{00}\right)} + {g_{01}}^{2\left(N-N_{00}-1\right)} + \cdots + {g_{01}}^{2\left(N-N_{00}-N_{01}\right)} \right\}, \end{aligned} \tag{9.13}$$

where E_s denotes the energy of the QAM modulated PU signal. The respective derivations of P_n and P_s are given in (V.1) and (V.2) of Appendix V. The normalizing factor of modulated PU signal can be represented as [174]

$$f_o = \begin{cases} \sqrt{\frac{3}{2(M-1)}}, \text{for QPSK, 16-QAM, 64-QAM;} \\ 1, \qquad\quad \text{for BPSK} \end{cases} \tag{9.14}$$

where M is assumed as 2, 4, 16, and 64 representing BPSK, QPSK, 16-QAM, and 64-QAM, respectively.

Similarly, under hypothesis H_1, P_n and P_s can be represented as

$$\begin{aligned} P_n = 2\kappa^2 \bigg\{ & {g_{10}}^{2\left(N-1\right)} + {g_{10}}^{2\left(N-2\right)} + \cdots + {g_{10}}^{2\left(N-N10\right)} + {g_{11}}^{2\left(N-N10\right)} \\ & + {g_{11}}^{2\left(N-N10-1\right)} + \cdots + {g_{11}}^{2\left(N-N10-N_{11}\right)} \bigg\}; \\ P_s = \frac{2\alpha^2 f_o^2 E_s}{M} & \left\{ {g_{11}}^{2\left(N-N10\right)} + {g_{11}}^{2\left(N-N10-1\right)} + \cdots + {g_{11}}^{2\left(N-N10-N_{11}\right)} \right\}. \end{aligned} \tag{9.15}$$

The respective derivations of P_n and P_s are given in (V.3) and (V.4) of Appendix B. Finally, the ratio of P_s and P_n yields the average SNR as

$$\gamma = P_s/P_n. \tag{9.16}$$

9.3.2 Mean and variance of $\Upsilon(\mathbf{y})$

Now, mean under hypothesis H_o can be expressed as

$$E[\Upsilon(\mathbf{y})] = \Phi_o \sum_{m=1}^{N_{00}} g_{00}^{(L)} + \Phi_1 \sum_{m=N_{00}+1}^{N_{00}+N_{01}} g_{01}^{(L)}. \tag{9.17}$$

The Φ_o and Φ_1 can be derived as

$$\begin{aligned}
&\Phi_o = \kappa^P \Gamma\big(P+1\big),\\
&\Phi_1 = \exp\big(-u^P\big)\Gamma\big(P+1,u\big)ln\big(|u|\big)\exp\big(-u^P\big)\\
&\quad + \exp\big(-u^P\big)\Gamma\big(P+1\big) + \exp\big(-a^P\big)\Gamma\big(P+1,a\big)ln\big(|a|\big)H\left(a^{P+1},\frac{1}{2},u^{P+1}\right),
\end{aligned} \tag{9.18}$$

where

$$\begin{aligned}
u &= \frac{\alpha^2\phi_o\sqrt{\gamma}}{2\kappa^2}; a = \frac{\alpha\phi_o\sqrt{\gamma}}{\sqrt{2}\kappa},\\
\phi_o &= \sum_{m=1}^{\frac{\sqrt{M}}{2}} b_o f_o(2m-1); b_o = log_2(M),\\
H(u,v,w) &= \frac{1}{\Gamma(u)}\bigg\{\int_0^\infty e^{-wt}t^{u-1}(1+t)^{v-u-1}dt\bigg\}.
\end{aligned} \tag{9.19}$$

Here, H(u,v,w) is the confluent hypergeometric function [77]. Similarly, under hypothesis H_o, variance can be expressed as

$$var[\Upsilon(\mathbf{y})] = \sigma_o^2 \sum_{m=1}^{N_{00}} \left\{g_{00}^{(L)}\right\}^2 + \sigma_1^2 \sum_{m=N_{00}+1}^{N_{00}+N_{01}} \left\{g_{01}^{(L)}\right\}^2, \tag{9.20}$$

where σ_o^2 and σ_1^2 can be derived as

$$\begin{aligned}
&\sigma_o^2 = \kappa^{2P}\left(\Gamma(2P+1) - \Gamma^2(P+1)\right),\\
&\sigma_1^2 = \exp\big(-u^{2P}\big)\Gamma\big(2P+1,u\big)ln\big(|u|\big)\exp\big(-u^{2P}\big) + \exp\big(-u^{2P}\big)\Gamma\big(2P+1\big) + \exp\big(-a^{2P}\big)\\
&\quad \Gamma\big(2P+1,a\big)ln\big(|a|\big)H\left(a^{2P+1},\frac{1}{2},u^{2P+1}\right) - \Phi_1^2.
\end{aligned} \tag{9.21}$$

Similar steps are followed to obtain the mean and variance of $\Upsilon(\mathbf{y})$ under hypothesis H_1. We have

$$\begin{aligned}
E[\Upsilon(\mathbf{y})] &= \Phi_o \sum_{m=1}^{N10} g_{10}^{(L)} + \Phi_1 \sum_{m=N10+1}^{N10+N_{11}} g_{11}^{(L)},\\
var[\Upsilon(\mathbf{y})] &= \sigma_o^2 \sum_{m=1}^{N10} \left\{g_{10}^{(L)}\right\}^2 + \sigma_1^2 \sum_{m=N10+1}^{N10+N_{11}} \left\{g_{11}^{(L)}\right\}^2.
\end{aligned} \tag{9.22}$$

The Algorithm 1 presents $\mathcal{M}_r$: i-AVCD based sensing scheme.

Algorithm 1 $\mathcal{M}_r$: i-AVCD based sensing scheme for dynamic PU with multiple transitions

Require: $\{N, P, \kappa\} \geq 0$;
Require: g_{00}, g_{01}, g_{10} and g_{11} ▷ For fixed τ_s and τ_d using (8.2)
Calculate $I_{\{ij\}}$ using (9.3) ▷ $I_{00} + I_{01} = N$; $I_{10} + I_{11} = N$
for $m = I_{\{ij\}}, I_{\{ij\}} + 1, \cdots, N$ **do**
  L=N-m
  Calculate $m^{L}_{\{ij\}}$
  Calculate $N_{\{ij\}}$= $N\{m^{L}_{\{ij\}}\}$
Generate $n_m = [w_1, w_2, \cdots w_{\{N_{\{ij\}}\}}]$ and $u_m = [u_1, u_2, \cdots u_{\{N_{\{ij\}}\}}]$.
for $i = 1, 2, \cdots$, length(P_F) **do**
  true_decision=0. ▷ initial variable for true detection
  Evaluate Ψ using (9.10).
  for $j = 1, 2, \cdots, M$ **do**
    Generate y_m from (9.1). ▷ There will be $N10$ values of n_m and N_{11} values of u_m
    final_decision_statistic=0.
    for m **do**=1: $N_{\{ij\}}$ ▷ $ij = 10$
      decision_statistic=$|n_m(m)|^P$
      for m **do**=1: $N_{\{ij\}}$ ▷ $ij = 11$
        decision_statistic=$|y_m(m)|^P$
        final_decision_statistic=final_decision_statistic+decision_statistic.
    if final_decision_statistic$\geq$ Ψ **then**
      true_decision=true_decision+1
  $P_D(i)$=true_decision/M. ▷ detection Probability at each value of P_F

9.4 EGC with $\mathcal{M}_r$: i-AVCD

In this section, we analyze the performance of EGC with $\mathcal{M}_r$: i-AVCD scheme when SU is equipped with K number of receiver antennas. We have neglected the correlation between antennas. Further, it is assumed that channel attenuation is independent for all antennas. The system model can be represented as

$$\begin{aligned} H_o : y_{m,k'} &= g^{(L)}_{00} w_{m,k'}\Big|_{m=1,2,\ldots,N_{00}} + g^{(L)}_{01} u_{m,k'}\Big|_{m=N_{00}+1,N_{00}+2\ldots,N_{00}+N_{01};} \\ H_1 : y_{m,k'} &= g^{(L)}_{10} w_{m,k'}\Big|_{m=1,2,\ldots,N10} + g^{(L)}_{11} u_{m,k'}\Big|_{m=N10+1,N10+2,\ldots,N10+N_{11},} \end{aligned} \tag{9.23}$$

where $k' = 1, 2, \ldots, K$. All K antennas present at the receiver combines the received observations over sensing period. The decision statistic can be represented as

$$\Upsilon(\mathbf{y}) = \sum_{n} \left\{ \sum_{k'=1}^{K} m^{(L,k')}_{\{ij\}} |y_{m,k'}|^P \right\}. \tag{9.24}$$

Under hypothesis H_o, $\Upsilon(\mathbf{y})$ can be represented as

$$\Upsilon(\mathbf{y}) = \sum_{n=1}^{N_{00}} \left\{ \sum_{k'=1}^{K} g^{(L,k')}_{00} |y_{m,k'}|^P \right\} + \sum_{n=N_{00}+1}^{N_{00}+N_{01}} \left\{ \sum_{k'=1}^{K} g^{(L,k')}_{01} |y_{m,k'}|^P \right\}. \tag{9.25}$$

Similarly, under hypothesis H_1, we have

$$\Upsilon(\mathbf{y}) = \sum_{n=1}^{N10} \left\{ \sum_{k'=1}^{K} g_{10}^{(L,k')} |y_{m,k'}|^P \right\} + \sum_{n=N10+1}^{N10+N_{11}} \left\{ \sum_{k'=1}^{K} g_{11}^{(L,k')} |y_{m,k'}|^P \right\}. \tag{9.26}$$

Finally, the EGC with $\mathcal{M}_r$: i-AVCD scheme can be represented as

$$\Upsilon(\mathbf{y}) \underset{H_o}{\overset{H_1}{\gtrless}} \Psi, \tag{9.27}$$

where Ψ is the detection threshold obtained using NP approach. The mean and variance under H_o can be represented as

$$\begin{aligned} E[\Upsilon(\mathbf{y})] &= \Phi_o' \sum_{m=1}^{N_{00}} g_{00}^{(L)} + \Phi_1' \sum_{m=N_{00}+1}^{N_{00}+N_{01}} g_{01}^{(L)}, \\ var[\Upsilon(\mathbf{y})] &= \sigma_o^{2'} \sum_{m=1}^{N_{00}} \left\{ g_{00}^{(L)} \right\}^2 + \sigma_1^{2'} \sum_{m=N_{00}+1}^{N_{00}+N_{01}} \left\{ g_{01}^{(L)} \right\}^2, \end{aligned} \tag{9.28}$$

where $\Phi_o' = K\Phi_o$, $\Phi_1' = K\Phi_1$, $\sigma_o^{2'} = K\sigma_o^2$ and $\sigma_1^{2'} = K\sigma_1^2$. Similarly, under hypothesis H_1, we have

$$\begin{aligned} E[\Upsilon(\mathbf{y})] &= \Phi_o \sum_{m=1}^{N10} g_{10}^{(L)} + \Phi_1 \sum_{m=N10+1}^{N10+N_{11}} g_{11}^{(L)}, \\ var[\Upsilon(\mathbf{y})] &= \sigma_o^{2'} \sum_{m=1}^{N10} \left\{ g_{10}^{(L)} \right\}^2 + \sigma_1^{2'} \sum_{m=N10+1}^{N10+N_{11}} \left\{ g_{11}^{(L)} \right\}^2. \end{aligned} \tag{9.29}$$

The mean and variance under both hypotheses for $\mathcal{M}_r$: AVCD can be obtained by substituting $P = 1$ in (9.28) and (9.29). Similarly, the mean and variance for $\mathcal{M}_r$: ED can be found by substituting $P = 2$ in (9.28) and (9.29).

9.5 $\mathcal{M}_r$: SL-PCA

The SL-PCA has been proposed as an improved detection scheme for a multiple antenna system for static PU. The PU signal distorted with ALN is passed through a soft-limiter. Using SL-PCA, decision statistic can be expressed as [117]

$$\Upsilon(\mathbf{y}) = \sum_{n=1}^{N} \left\{ \sum_{k'=1}^{K} F_S(y_{m,k'}) \right\}^2, \tag{9.30}$$

where soft limiting function $F_S(v)$ can be expressed as

$$F_S(v) = \begin{cases} 1, & S < v \\ \frac{1}{S}v, & -S \leqslant v \leqslant S \\ -1, & v < -S. \end{cases} \tag{9.31}$$

The S denotes the degree of softness. With an increase in S, the limiter becomes softer and probability of detection increases. We modify the SL-PCA detection scheme for the dynamic PU environment. We call it $\mathcal{M}_r$: SL-PCA detection scheme. Hence, the modified decision statistic can be represented as

$$\Upsilon(\mathbf{y}) = \sum_n m_{\{ij\}}^{(L)} \left\{ \sum_{k'=1}^{K} F_S(y_{m,k'}) \right\}^2 . \tag{9.32}$$

Under hypothesis H_o, $\Upsilon(\mathbf{y})$ can be represented as

$$\Upsilon(\mathbf{y}) = \sum_{n=1}^{N_{00}} g_{00}^{(L,k')} \left\{ \sum_{k'=1}^{K} F_S(y_{m,k'}) \right\}^2 + \sum_{n=N_{00}+1}^{N_{00}+N_{01}} g_{01}^{(L,k')} \left\{ \sum_{k'=1}^{K} F_S(y_{m,k'}) \right\}^2 . \tag{9.33}$$

Similarly, under hypothesis H_1, we have

$$\Upsilon(\mathbf{y}) = \sum_{n=1}^{N10} g_{10}^{(L,k')} \left\{ \sum_{k'=1}^{K} F_S(y_{m,k'}) \right\}^2 + \sum_{n=N10+1}^{N10+N_{11}} g_{11}^{(L,k')} \left\{ \sum_{k'=1}^{K} F_S(y_{m,k'}) \right\}^2 . \tag{9.34}$$

The mean and variance of (9.33) and (9.34) can be derived in the same way as obtained in Section 9.3.2. Finally, the $\mathcal{M}_r$: SL-PCA scheme can be represented as

$$\Upsilon(\mathbf{y}) \underset{H_o}{\overset{H_1}{\gtrless}} \Psi, \tag{9.35}$$

where Ψ is the detection threshold obtained using NP approach.

9.6 Simulation Results

In this section, we present the performance of the modified schemes such as $\mathcal{M}_r$: i-AVCD, $\mathcal{M}_r$: AVCD, and $\mathcal{M}_r$: ED with receiver operating characteristics (ROC) and P_D vs. γ using Monte Carlo simulations. Further, α and S are assumed to be 5 and 0.2, respectively, throughout the simulations. The values of g_{00} and g_{01} are determined as 0.03 and 0.0003, respectively. Similarly, the corresponding values of g_{10} and g_{11} are 0.0006 and 0.0294. We assume RDCA for the considered detection schemes. Using (9.10), we obtain detection threshold Ψ for corresponding values of P_F. Finally, using (9.11), we obtain P_D. Without loss of generality, we assume the values of E_s and κ to be 1 for simulations. Under hypothesis H_o and H_1, total number of PU transitions are $N_{01} + 1$ and $N10 + 1$, respectively [146].

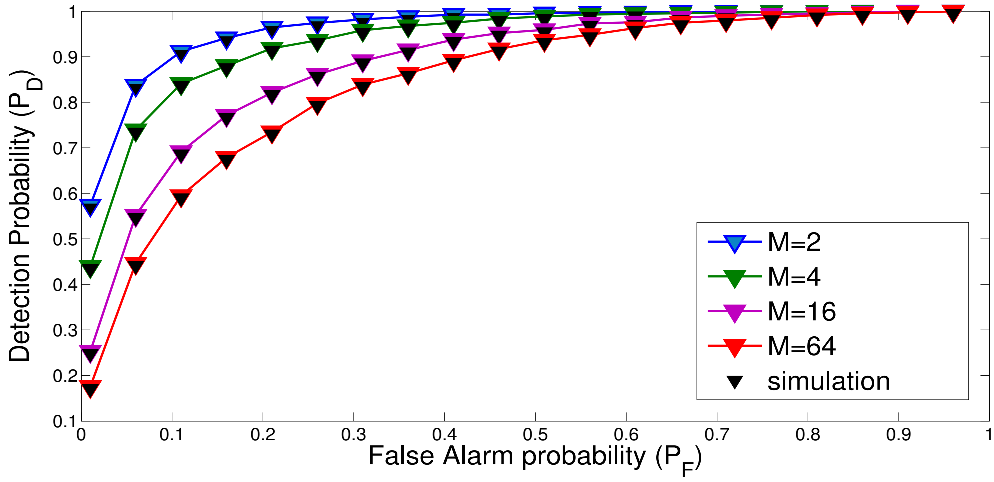

Figure 9.1: ROC using $\mathcal{M}_r$: i-AVCD with RDCA for QAM schemes at $\tau_s = 50$, $\tau_d = 100$, $N = 100$, $\gamma = -2$ dB.

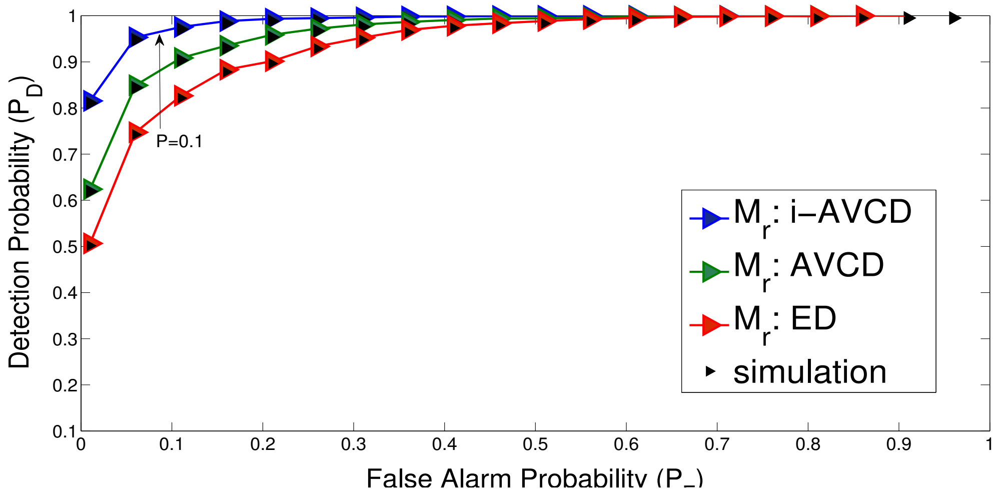

Figure 9.2: ROC for the MDS with RDCA at $\tau_s = 50$, $\tau_d = 100$, $N = 50$, $\gamma = 2$ dB and $M = 2$.

Figure 9.1 presents ROC using $\mathcal{M}_r$: i-AVCD scheme ($P = 0.1$) for different values of modulation order $M = 2$, 4, 16 and 64. We assume $\tau_s = 50$ and $\tau_d = 100$. Further, γ and N is assumed to be -2 dB and 100, respectively. We observe that simulations closely match with analytical results. The performance of the scheme improves with decrease in the value of M. It is due to the fact that as M increases, constellation points of the QAM schemes comes closer. Thus, mean and variance of the proposed $\mathcal{M}_r$: i-AVCD based decision statistic are adversely effected. It results in decrease in the value of P_D with increase in M.

Figure 9.2 presents ROC for $\mathcal{M}_r$: i-AVCD ($P = 0.1$), $\mathcal{M}_r$: AVCD ($P = 1$) and $\mathcal{M}_r$: ED ($P = 2$). For this, we assume $N = 50$, $\tau_s = 50$ and $\tau_d = 100$. Further, γ is assumed as 2 dB. Besides this, we also assume the BPSK modulation scheme , i.e., $M = 2$ for the PU. Using P_F and P_D obtained in (9.10) and (9.11), respectively, ROC is presented. At $P_F = 0.1$, the respective values of P_D for

$\mathcal{M}_r$: i-AVCD, $\mathcal{M}_r$: AVCD and $\mathcal{M}_r$: ED schemes are 0.967, 0.851 and 0.756. The $\mathcal{M}_r$: i-AVCD

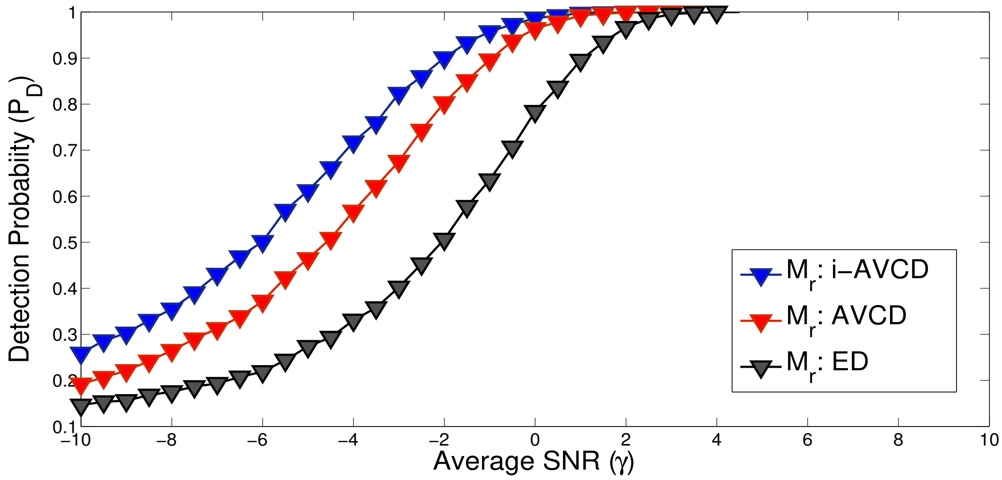

Figure 9.3: P_D vs. SNR for MDS with RDCA at $\tau_s = 50$, $\tau_d = 100$, $N = 100$, $P_F = 0.1$ dB and $M = 2$.

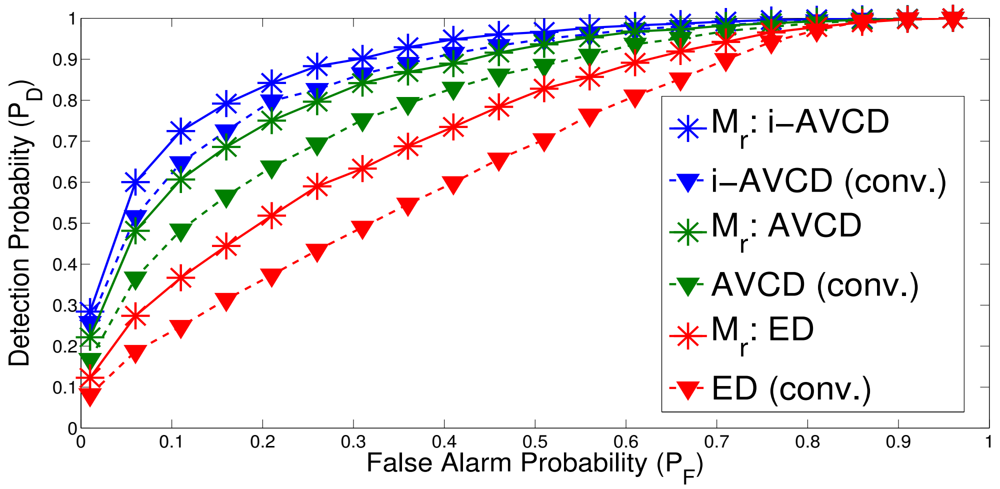

Figure 9.4: ROC for the MDS and their conventional counterparts at $N = 50$, $P = 0.1$, $\gamma = -2$ dB and $M = 2$.

outperforms its special cases of $P = 1$ and $P = 2$, which corresponds $\mathcal{M}_r$: AVCD and $\mathcal{M}_r$: ED, respectively. The fact that simulation results closely match their analytical counterparts validates our interpretation of the CLT.

Figure 9.3 presents P_D vs. SNR plot of MDS such as $\mathcal{M}_r$: i-AVCD, $\mathcal{M}_r$: AVCD and $\mathcal{M}_r$: ED. The range of SNR γ is from -10 to 10 dB. We assume P_F to be 0.1. Further, it is assumed that $\tau_d = 100$, $\tau_s = 50$ and $M = 2$. We observe that $\mathcal{M}_r$: i-AVCD outperforms $\mathcal{M}_r$: AVCD and $\mathcal{M}_r$: ED over a wide range of γ.

We present ROC of the modified schemes such as $\mathcal{M}_r$: i-AVCD, $\mathcal{M}_r$: AVCD and $\mathcal{M}_r$: ED along with their conventional counterparts in Figure 9.4. In conventional schemes, we assume that no information on MCPs τ_s and τ_d is available at the SU a priori. Here, N is assumed to be 50. Further, we assume $\tau_d = 100$, $\tau_s = 50$, $\gamma = -2$ dB and $M = 2$. For the $\mathcal{M}_r$: i-AVCD, we have assumed the value of P as 0.1. We observe that $\mathcal{M}_r$: i-AVCD outperforms its conventional counterpart. The two special cases considered likewise show a similar trend. For modified schemes, higher average SNR is available than the conventional schemes since MCPs are assumed to be known at the cognitive terminal a priori.

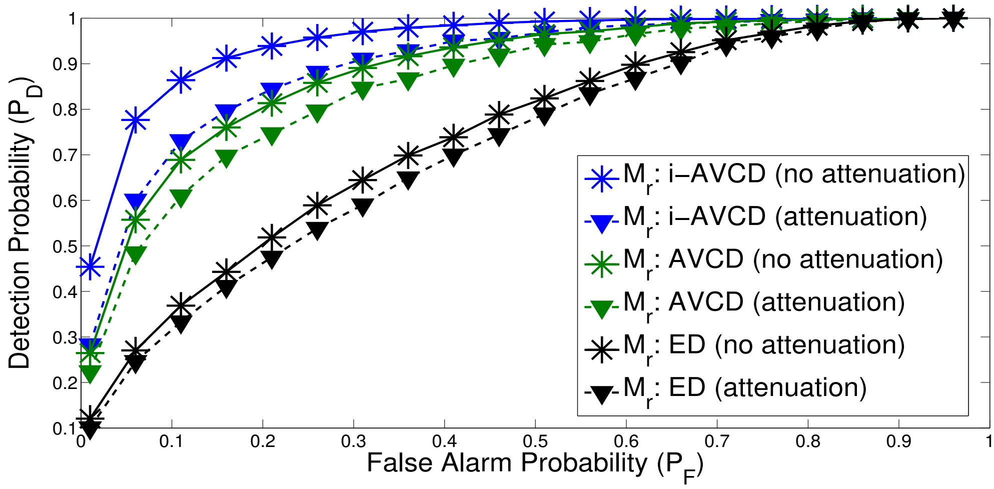

Figure 9.5: ROC for the MDS showing the effect of attenuation and non-attenuation at $N = 50$, $\tau_d = 100$, $\tau_s = 50$, $\gamma = -2$ dB and $M = 2$.

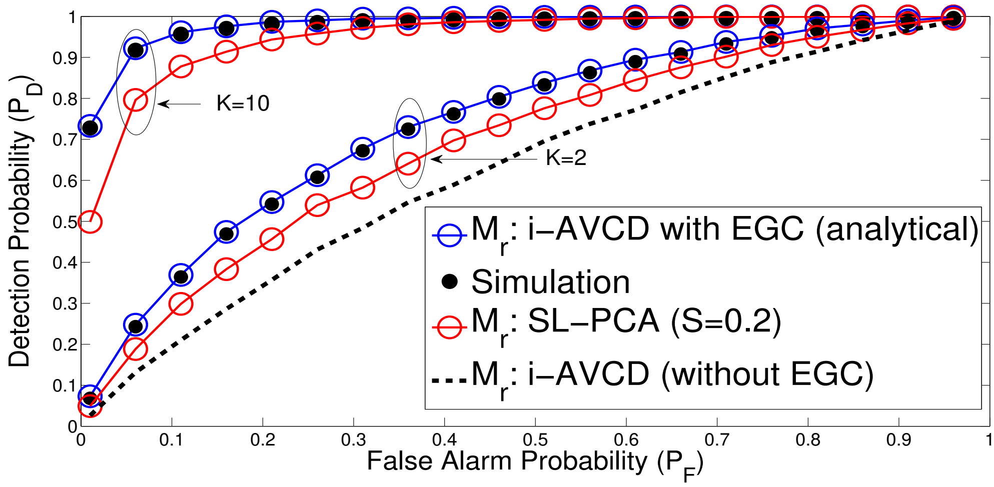

Figure 9.6: ROC for the $\mathcal{M}_r$: i-AVCD with EGC and $\mathcal{M}_r$: SL-PCA for different K at $N = 50$, $S = 0.2$ and $\gamma = -10$ dB.

We compare the performance of MDS assuming both channel attenuation and non-attenuation scenarios and present the results with ROC in Figure 9.5. In a non-attenuation scenario, the channel coefficient h_m is assumed as 1. Further, N is assumed as 50. Further, we assume $\tau_d = 100$, $\tau_s = 50$, $\gamma = -2$ dB and $M = 2$. We observe that the performance of MDS without channel attenuation outperforms the attenuation counterparts as expected.

Finally, we consider a multiple antenna scenario at the CR terminal, where a CR is equipped with K number of receiver antennas. We have neglected correlation between antennas. We use diversity schemes such as EGC followed by $\mathcal{M}_r$: i-AVCD scheme at the CR terminal. Further, we also modify the prevailing SL-PCA detection scheme for the dynamic PU scenario and call it $\mathcal{M}_r$: SL-PCA detection scheme. We observe that performance of the scheme improves with an increase in the number of antennas K. Figure 9.6 presents the performance of $\mathcal{M}_r$: i-AVCD with EGC and $\mathcal{M}_r$: SL-PCA detection schemes for $K = 2$ and $K = 10$. We assume $\tau_d = 100$, $\tau_s = 10$ and $\gamma = -10$ dB. It is observed that the performance significantly improves with diversity schemes such as $\mathcal{M}_r$: i-AVCD with EGC and $\mathcal{M}_r$: SL-PCA with an increase in the number of receiver antennas at a low value of SNR.

9.7 Conclusion

We considered multiple PU transitions in the sensing interval with the $\mathcal{M}_r$: i-AVCD spectrum sensing technique, assuming ALN environment. We also assumed Rayleigh distribution to model the channel attenuation. For PU, we assumed QAM modulation scheme with its modulation order M. The underlying MCPs τ_d and τ_s were considered while modeling the random transitions of the PU. Further, the assumption of MCPs at the cognitive terminal modified the i-AVCD scheme. We derived closed-form expressions of P_D and P_F for the MDS. We have shown the performance of the MDS using ROC and P_D vs. average SNR. Our mathematical analyses were validated by simulations that closely matched with their analytical counterparts. We presented the effect of M on ROC for $\mathcal{M}_r$: i-AVCD scheme. We considered the BPSK modulation scheme as one of the special cases of QAM at a fixed value of $M = 2$. Further, we discussed special cases of $P = 1$ which corresponds to $\mathcal{M}_r$: AVCD, and $P = 2$ which corresponds to $\mathcal{M}_r$: ED schemes. We also discussed the conventional detection technique for $\mathcal{M}_r$: i-AVCD with an assumption that MCPs τ_d and τ_s are not available at the cognitive terminal a priori. We compared the effect of increasing the number of receiver antennas K on the detection performance. We conclude that the ROC for the $\mathcal{M}_r$: i-AVCD scheme improves as M decreases and vice-versa. We also conclude that the performance of the $\mathcal{M}_r$: i-AVCD scheme improves with an increase in the number of receiver antennas K. Further, the $\mathcal{M}_r$: i-AVCD scheme outperforms its conventional counterpart. Finally, we observe that the channel attenuation deteriorates the performance of the considered modified scheme.

Chapter 10

Conclusion

In this section, we present a brief conclusion of our research work.

Spectrum sensing in cognitive radio is a challenging topic for the effective utilization of the licensed spectrum. We have considered seven different system models of spectrum sensing, assuming additive Laplacian noise environment. In the first two models, we assumed the static behavior of the PU and used modified versions of the coherent detector (MCD). More precisely, in the MCD, we have used exponent P in the detection variable, where $0 < P \leq 2$. Using simulations, we observed that the ROC performance improves for $P < 1$ up to optimum value P_o. Below P_o, no significant improvement was achieved. Subsequently, we improved the detection performance by using a centralized CSS scheme. In this scheme, each surrounding CR performed localized sensing using the MCD scheme. Then, they sent their hard decisions to the fusion center, where all the received decisions were logically combined according to fusion schemes such as CSS: AND, CSS: OR and CSS: majority. We conclude that CSS: OR outperformed the other two fusion schemes. Next, in order to deal with the real communication scenario, we shifted our focus from the case of static PU to dynamic PU. Here, we assumed that the PU is not known. The rate of random arrival and/or departure rate of the PU followed the Poisson process. In this case, the probability of the non-arrival of the PU followed the Poisson distribution. We considered the i-AVCD scheme, with AVCD and ED as its special cases at $P = 1$ and $P = 2$, respectively. Next, we improved the performance of the i-AVCD scheme in the dynamic PU scenario using the CSS scheme. The performance was improved over a specified range of γ in the case of CSS: majority fusion scheme. Next, we increased the number of transitions of the PU from 1 to 2. We estimated the LSCP of the PU. Then, we use the samples available from the LSCP to the end of sensing samples to detect the PU. We conclude that the i-AVCD scheme outperformed the prevailing SMD and ED schemes. Next, we extend our work from two PU transitions to multiple PU transitions. In this work, multiple PU transitions were modeled using Markov parameters. We assumed M-QAM modulation for the PU. It was assumed that Markov parameters were known to the receiver. The i-AVCD with Markov parameters was referred to as Modified i-AVCD. We conclude that the modified i-AVCD and its two special cases such as modified AVCD and modified ED outperformed corresponding conventional schemes such as i-AVCD, AVCD and ED. Finally, we assumed random channel attenuation modeled by Rayleigh distribution, in the dynamic PU environment. Here also, we assumed multiple transitions of PU using Markov parameters. We also used diversity techniques such as EGC and SL-PCA to further improve the detection performance. We conclude that the performance of modified i-AVCD deteriorates due to the presence of attenuation coefficients. However, the performance was improved using SL-PCA and EGC. In the case of the Poisson distribution, we derived the closed-form expressions of P_F and plot the ROC using simulations. For other cases, we derived closed-form expressions of P_D and P_F and shown the ROC. We also presented simulation results and found a close match between analysis and simulation results.

10.1 Future Scope

In this section, we discuss the future scope of our work discussed above.

- The Laplacian noise is a special case of generalized noises such as McLeish noise and GGN. Besides this, these noises also model several other impulsive noises such as Dirac Delta noise and specific atmospheric noise. Hence, further research could look into considering these generalized noises to model dynamic PU.

- In the considered system models for spectrum sensing (Chapter 3-8), the effect of channel fading is not considered. However, in Chapter 9, the Rayleigh distributed channel attenuation is considered. It would be highly interesting to include the effect of channel fading in the system model for modeling of the dynamic PU.

- In Chapter 9, a multiple antenna scenario at the CR is considered. One can also consider a multiple antenna scenario at the PU. The application of Multiple Input Multiple Output (MIMO) transmit-receive diversity techniques in such a scenario would be an interesting area to explore.

- The cooperative spectrum sensing scheme (CSS) is explored using hard decision fusion at the fusion center. However, one can also investigate the soft decision fusion scheme of CSS for dynamic PU.

- We have focused on modeling of the transition of the PU using different dynamic parameters such as arrival and/or departure rate, Markov parameters, etc. In practice, another factor such as the Doppler effect also affects the detection performance. It would be interesting to consider the Doppler effect in spectrum sensing.

Appendix I

Appendix: Derivation of mean and variance under H_o and H_1

In this section, we include proofs of $E\Big[w_1^P\Big]$, $var\Big[w_1^P\Big]$, $E\big[u_1^P\big]$ and $var\Big[u_1^P\Big]$.

I.1 Proof of expectation $E\Big[w_1^P\Big]$

$$
\begin{aligned}
E\Big[w_1^P\Big] &= \int_{-\infty}^{\infty} x^P f_{w_1}(x)dx \\
&= \frac{1}{2\kappa\sqrt{\gamma}}\Bigg\{\underbrace{\int_{-\infty}^{0} x^P \exp\bigg(-\frac{|x|}{\kappa\sqrt{\gamma}}\bigg)dx}_{\beta_1} + \underbrace{\int_{0}^{\infty} x^P \exp\bigg(-\frac{|x|}{\kappa\sqrt{\gamma}}\bigg)dx}_{\beta_2}\Bigg\},
\end{aligned} \tag{I.1}
$$

where f_{w_1} represents the PDF of w_1. Now, β_1 and β_2 can be solved as

$$
\begin{aligned}
\beta_1 &= \int_{-\infty}^{0} x^P \exp\bigg(-\frac{|x|}{\kappa\sqrt{\gamma}}\bigg)dx \\
&= \int_{-\infty}^{0} x^P \exp\bigg(\frac{x}{\kappa\sqrt{\gamma}}\bigg)dx.
\end{aligned} \tag{I.2}
$$

Let $\frac{x}{\kappa\sqrt{\gamma}} = -t$, $dx = -\kappa\sqrt{\gamma}dt$, hence (I.2) can be expressed as

$$
\begin{aligned}
\beta_1 &= \int_{\infty}^{0} -\exp(-t)\kappa\sqrt{\gamma}(-t\kappa\sqrt{\gamma})^P dt \\
&= \int_{0}^{\infty} \exp(-t)\sqrt{\gamma}^{P+1}(-t)^P\kappa^{P+1}dt \\
&= (-1)^P\kappa^{P+1}\int_{0}^{\infty} \exp(-t)(\sqrt{\gamma})^{P+1}(t)^P dt \\
&= (-1)^P\kappa^{P+1}(\sqrt{\gamma})^{P+1}\Gamma(P+1),
\end{aligned} \tag{I.3}
$$

where $\Gamma\left(v\right)=\int_0^{+\infty}\exp\left(-t\right)t^{v-1}dt$.

From (I.1), β_2 can be expressed as

$$\beta_2=\int_0^{\infty}x^P\exp\left(-\frac{|x|}{\kappa\sqrt{\gamma}}\right)dx. \tag{I.4}$$

Let $\frac{x}{\kappa\sqrt{\gamma}}=t$ in this case, hence $dx=\kappa\sqrt{\gamma}dt$, hence (I.4) can be expressed as

$$\begin{aligned}\beta_2&=\int_0^{\infty}\exp\left(-t\right)\kappa\sqrt{\gamma}(t\kappa\sqrt{\gamma})^Pdt\\&=\int_0^{\infty}\exp\left(-t\right)\kappa^{P+1}\sqrt{\gamma}^{P+1}(t)^Pdt\\&=\Gamma(P+1)\kappa^{P+1}(\sqrt{\gamma})^{P+1}.\end{aligned} \tag{I.5}$$

From (I.1), $E\Big[w_1^P\Big]$ can be expressed as

$$\begin{aligned}E\Big[w_1^P\Big]&=\frac{1}{2\kappa\sqrt{\gamma}}\Big\{\beta_1+\beta_2\Big\}\\&=\frac{1}{2\kappa\sqrt{\gamma}}\Big\{\big(-1\big)^P\Gamma\big(P+1\big)\kappa^{P+1}\big(\sqrt{\gamma}\big)^{P+1}+\Gamma\big(P+1\big)\kappa^{P+1}\big(\sqrt{\gamma}\big)^{P+1}\Big\}\\&=\frac{\kappa^P}{2\sqrt{\gamma}}\Big\{\big(-1\big)^P\Gamma\big(P+1\big)\big(\sqrt{\gamma}\big)^{P+1}+\Gamma\big(P+1\big)\big(\sqrt{\gamma}\big)^{P+1}\Big\}.\end{aligned} \tag{I.6}$$

I.2 Proof of variance $var\Big[w_1^P\Big]$

$$var\Big[w_1^P\Big]=E\Big[w_1^{2P}\Big]-E^2\Big[w_1^P\Big], \tag{I.7}$$

where

$$\begin{aligned}E\Big[w_1^{2P}\Big]&=\int_{-\infty}^{\infty}x^{2P}f_{w_1}\big(x\big)dx\\&=\frac{1}{2\kappa\sqrt{\gamma}}\Bigg\{\underbrace{\int_{-\infty}^{0}x^{2P}\exp\left(-\frac{|x|}{\kappa\sqrt{\gamma}}\right)dx}_{\beta_1^{'}}+\underbrace{\int_0^{\infty}x^{2P}\exp\left(-\frac{|x|}{\kappa\sqrt{\gamma}}\right)dx}_{\beta_2^{'}}\Bigg\}.\end{aligned} \tag{I.8}$$

$\beta_1^{'}$ and $\beta_2^{'}$ can be obtained by applying similar concepts used to solve β_1 and β_2 in (I.3) and (I.5) as

$$\begin{aligned}\beta_1^{'}&=\int_0^{\infty}\big(\sqrt{\gamma}\big)^{2P+1}\kappa^{2P+1}\big(-t\big)^{2P}\exp\left(-t\right)dt\\&=\Gamma\big(2P+1\big)\big(\sqrt{\gamma}\big)^{2P+1}\kappa^{2P+1}\big(-1\big)^{2P}.\end{aligned} \tag{I.9}$$

$$\begin{aligned}
\beta_2^{'} &= \int_0^{\infty} \left(\sqrt{\gamma}\right)^{2P+1} \kappa^{2P+1} t^{2P} \exp\left(-t\right) dt \\
&= \Gamma\left(2P+1\right)\left(\sqrt{\gamma}\right)^{2P+1} \kappa^{2P+1}.
\end{aligned} \tag{I.10}$$

From (I.8), $E\left[w_1^{2P}\right]$ can be represented as

$$\begin{aligned}
E\left[w_1^{2P}\right] &= \frac{1}{2\kappa\sqrt{\gamma}}\left\{\beta_1^{'} + \beta_2^{'}\right\} \\
&= \frac{1}{2\kappa\sqrt{\gamma}}\left\{\Gamma\left(2P+1\right)\left(\sqrt{\gamma}\right)^{2P+1}\kappa^{2P+1}\left(-1\right)^{2P} + \Gamma\left(2P+1\right)\left(\sqrt{\gamma}\right)^{2P+1}\kappa^{2P+1}\right\} \\
&= \frac{\kappa^{2P}}{2\sqrt{\gamma}}\left\{\Gamma\left(2P+1\right)\left(\sqrt{\gamma}\right)^{2P+1}\left(-1\right)^{2P} + \Gamma\left(2P+1\right)\left(\sqrt{\gamma}\right)^{2P+1}\right\}.
\end{aligned} \tag{I.11}$$

In the similar way, $E^2\left[w_1^P\right]$ is obtained by squaring the $E\left[w_1^P\right]$ derived in (I.6). Subsequently, the variance can be calculated by substituting the values of $E^2\left[w_1^P\right]$ and $E\left[w_1^{2P}\right]$ in the expression obtained in (I.7).

I.3 Proof of expectation $E\left[u_1^P\right]$

$$\begin{aligned}
E\left[u_1^P\right] &= \int_{-\infty}^{\infty} x^P f_{u_1}(x) dx \\
&= \frac{1}{2\kappa\sqrt{\alpha_o}}\left\{\underbrace{\int_{-\infty}^{0} x^P \exp\left(-\frac{\left|x-\alpha_o\right|}{\kappa\sqrt{\alpha_o}}\right) dx}_{\xi_1} + \underbrace{\int_{0}^{\infty} x^P \exp\left(-\frac{\left|x-\alpha_o\right|}{\kappa\sqrt{\alpha_o}}\right) dx}_{\xi_2}\right\}.
\end{aligned} \tag{I.12}$$

Now ξ_1 and ξ_2 can be solved as

$$\begin{aligned}
\xi_1 &= \int_{-\infty}^{0} x^P \exp\left(-\frac{\left|x-\alpha_o\right|}{\kappa\sqrt{\alpha_o}}\right) dx \\
&= \int_{-\infty}^{0} x^P \exp\left(\frac{x-\alpha_o}{\kappa\sqrt{\alpha_o}}\right) dx.
\end{aligned} \tag{I.13}$$

Let $\kappa\sqrt{\alpha_o} = c_o$, hence (I.13) can be expressed as

$$\begin{aligned}
\xi_1 &= \int_{-\infty}^{0} x^P \exp\left(\frac{x}{c_o}\right) \exp\left(-\frac{\alpha_o}{c_o}\right) dx \\
&= \exp\left(-\frac{\alpha_o}{c_o}\right) \int_{-\infty}^{0} x^P \exp\left(\frac{x}{c_o}\right) dx \\
&= -\exp\left(-\frac{\alpha_o}{c_o}\right) \int_{0}^{-\infty} x^P \exp\left(\frac{x}{c_o}\right) dx.
\end{aligned} \tag{I.14}$$

Substituting $\frac{x}{c_o} = -t$ and $dx = -c_o dt$, we get

$$\begin{aligned}\xi_1 &= e^{-\frac{\alpha_o}{c_o}} \int_0^{\infty} (-1)^P \exp\left(-t\right) c_o^{P+1} \big(t\big)^P dt \\ &= \big(-1\big)^P \exp\left(\frac{-\alpha_o}{c_o}\right) c_o^{P+1} \Gamma\big(P+1\big).\end{aligned} \tag{I.15}$$

From (I.12), ξ_2 can be expressed as

$$\begin{aligned}\xi_2 &= \int_0^{\infty} x^P \exp\left(-\frac{\big|x-\alpha_o\big|}{\kappa\sqrt{\alpha_o}}\right) dx \\ &= \int_0^{\infty} x^P \exp\left(-\frac{x-\alpha_o}{\kappa\sqrt{\alpha_o}}\right) dx \\ &= \exp\left(\frac{\alpha_o}{c_o}\right) c_o^{P+1} \Gamma\big(P+1\big).\end{aligned} \tag{I.16}$$

From (I.12), $E\Big[u_1^P\Big]$ can be represented as

$$\begin{aligned}E\Big[u_1^P\Big] &= \frac{1}{2\kappa\sqrt{\alpha_o}} \Big\{\xi_1 + \xi_2\Big\}, \\ &= \frac{1}{2\kappa\sqrt{\alpha_o}} \Big\{\big(-1\big)^P \exp\left(-\frac{\alpha_o}{c_o}\right) c_o^{P+1} \Gamma\big(P+1\big) + \exp\left(\frac{\alpha_o}{c_o}\right) c_o^{P+1} \Gamma\big(P+1\big)\Big\} \\ &= \frac{c_o^P}{2} \Big\{\big(-1\big)^P \exp\left(-\frac{\alpha_o}{c_o}\right) \Gamma\big(P+1\big) + \exp\left(\frac{\alpha_o}{c_o}\right) \Gamma\big(P+1\big)\Big\}.\end{aligned} \tag{I.17}$$

I.4 Proof of variance $var\Big[u_1^P\Big]$

$$var\Big[u_1^P\Big] = E\Big[u_1^{2P}\Big] - E^2\Big[u_1^P\Big], \tag{I.18}$$

where

$$\begin{aligned}E\Big[u_1^{2P}\Big] &= \int_{-\infty}^{\infty} x^{2P} f_{u_1}\big(x\big) dx \\ &= \frac{1}{2\kappa\sqrt{\alpha_o}} \Bigg\{ \underbrace{\int_{-\infty}^{0} x^{2P} \exp\left(-\frac{\big|x-\alpha_o\big|}{\kappa\sqrt{\alpha_o}}\right) dx}_{\xi_1'} + \underbrace{\int_0^{\infty} x^{2P} \exp\left(-\frac{\big|x-\alpha_o\big|}{\kappa\sqrt{\alpha_o}}\right) dx}_{\xi_2'} \Bigg\}.\end{aligned} \tag{I.19}$$

ξ_1' and ξ_2' can be derived using similar steps involved in the analytical derivation of ξ_1 and ξ_2 as

$$\begin{aligned}
\xi_1' &= \exp\left(-\frac{\alpha_o}{c_o}\right)\int_0^\infty e^{\frac{-t}{c_o}}\big(-t\big)^{2P}dt \\
&= \big(-1\big)^{2P}\exp\left(-\frac{\alpha_o}{c_o}\right)a^{2P+1}\Gamma\big(2P+1\big). \\
\xi_2' &= \exp\left(\frac{\alpha_o}{c_o}\right)\int_0^\infty e^{\frac{-t}{c_o}}\big(t\big)^{2P}dt \\
&= \exp\left(\frac{\alpha_o}{c_o}\right)a^{2P+1}\Gamma\big(2P+1\big).
\end{aligned} \tag{I.20}$$

From (I.19), $E\Big[u_1^{2P}\Big]$ can be expressed as

$$\begin{aligned}
E\Big[u_1^{2P}\Big] &= \frac{1}{2\kappa\sqrt{\alpha_o}}\Big\{\xi_1' + \xi_2'\Big\} \\
&= \frac{1}{2\kappa\sqrt{\alpha_o}}\left\{\big(-1\big)^{2P}\exp\left(-\frac{\alpha_o}{c_o}\right)c_o^{2P+1}\Gamma\big(2P+1\big) + \exp\left(\frac{\alpha_o}{c_o}\right)c_o^{2P+1}\Gamma\big(2P+1\big)\right\} \\
&= \frac{c_o^{2P}}{2}\left\{\big(-1\big)^{2P}\exp\left(-\frac{\alpha_o}{c_o}\right)\Gamma\big(2P+1\big) + \exp\left(\frac{\alpha_o}{c_o}\right)\Gamma\big(2P+1\big)\right\}.
\end{aligned}$$

$E^2\Big[u_1^P\Big]$ can be obtained by squaring $E\Big[u_1^P\Big]$ derived in (I.17). Finally, variance is derived using the expression given in (I.18).

Appendix II

Appendix: Derivation of mean and variance under H_o' and H_1'

In this section, we include proofs of $E\Big[\Upsilon(\mathbf{y})\Big]$ and $var\Big[\Upsilon(\mathbf{y})\Big]$ under H_o' and H_1'. Here, for convenience, $E\Big[\Upsilon(\mathbf{y})\Big]$ and $var\Big[\Upsilon(\mathbf{y})\Big]$ under H_o' are respectively denoted as $E\Big[\Upsilon(\mathbf{y})|H_o'\Big]$ and $var\Big[\Upsilon(\mathbf{y})|H_o'\Big]$. Similarly, Under H_1', $E\Big[\Upsilon(\mathbf{y})\Big]$ and $var\Big[\Upsilon(\mathbf{y})\Big]$ are respectively denoted as $E\Big[\Upsilon(\mathbf{y})|H_1'\Big]$ and $var\Big[\Upsilon(\mathbf{y})|H_1'\Big]$.

II.1 Proof of $E\Big[\Upsilon(\mathbf{y})|H_o'\Big]$

From (7.6), we have

$$\Upsilon(\mathbf{y}) = \frac{1}{N - l_{scp}}\left(\sum_{m=1}^{N-l_{scp}} (N - l_{scp} - m + 1) y_{N-m+1}\right). \tag{II.1}$$

Expanding the above expression, we get

$$E\Big[\Upsilon(\mathbf{y})|H_o'\Big] = \frac{1}{N - l_{scp}} E\Bigg[(N - l_{scp})n_N + (N - l_{scp} - 1)n_{N-1} + \cdots + n_{l_{scp}+1}\Bigg]. \tag{II.2}$$

As $n_N, n_{N-1}, n_{N-2}\ldots$ are all iid, hence $E\big[n_N\big] = E[n_{N-1}] = \cdots = E\big[n_{l_{scp}+1}\big] = 0$. The above expression of $E\Big[\Upsilon(\mathbf{y})|H_o'\Big]$ can be further simplified as

$$E\Big[\Upsilon(\mathbf{y})|H_o'\Big] = 0.$$

II.2 Proof of $var\Big[\Upsilon(\mathbf{y})|H_o'\Big]$

We have

$$var\Big[\Upsilon(\mathbf{y})|H_o'\Big] = var\left[\frac{1}{N-l_{scp}}\left(\sum_{m=1}^{N-l_{scp}}(N-l_{scp}-m+1)y_{N-m+1}\right)\right]$$
$$= \left(\frac{1}{N-l_{scp}}\right)var\Big[(N-l_{scp})n_N + (N-l_{scp}-1)n_{N-1} + \cdots + n_{l_{scp}+1}\Big]. \quad \text{(II.3)}$$

As $n_N, n_{N-1}, n_{N-2}\ldots$ are all iid, hence $var\big[n_N\big] = var[n_{N-1}\big] = \cdots = var\big[n_{l_{scp}+1}\big] = 2\kappa^2$. The above expression of $var\Big[\Upsilon(\mathbf{y})|H_o'\Big]$ can be further simplified as

$$var\Big[\Upsilon(\mathbf{y})|H_o'\Big] = \frac{2\kappa^2}{(N-l_{scp})^2}\Big[(N-l_{scp})^2(N-l_{scp}-1)^2 + \cdots + 1^2\Big]$$
$$= \frac{2\kappa^2}{(N-l_{scp})^2}\Big[1^2 + 2^2 + \cdots + (N-L_{scp-2})^2 + (N-l_{scp}-1)^2 + (N-l_{scp})^2\Big]$$
$$= \frac{2\kappa^2}{6}\left[\frac{(N-l_{scp}+1)\big\{(2(N-l_{scp})+1\big\}}{N-l_{scp}}\right].$$

As $l_{scp} = \hat{\vartheta}_o'$, the final expression becomes

$$var\Big[\Upsilon(\mathbf{y})|H_o'\Big] = \frac{2\kappa^2}{6}\left[\frac{(N-\hat{\vartheta}_o'+1)\big\{(2(N-\hat{\vartheta}_o')+1\big\}}{N-\hat{\vartheta}_o'}\right]. \quad \text{(II.4)}$$

II.3 Proof of $E\Big[\Upsilon(\mathbf{y})|H_1'\Big]$

We have

$$E\Big[\Upsilon(\mathbf{y})|H_1'\Big] = E\left[\frac{1}{N-l_{scp}}\left(\sum_{m=1}^{N-l_{scp}}(N-l_{scp}-m+1y_{N-m+1}\right)\right]. \quad \text{(II.5)}$$

Expanding the above expression, we get

$$E\Big[\Upsilon(\mathbf{y})|H_1'\Big] = \frac{1}{N-l_{scp}}E\Big[(N-l_{scp})\big\{n_N + C\big\} + (N-l_{scp}-1)\big\{n_{N-1}+C\big\} + \cdots + \big\{n_{l_{scp}+1}+C\big\}\Big].$$

As $n_N, n_{N-1}, n_{N-2}\dots$ are all iid, hence $E\Big[n_N\Big] = E[n_{N-1}\Big] = \cdots = E\Big[n_{l_{scp}+1}\Big] = 0$. The above expression of $E\Big[\Upsilon(\mathbf{y})|H_1'\Big]$ can be further simplified as

$$
\begin{aligned}
E\Big[\Upsilon(\mathbf{y})|H_1'\Big] &= \frac{1}{N-l_{scp}}\Bigg[C(N-l_{scp}) + C(N-l_{scp}-1) + C(N-l_{scp}-2) + \cdots + C\Bigg] \\
&= \frac{C}{N-l_{scp}}\Bigg[(N-l_{scp}) + (N-l_{scp}-1) + (N-l_{scp}-2) + \cdots + 1\Bigg] \\
&= \frac{C}{2}\Bigg\{N-l_{scp}-1\Bigg\}.
\end{aligned}
$$

As $l_{scp} = \hat{\vartheta}_1'$, the final expression becomes

$$
E\Big[\Upsilon(\mathbf{y})|H_1'\Big] = \frac{C}{2}\Bigg\{N-\hat{\vartheta}_1'-1\Bigg\}. \tag{II.6}
$$

II.4 Proof of $var\Big[\Upsilon(\mathbf{y})|H_1'\Big]$

We have

$$
\begin{aligned}
var\Big[\Upsilon(\mathbf{y})|H_1'\Big] &= var\Bigg[\frac{1}{N-l_{scp}}\Bigg(\sum_{m=1}^{N-l_{scp}}(N-l_{scp}-m+1)y_{N-m+1}\Bigg)\Bigg] \\
&= \Bigg(\frac{1}{N-l_{scp}}\Bigg)var\Bigg[(N-l_{scp})\{n_N+C\} + (N-l_{scp}-1)\{n_{N-1}+C\} + \\
&\quad \cdots + \{n_{l_{scp}+1}+C\}\Bigg].
\end{aligned} \tag{II.7}
$$

As $n_N, n_{N-1}, n_{N-2}\dots$ are all iid, hence $var\Big[n_N\Big] = var[n_{N-1}\Big] = \cdots = var\Big[n_{l_{scp}+1}\Big] = 2\kappa^2$. The above expression of $var\Big[\Upsilon(\mathbf{y})|H_1'\Big]$ can be further simplified as

$$
\begin{aligned}
var\Big[\Upsilon(\mathbf{y})|H_1'\Big] &= \frac{2\kappa^2}{(N-l_{scp})^2}\Bigg[(N-l_{scp})^2 + (N-l_{scp}-1)^2 + \cdots + 1^2\Bigg] \\
&= \frac{2\kappa^2}{(N-l_{scp})^2}\Bigg[1^2 + 2^2 + \cdots + (N-L_{scp-2})^2 + (N-l_{scp}-1)^2 + (N-l_{scp})^2\Bigg] \\
&= \frac{2\kappa^2}{6}\Bigg[\frac{(N-l_{scp}+1)\{(2(N-l_{scp})+1\}}{N-l_{scp}}\Bigg] \\
&= \frac{2\kappa^2}{6}\Bigg[\frac{(N-\hat{\vartheta}_1'+1)\{(2(N-\hat{\vartheta}_1')+1\}}{N-\hat{\vartheta}_1'}\Bigg].
\end{aligned} \tag{II.8}
$$

Appendix III

Appendix: Derivation of mean and variance under H_o and H_1 for dynamic PU based on Markov parameters

In this section, we include proofs of $E\Big[\Upsilon(\mathbf{y})|H_o\Big]$ and $var\Big[\Upsilon(\mathbf{y})|H_o\Big]$.

III.1 Derivation of $E\Big[\Upsilon(\mathbf{y})|H_o\Big]$

$$\Upsilon(\mathbf{y})|H_o = \sum_{m=1}^{N_{00}} g_{00}^{(N-m)}|y_m|^P + \sum_{m=1}^{N_{01}} g_{01}^{(N-m)}|y_m|^P. \tag{III.1}$$

Hence,

$$E[\Upsilon(\mathbf{y})|H_o] = \underbrace{E\left[\sum_{m=1}^{N_{00}} g_{00}^{(N-m)} n_m\Big|_{m=1,2,\dots,N_{00}}\right]}_{\beta_1} + \underbrace{E\left[\sum_{m=1}^{N_{01}} g_{01}^{(N-m)} s_m\Big|_{m=1,2,\dots,N_{01}}\right]}_{\beta_2}. \tag{III.2}$$

Now, solving β_1 and β_2, we get

$$\begin{aligned}\beta_1 &= E\left[\sum_{m=1}^{N_{00}} g_{00}^{(N-m)} n_m\Big|_{m=1,2,\dots,N_{00}}\right]\\ &= E\Big[g_{00}^{(N-1)}n_1 + g_{00}^{(N-2)}n_2 + \cdots + g_{00}^{(N-m_{00})}n_{N_{00}}\Big],\end{aligned} \tag{III.3}$$

where $n_1, n_2, \ldots, n_{N_{00}}$ are assumed to be independent and identically distributed (i.i.d). Hence, $E[n_1] = E[n_2] = \cdots = E[n_{N_{00}}] = \zeta_o$. Hence,

$$\begin{aligned}\beta_1 &= \zeta_o E\left[g_{00}^{(N-1)} + g_{00}^{(N-2)} + \cdots + g_{00}^{(N-m_{00})}\right] \\ &= \zeta_o \left\{g_{00}^{(N-1)} + g_{00}^{(N-2)} + \cdots + g_{00}^{(N-m_{00})}\right\} \\ &= \zeta_o \sum_{m=1}^{N_{00}} g_{00}^{(N-m)}. \end{aligned} \tag{III.4}$$

Similarly,

$$\beta_2 = \zeta_1 \sum_{m=1}^{N_{01}} g_{01}^{(N-m)}. \tag{III.5}$$

III.2 Derivation of $var\Big[\Upsilon(\mathbf{y})|H_o\Big]$

$$\Upsilon(\mathbf{y})|H_o = \sum_{m=1}^{N_{10}} g_{10}^{(N-m)} |y_m|^P + \sum_{m=1}^{N_{11}} g_{11}^{(N-m)} |y_m|^P. \tag{III.6}$$

Hence,

$$var[\Upsilon(\mathbf{y})|H_o] = \underbrace{var\left[\sum_{m=1}^{N_{10}} g_{10}^{(N-m)} n_m \Big|_{m=1,2,\ldots,N_{10}}\right]}_{\xi_o} + \underbrace{var\left[\sum_{m=1}^{N_{11}} g_{11}^{(N-m)} s_m \Big|_{m=1,2,\ldots,N_{11}}\right]}_{\xi_1}. \tag{III.7}$$

Now, solving ξ_o and ξ_1, we get

$$\begin{aligned}\xi_o &= var\left[\sum_{m=1}^{N_{10}} g_{10}^{(N-m)} n_m \Big|_{m=1,2,\ldots,N_{10}}\right] \\ &= var\left[g_{10}^{(N-1)} n_1 + g_{10}^{(N-2)} n_2 + \cdots + g_{10}^{(N-m_{10})} n_{N_{10}}\right], \end{aligned} \tag{III.8}$$

where $n_1, n_2, \ldots, n_{N_{10}}$ are assumed to be independent and identically distributed (i.i.d). Hence, $var[n_1] = var[n_2] = \cdots = var[n_{N_{10}}] = \sigma_o^2$. Hence,

$$\begin{aligned}\xi_o &= \sigma_o^2 var\left[g_{10}^{(N-1)} + g_{10}^{(N-2)} + \cdots + g_{10}^{(N-m_{10})}\right] \\ &= \sigma_o^2\left[\left\{g_{10}^{(N-1)}\right\}^2 + \left\{g_{10}^{(N-2)}\right\}^2 + \cdots + \left\{g_{10}^{(N-m_{10})}\right\}^2\right] \\ &= \sigma_o^2 \sum_{m=1}^{N_{10}} \left\{g_{10}^{(N-m)}\right\}^2. \end{aligned} \tag{III.9}$$

Similarly,

$$\xi_1 = \sigma_1^2 \sum_{m=1}^{N_{11}} \left\{g_{11}^{(N-m)}\right\}^2 \tag{III.10}$$

Appendix IV

Appendix: Gamma functions and its derivatives

We have used Gamma functions in few chapters. In this section, we include some of the mathematical intricacies of Gamma functions [180].

$$\Gamma(v) = \int_0^{+\infty} e^{-t} t^{v-1} dt, \tag{IV.1}$$

where $t > 0$. Splitting the above gamma function about a point $i \geq 0$, we obtain

$$\gamma(v, i) = \int_0^{i} e^{-t} t^{v-1} dt, \tag{IV.2}$$

where $\gamma(v, i)$ is known as lower-incomplete gamma function. Similarly, upper incomplete gamma function can be represented as

$$\Gamma(v, i) = \int_i^{\infty} e^{-t} t^{v-1} dt. \tag{IV.3}$$

Clearly, $\Gamma(v, i) + \gamma(v, i) = \Gamma(v)$ for all $v > 0$ and $i \geq 0$. Using the fundamentals of Calculus,

$$\begin{aligned} \frac{d}{di}\gamma(v, i) &= -\frac{d}{di}\Gamma(v, i) \\ &= e^{-i} i^{v-1}. \end{aligned} \tag{IV.4}$$

Further,

$$\frac{d}{dv}\gamma(v, i) = \int_0^{i} e^{-t} t^{v-1} logt dt. \tag{IV.5}$$

As $v \to \infty$, both $\gamma(v, i)$ and $\Gamma(v, i)$ tends to infinity.

Appendix V

Appendix: Derivation of average signal-to-noise ratio under H_o and H_1

V.1 Derivation of average signal-to-noise ratio under H_o

With reference to Eq. (9.1), under hypothesis H_o, noise power P_n can be represented as

$$\begin{aligned} P_n &= \sum_{n=1}^{I'_{00}} E\left[\left\{ {m_{00}}^{(L)} w_n \right\}^2\right] + \sum_{n=I'_{00}+1}^{I'_{00}+I'_{01}} E\left[\left\{ {m_{01}}^{(L)} w_n \right\}^2\right] \\ &= 2b_l^2 \Big\{ {m_{00}}^{2\left(N-1\right)} + {m_{00}}^{2\left(N-2\right)} + \cdots + {m_{00}}^{2\left(N-I'_{00}\right)} + {m_{01}}^{2\left(N-I'_{00}\right)} + {m_{01}}^{2\left(N-I'_{00}-1\right)} + \cdots + {m_{01}}^{2\left(N-I'_{00}-I'_{01}\right)} \end{aligned} \tag{V.1}$$

Similarly, signal power P_s can be represented as

$$\begin{aligned} P_s &= \sum_{n=I'_{00}+1}^{I'_{00}+I'_{01}} E\left[\left\{ {m_{01}}^{(L)} s_n \right\}^2\right] \\ &= \frac{2\alpha^2 e_o^2 E_Q}{M} \left\{ {m_{01}}^{2\left(N-I'_{00}\right)} + {m_{01}}^{2\left(N-I'_{00}-1\right)} + \cdots + {m_{01}}^{2\left(N-I'_{00}-I'_{01}\right)} \right\}. \end{aligned} \tag{V.2}$$

V.2 Derivation of average signal-to-noise ratio under H_1

Under hypothesis H_1, P_n and P_s can be represented as

$$\begin{aligned} P_n &= \sum_{n=1}^{I'_{10}} E\left[\left\{m_{10}{}^{(L)} w_n\right\}^2\right] + \sum_{n=I'_{10}+1}^{I'_{10}+I'_{11}} E\left[\left\{m_{11}{}^{(L)} w_n\right\}^2\right] \\ &= 2b_l^2 \Big\{ m_{10}{}^{2\left(N-1\right)} + m_{10}{}^{2\left(N-2\right)} + \cdots + m_{10}{}^{2\left(N-I'_{10}\right)} + m_{11}{}^{2\left(N-I'_{10}\right)} + m_{11}{}^{2\left(N-I'_{10}-1\right)} + \cdots + m_{11}{}^{2\left(N-I'_{10}-I'_{11}\right)} \end{aligned} \tag{V.3}$$

Similarly, signal power P_s can be represented as

$$\begin{aligned} P_s &= \sum_{n=I'_{10}+1}^{I'_{10}+I'_{11}} E\left[\left\{m_{11}{}^{(L)} s_n\right\}^2\right] \\ &= \frac{2\alpha^2 e_o^2 E_Q}{M} \left\{ m_{11}{}^{2\left(N-I'_{10}\right)} + m_{11}{}^{2\left(N-I'_{10}-1\right)} + \cdots + m_{11}{}^{2\left(N-I'_{10}-I'_{11}\right)} \right\}. \end{aligned} \tag{V.4}$$

.

Bibliography

[1] S. Solanki, V. Dehalwar, J. Choudhary, M. L. Kolhe, and K. Ogura, "Spectrum sensing in cognitive radio using cnn-rnn and transfer learning," *IEEE Access*, vol. 10, pp. 113 482–113 492, 2022.

[2] L. Cai, K. Cao, Y. Wu, and Y. Zhou, "Spectrum sensing based on spectrogram-aware cnn for cognitive radio network," *IEEE Wireless Communications Letters*, vol. 11, no. 10, pp. 2135–2139, 2022.

[3] J. Manco, I. Dayoub, A. Nafkha, M. Alibakhshikenari, and H. B. Thameur, "Spectrum sensing using software defined radio for cognitive radio networks: A survey," *IEEE Access*, vol. 10, pp. 131 887–131 908, 2022.

[4] FCC, "Report of the spectrum efficiency working group," Federal Communications Commission, Washington, DC, USA, Tech. Rep. ET Docket 02-135, 2002.

[5] T. Xu, M. Zhang, H. Hu, and H.-H. Chen, "Sliced spectrum sensing—a channel condition aware sensing technique for cognitive radio networks," *IEEE Transactions on Vehicular Technology*, vol. 67, no. 11, pp. 10 815–10 829, 2018.

[6] Z. Gu, Y. Wang, T. Shen, and F. C. Lau, "On heterogeneous sensing capability for distributed rendezvous in cognitive radio networks," *IEEE Transactions on Mobile Computing*, vol. 20, no. 11, pp. 3211–3226, 2021.

[7] J. Gong, X. Qin, and X. Xu, "Multi-task based deep learning approach for open-set wireless signal identification in ism band," *IEEE Transactions on Cognitive Communications and Networking*, vol. 8, no. 1, pp. 121–135, 2022.

[8] N. Radhakrishnan, S. Kandeepan, X. Yu, and G. Baldini, "Performance analysis of long short-term memory-based markovian spectrum prediction," *IEEE Access*, vol. 9, pp. 149 582–149 595, 2021.

[9] S. M. Kim, J. Kim, H. Cha, M. S. Sim, J. Choi, S. W. Ko, C. B. Chae, and S. L. Kim, "Opportunism in spectrum sharing for beyond 5g with sub-6 ghz: A concept and its application to duplexing," *IEEE Access*, vol. 8, pp. 148 877–148 891, 2020.

[10] Y. Tao, B. Li, and C. Zhao, "Channel detection under impulsive noise and fading environments for smart grid," *IEEE Internet of Things Journal*, vol. 8, no. 20, pp. 15 407–15 421, 2021.

[11] M. Nouri, H. Behroozi, N. K. Mallat, and S. A. Aghdam, "A wideband 5g cyclostationary spectrum sensing method by kernel least mean square algorithm for cognitive radio networks," *IEEE Transactions on Circuits and Systems II: Express Briefs*, vol. 68, no. 7, pp. 2700–2704, 2021.

[12] A. Arteaga, S. Céspedes, and C. Azurdia-Meza, "Vehicular communications over tv white spaces in the presence of secondary users," *IEEE Access*, vol. 7, pp. 53 496–53 508, 2019.

[13] A. B. Flores, R. E. Guerra, E. W. Knightly, P. Ecclesine, and S. Pandey, "Ieee 802.11af: a standard for tv white space spectrum sharing," *IEEE Communications Magazine*, vol. 51, no. 10, pp. 92–100, 2013.

[14] J. Mitola and G. Maguire, "Cognitive radio: making software radios more personal," *IEEE Personal Communications*, vol. 6, no. 4, pp. 13–18, 1999.

[15] J. Mitola, "Software radio architecture: a mathematical perspective," *IEEE Journal on Selected Areas in Communications*, vol. 17, no. 4, pp. 514–538, 1999.

[16] S. Haykin, "Cognitive radio: brain-empowered wireless communications," *IEEE Journal on Selected Areas in Communications*, vol. 23, no. 2, pp. 201–220, 2005.

[17] H. Liao, X. Chen, Z. Zhou, N. Liu, and B. Ai, "Licensed and unlicensed spectrum management for cognitive m2m: A context-aware learning approach," *IEEE Transactions on Cognitive Communications and Networking*, vol. 6, no. 3, pp. 915–925, 2020.

[18] F. Mehmeti and T. Spyropoulos, "Performance analysis, comparison, and optimization of interweave and underlay spectrum access in cognitive radio networks," *IEEE Transactions on Vehicular Technology*, vol. 67, no. 8, pp. 7143–7157, 2018.

[19] F. A. Awin, Y. M. Alginahi, E. Abdel-Raheem, and K. Tepe, "Technical issues on cognitive radio-based internet of things systems: A survey," *IEEE Access*, vol. 7, pp. 97 887–97 908, 2019.

[20] F. Li, K.-Y. Lam, X. Li, Z. Sheng, J. Hua, and L. Wang, "Advances and emerging challenges in cognitive internet-of-things," *IEEE Transactions on Industrial Informatics*, vol. 16, no. 8, pp. 5489–5496, 2020.

[21] F. Hu, B. Chen, and K. Zhu, "Full spectrum sharing in cognitive radio networks toward 5g: A survey," *IEEE Access*, vol. 6, pp. 15 754–15 776, 2018.

[22] G. Kakkavas, K. Tsitseklis, V. Karyotis, and S. Papavassiliou, "A software defined radio cross-layer resource allocation approach for cognitive radio networks: From theory to practice," *IEEE Transactions on Cognitive Communications and Networking*, vol. 6, no. 2, pp. 740–755, 2020.

[23] F. Liu, Z. Zhang, R. Du, J. Sheng, and C. Huang, “Frequency-angle spectrum hole detection with taylor expansion based focusing transformation,” *IEEE Transactions on Mobile Computing*, vol. 19, no. 10, pp. 2330–2343, 2020.

[24] T. Xiong, Y.-D. Yao, Y. Ren, and Z. Li, “Multiband spectrum sensing in cognitive radio networks with secondary user hardware limitation: Random and adaptive spectrum sensing strategies,” *IEEE Transactions on Wireless Communications*, vol. 17, no. 5, pp. 3018–3029, 2018.

[25] S. Lin, B. Zheng, F. Chen, and R. Zhang, “Intelligent reflecting surface-aided spectrum sensing for cognitive radio,” *IEEE Wireless Communications Letters*, vol. 11, no. 5, pp. 928–932, 2022.

[26] L. Yang, J. Fang, H. Duan, and H. Li, “Fast compressed power spectrum estimation: Toward a practical solution for wideband spectrum sensing,” *IEEE Transactions on Wireless Communications*, vol. 19, no. 1, pp. 520–532, 2020.

[27] A. G. Fragkiadakis, E. Z. Tragos, and I. G. Askoxylakis, “A survey on security threats and detection techniques in cognitive radio networks,” *IEEE Communications Surveys Tutorials*, vol. 15, no. 1, pp. 428–445, 2013.

[28] O. S. Badarneh, “Error rate analysis of m-ary phase shift keying in $\alpha{-}\eta{-}\mu$ fading channels subject to additive laplacian noise,” *IEEE Communications Letters*, vol. 19, no. 7, pp. 1253–1256, 2015.

[29] T.-Y. Wang, F.-T. Chien, and C.-K. Hsieh, “Collaborative sampling and binary local output generation for distributed blind cooperative spectrum sensing,” *IEEE Transactions on Communications*, vol. 69, no. 8, pp. 5471–5486, 2021.

[30] S. M. Kay, “Fundamentals of statistical signal processing,” *PTR Prentice-Hall, Englewood Cliffs, NJ*, vol. II, 1998.

[31] L. Zheng, C. Yang, X. Deng, and W. Ge, “Linearized model for mimo-mfsk systems with energy detection,” *IEEE Communications Letters*, vol. 26, no. 6, pp. 1408–1412, 2022.

[32] M. V. Lipski, S. Kompella, and R. M. Narayanan, “Practical implementation of adaptive threshold energy detection using software defined radio,” *IEEE Transactions on Aerospace and Electronic Systems*, vol. 57, no. 2, pp. 1227–1241, 2021.

[33] A. Singh, M. R. Bhatnagar, and R. K. Mallik, “Cooperative spectrum sensing in multiple antenna based cognitive radio network using an improved energy detector,” *IEEE Communications Letters*, vol. 16, no. 1, pp. 64–67, 2012.

[34] S. Kavaiya and D. K. Patel, “On the performance of an improved energy detector over shadow fading channels for vehicular networks,” pp. 275–279, 2022.

[35] A. Parmar, K. Captain, R. Kumar, and A. Chouhan, "On the performance of cooperative spectrum sensing under binary erasure reporting channels," in *2022 National Conference on Communications (NCC)*, 2022, pp. 142–147.

[36] M. Golvaei and M. Fakharzadeh, "A fast soft decision algorithm for cooperative spectrum sensing," *IEEE Transactions on Circuits and Systems II: Express Briefs*, vol. 68, no. 1, pp. 241–245, 2021.

[37] P. B. Gohain, S. Chaudhari, and V. Koivunen, "Cooperative energy detection with heterogeneous sensors under noise uncertainty: Snr wall and use of evidence theory," *IEEE Transactions on Cognitive Communications and Networking*, vol. 4, no. 3, pp. 473–485, 2018.

[38] J. Perez, J. Via, L. Vielva, and D. Ramírez, "Online detection and snr estimation in cooperative spectrum sensing," *IEEE Transactions on Wireless Communications*, vol. 21, no. 4, pp. 2521–2533, 2022.

[39] L. Li, H. Jiang, and H. He, "Deep transfer cooperative sensing in cognitive radio," *IEEE Wireless Communications Letters*, vol. 10, no. 6, pp. 1354–1358, 2021.

[40] A.-Z. Chen and Z.-P. Shi, "Covariance-based spectrum sensing for noncircular signal in cognitive radio networks with uncalibrated multiple antennas," *IEEE Wireless Communications Letters*, vol. 9, no. 5, pp. 662–665, 2020.

[41] M. Jin, Q. Guo, J. Xi, Y. Li, Y. Yu, and D. Huang, "Spectrum sensing using weighted covariance matrix in rayleigh fading channels," *IEEE Transactions on Vehicular Technology*, vol. 64, no. 11, pp. 5137–5148, 2015.

[42] K. Bouallegue, I. Dayoub, M. Gharbi, and K. Hassan, "Blind spectrum sensing using extreme eigenvalues for cognitive radio networks," *IEEE Communications Letters*, vol. 22, no. 7, pp. 1386–1389, 2018.

[43] W. Zhao, S. S. Ali, M. Jin, G. Cui, N. Zhao, and S.-J. Yoo, "Extreme eigenvalues-based detectors for spectrum sensing in cognitive radio networks," *IEEE Transactions on Communications*, vol. 70, no. 1, pp. 538–551, 2022.

[44] C. Liu, J. Wang, X. Liu, and Y.-C. Liang, "Maximum eigenvalue-based goodness-of-fit detection for spectrum sensing in cognitive radio," *IEEE Transactions on Vehicular Technology*, vol. 68, no. 8, pp. 7747–7760, 2019.

[45] W. Zhao, S. S. Ali, M. Jin, G. Cui, N. Zhao, and S.-J. Yoo, "Extreme eigenvalues-based detectors for spectrum sensing in cognitive radio networks," *IEEE Transactions on Communications*, vol. 70, no. 1, pp. 538–551, 2022.

[46] J. Gao, X. Yi, C. Zhong, X. Chen, and Z. Zhang, "Deep learning for spectrum sensing," *IEEE Wireless Communications Letters*, vol. 8, no. 6, pp. 1727–1730, 2019.

[47] R. Liu, Y. Ma, X. Zhang, and Y. Gao, "Deep learning-based spectrum sensing in space-air-ground integrated networks," *Journal of Communications and Information Networks*, vol. 6, no. 1, pp. 82–90, 2021.

[48] A. Singh, M. R. Bhatnagar, and R. K. Mallik, "Performance of an improved energy detector in multihop cognitive radio networks," *IEEE Transactions on Vehicular Technology*, vol. 65, no. 2, pp. 732–743, 2016.

[49] R. B. Chaurasiya and R. Shrestha, "Hardware-efficient vlsi architecture and asic implementation of grcr-based cooperative spectrum sensor for cognitive-radio network," *IEEE Transactions on Very Large Scale Integration (VLSI) Systems*, vol. 30, no. 2, pp. 166–176, 2022.

[50] N. R. Banavathu and M. Z. A. Khan, "Optimization of n-out-of-k rule for heterogeneous cognitive radio networks," *IEEE Signal Processing Letters*, vol. 26, no. 3, pp. 445–449, 2019.

[51] A. Kumar, S. Pandit, P. Thakur, and G. Singh, "Optimization of fusion center parameters with threshold selection in multiple antenna and censoring-based cognitive radio network," *IEEE Sensors Journal*, vol. 22, no. 5, pp. 4709–4721, 2022.

[52] S. D. Arthur Nkalango, H. Zhao, Y. Song, and T. Zhang, "Energy efficiency under double deck relay assistance on cluster cooperative spectrum sensing in hybrid spectrum sharing," *IEEE Access*, vol. 8, pp. 41 298–41 308, 2020.

[53] K. Gupta, S. N. Merchant, and U. B. Desai, "Inherence of hard decision fusion in soft decision fusion and a generalized radix-2 multistage decision fusion strategy," *IEEE Access*, vol. 6, pp. 55 701–55 711, 2018.

[54] H. Soury and M.-S. Alouini, "Symbol error rate of mpsk over egk channels perturbed by a dominant additive laplacian noise," *IEEE Transactions on Communications*, vol. 63, no. 7, pp. 2511–2523, 2015.

[55] S. Gurugopinath and R. Muralishankar, "Geometric power detector for spectrum sensing under symmetric alpha stable noise," *Electronics Letters*, vol. 54, no. 22, pp. 1284–1286, 2018.

[56] D. Patel and Y. Trivedi, "Goodness-of-fit-based non-parametric spectrum sensing under middleton noise for cognitive radio," *Electronics Letters*, vol. 51, no. 5, pp. 419–421, 2015.

[57] D. K. Patel, S. Kavaiya, Z. Ding, Y. L. Guan, and S. Sun, "Impact of primary user activity statistics in cognitive vehicular networks," *IEEE Transactions on Vehicular Technology*, vol. 71, no. 3, pp. 2859–2873, 2022.

[58] B. Soni, D. K. Patel, Z. Ding, Y. L. Guan, and S. Sun, “On sensing performance of multi-antenna mobile cognitive radio conditioned on primary user activity statistics,” *IEEE Transactions on Wireless Communications*, vol. 21, no. 5, pp. 3381–3394, 2022.

[59] A. W. Min and K. G. Shin, “Robust tracking of small-scale mobile primary user in cognitive radio networks,” *IEEE Transactions on Parallel and Distributed Systems*, vol. 24, no. 4, pp. 778–788, 2013.

[60] X. He, R. Jin, and H. Dai, “Camouflaging mobile primary users in database-driven cognitive radio networks,” *IEEE Wireless Communications Letters*, vol. 8, no. 1, pp. 21–24, 2019.

[61] M. J. Rahman, “On mutual interference analysis in hybrid interweave-underlay cognitive communications,” *IEEE Transactions on Mobile Computing*, vol. 18, no. 11, pp. 2577–2588, 2019.

[62] K. Zheng, X.-Y. Liu, X. Liu, and Y. Zhu, “Hybrid overlay-underlay cognitive radio networks with energy harvesting,” *IEEE Transactions on Communications*, vol. 67, no. 7, pp. 4669–4682, 2019.

[63] T. Shongwe, A. J. H. Vinck, and H. C. Ferreira, “A study on impulse noise and its models,” *SAIEE Africa Research Journal*, vol. 106, no. 3, pp. 119–131, 2015.

[64] M. Shao and C. Nikias, “Signal processing with fractional lower order moments: stable processes and their applications,” *Proceedings of the IEEE*, vol. 81, no. 7, pp. 986–1010, 1993.

[65] S. Niranjayan and N. Beaulieu, “Receiver parameter estimation for the simplified gaussian-laplacian multiple access uwb receiver,” in *2009 IEEE International Conference on Ultra-Wideband*, 2009, pp. 707–712.

[66] C. Vlădeanu, A. Marţian, and D. C. Popescu, “Spectrum sensing with energy detection in multiple alternating time slots,” *IEEE Access*, vol. 10, pp. 38 565–38 574, 2022.

[67] A. Karimi, A. Taherpour, and D. Cabric, “Smart traffic-aware primary user emulation attack and its impact on secondary user throughput under rayleigh flat fading channel,” *IEEE Transactions on Information Forensics and Security*, vol. 15, pp. 66–80, 2020.

[68] A. A. Sharifi and M. J. Musevi Niya, “Defense against ssdf attack in cognitive radio networks: Attack-aware collaborative spectrum sensing approach,” *IEEE Communications Letters*, vol. 20, no. 1, pp. 93–96, 2016.

[69] K. Hassan, R. Gautier, I. Dayoub, M. Berbineau, and E. Radoi, “Multiple-antenna-based blind spectrum sensing in the presence of impulsive noise,” *IEEE Transactions on Vehicular Technology*, vol. 63, no. 5, pp. 2248–2257, 2014.

[70] M. Fernández, I. Landa, A. Arrinda, R. Torre, and M. M. Vélez, "Measurements of impulsive noise from specific sources in medium wave band," *IEEE Antennas and Wireless Propagation Letters*, vol. 13, pp. 1263–1266, 2014.

[71] H. Shao and N. C. Beaulieu, "An investigation of block coding for laplacian noise," *IEEE Transactions on Wireless Communications*, vol. 11, no. 7, pp. 2362–2372, 2012.

[72] F. Awin, E. Abdel-Raheem, and K. Tepe, "Blind spectrum sensing approaches for interweaved cognitive radio system: A tutorial and short course," *IEEE Communications Surveys Tutorials*, vol. 21, no. 1, pp. 238–259, 2019.

[73] T. Liu, T. Qiu, and S. Luan, "Cyclic frequency estimation by compressed cyclic correntropy spectrum in impulsive noise," *IEEE Signal Processing Letters*, vol. 26, no. 6, pp. 888–892, 2019.

[74] S. Bernstein, M. Burrows, J. Evans, A. Griffiths, D. McNeill, C. Niessen, I. Richer, D. White, and D. Willim, "Long-range communications at extremely low frequencies," *Proceedings of the IEEE*, vol. 62, no. 3, pp. 292–312, 1974.

[75] N. C. Beaulieu and S. Niranjayan, "Uwb receiver designs based on a gaussian-laplacian noise-plus-mai model," *IEEE Transactions on Communications*, vol. 58, no. 3, pp. 997–1006, 2010.

[76] F. Yilmaz, "Mcleish distribution: Performance of digital communications over additive white mcleish noise (awmn) channels," *IEEE Access*, vol. 8, pp. 19 133–19 195, 2020.

[77] K. Geddes, L. Glasser, R. Moore, and T. Scott, "Evaluation of classes of definite integrals involving elementary functions via differentiation of special functions," *Applicable Algebra in Engineering, Communication and Computing*, vol. 1, pp. 149–165, 09 1990.

[78] P. Narayanan and L. N. Theagarajan, "Capacity of peak and average power constrained additive generalized gaussian noise channels," *IEEE Communications Letters*, vol. 26, no. 12, pp. 2880–2883, 2022.

[79] M. Naseri and N. C. Beaulieu, "Fast simulation of additive generalized gaussian noise environments," *IEEE Communications Letters*, vol. 24, no. 8, pp. 1651–1654, 2020.

[80] J. Li, Q. Chen, Z. Long, W. Wang, H. Zhu, and L. Wang, "Spectrum sensing with non-gaussian noise over multi-path fading channels towards smart cities with iot," *IEEE Access*, vol. 9, pp. 11 194–11 202, 2021.

[81] L. Mohjazi, L. Bariah, S. Muhaidat, and M. A. Imran, "Performance of reconfigurable intelligent surfaces in the presence of generalized gaussian noise," *IEEE Communications Letters*, vol. 26, no. 4, pp. 773–777, 2022.

[82] F. Salahdine, H. E. Ghazi, N. Kaabouch, and W. F. Fihri, "Matched filter detection with dynamic threshold for cognitive radio networks," in *2015 International Conference on Wireless Networks and Mobile Communications (WINCOM)*, 2015, pp. 1–6.

[83] Y. Hama and H. Ochiai, "Matched-filter detector with quadrature interference cancellation for coded uplink multiuser mimo systems with massive iot devices," *IEEE Transactions on Wireless Communications*, vol. 21, no. 6, pp. 4025–4038, 2022.

[84] R. M. Narayanan, A. Z. Liu, and M. Rangaswamy, "An information elasticity framework for the adaptive matched filter," *IEEE Transactions on Aerospace and Electronic Systems*, vol. 56, no. 6, pp. 4916–4929, 2020.

[85] A. Brito, P. Sebastião, and F. J. Velez, "Hybrid matched filter detection spectrum sensing," *IEEE Access*, vol. 9, pp. 165 504–165 516, 2021.

[86] F. Robey, D. Fuhrmann, E. Kelly, and R. Nitzberg, "A cfar adaptive matched filter detector," *IEEE Transactions on Aerospace and Electronic Systems*, vol. 28, no. 1, pp. 208–216, 1992.

[87] G. Guo and M. Mandal, "On optimal threshold and structure in threshold system based detector," *Signal Processing*, vol. 92, no. 1, pp. 170–178, 2012.

[88] F. Chapeau-Blondeau, "Nonlinear test statistic to improve signal detection in non-gaussian noise," *IEEE Signal Processing Letters*, vol. 7, no. 7, pp. 205–207, 2000.

[89] M. Guerriero, S. Marano, V. Matta, and P. Willett, "Stochastic resonance in sequential detectors," *IEEE Transactions on Signal Processing*, vol. 57, no. 1, pp. 2–15, 2009.

[90] A. Saha, Aditya and G. Anand, "Design of detectors based on stochastic resonance," *Signal Processing*, vol. 83, no. 6, pp. 1193–1212, 2003.

[91] C. Sun and P. Lu, "Phase-rotated spectral correlation detector based sensing for wideband spectrum at low snrs," in *2019 IEEE International Conference on Signal, Information and Data Processing (ICSIDP)*, 2019, pp. 1–5.

[92] Z. Quan, W. Zhang, S. J. Shellhammer, and A. H. Sayed, "Optimal spectral feature detection for spectrum sensing at very low snr," *IEEE Transactions on Communications*, vol. 59, no. 1, pp. 201–212, 2011.

[93] E. Lagunas and M. Nájar, "Spectral feature detection with sub-nyquist sampling for wideband spectrum sensing," *IEEE Transactions on Wireless Communications*, vol. 14, no. 7, pp. 3978–3990, 2015.

[94] C. Guo, S. Chen, C. Feng, and Z. Zeng, "Correlation-statistics-based spectrum sensing exploiting energy and polarization for dual-polarized cognitive radios," *IEEE Transactions on Wireless Communications*, vol. 14, no. 3, pp. 1533–1554, 2015.

[95] M. Tavana, A. Rahmati, V. Shah-Mansouri, and B. Maham, “Cooperative sensing with joint energy and correlation detection in cognitive radio networks,” *IEEE Communications Letters*, vol. 21, no. 1, pp. 132–135, 2017.

[96] J. Lunden, S. A. Kassam, and V. Koivunen, “Robust nonparametric cyclic correlation-based spectrum sensing for cognitive radio,” *IEEE Transactions on Signal Processing*, vol. 58, no. 1, pp. 38–52, 2010.

[97] Y. Ye, Y. Li, G. Lu, and F. Zhou, “Improved energy detection with laplacian noise in cognitive radio,” *IEEE Systems Journal*, vol. 13, no. 1, pp. 18–29, 2019.

[98] Y. Ye, Y. Li, G. Lu, F. Zhou, and H. Zhang, “Performance of spectrum sensing based on absolute value cumulation in laplacian noise,” in *2017 IEEE 86th Vehicular Technology Conference (VTC-Fall)*, 2017, pp. 1–5.

[99] H. Shehata and T. Khattab, “Energy detection spectrum sensing in full-duplex cognitive radio: The practical case of rician rsi,” *IEEE Transactions on Communications*, vol. 67, no. 9, pp. 6544–6555, 2019.

[100] S. K. Yoo, P. C. Sofotasios, S. L. Cotton, S. Muhaidat, O. S. Badarneh, and G. K. Karagiannidis, “Entropy and energy detection-based spectrum sensing over $\mathcal{F}$ -composite fading channels,” *IEEE Transactions on Communications*, vol. 67, no. 7, pp. 4641–4653, 2019.

[101] L. Chen, N. Zhao, Y. Chen, F. R. Yu, and G. Wei, “Over-the-air computation for cooperative wideband spectrum sensing and performance analysis,” *IEEE Transactions on Vehicular Technology*, vol. 67, no. 11, pp. 10 603–10 614, 2018.

[102] L. Tlebaldiyeva, T. A. Tsiftsis, and B. Maham, “Performance analysis of improved energy detector with hardware impairments for accurate spectrum sensing,” *IEEE Access*, vol. 7, pp. 13 927–13 938, 2019.

[103] C. Vlădeanu, A. Marţian, and D. C. Popescu, “Spectrum sensing with energy detection in multiple alternating time slots,” *IEEE Access*, vol. 10, pp. 38 565–38 574, 2022.

[104] M. S. Oude Alink, A. B. J. Kokkeler, E. A. M. Klumperink, G. J. M. Smit, and B. Nauta, “Lowering the snr wall for energy detection using cross-correlation,” *IEEE Transactions on Vehicular Technology*, vol. 60, no. 8, pp. 3748–3757, 2011.

[105] A. Singh, M. R. Bhatnagar, and R. K. Mallik, “Optimization of cooperative spectrum sensing with an improved energy detector over imperfect reporting channels,” in *2011 IEEE Vehicular Technology Conference (VTC Fall)*, 2011, pp. 1–5.

[106] J. Wu, T. Song, Y. Yu, C. Wang, and J. Hu, “Generalized byzantine attack and defense in cooperative spectrum sensing for cognitive radio networks,” *IEEE Access*, vol. 6, pp. 53 272–53 286, 2018.

[107] S. Zhang, Y. Wang, Y. Zhang, P. Wan, and J. Zhuang, "A novel clustering algorithm based on information geometry for cooperative spectrum sensing," *IEEE Systems Journal*, vol. 15, no. 2, pp. 3121–3130, 2021.

[108] A. Ali and W. Hamouda, "Advances on spectrum sensing for cognitive radio networks: Theory and applications," *IEEE Communications Surveys and Tutorials*, vol. 19, no. 2, pp. 1277–1304, 2017.

[109] V. Rakovic, D. Denkovski, V. Atanasovski, P. Mähönen, and L. Gavrilovska, "Capacity-aware cooperative spectrum sensing based on noise power estimation," *IEEE Transactions on Communications*, vol. 63, no. 7, pp. 2428–2441, 2015.

[110] J. Wu, C. Wang, Y. Yu, T. Song, and J. Hu, "Performance optimisation of cooperative spectrum sensing in mobile cognitive radio networks," *IET Communications*, vol. 14, pp. 1028–1036(8), April 2020.

[111] X. Wu, L. Zhang, and M. Jiang, "Priority-based polarized transmission for feedback channels in cooperative spectrum sensing systems," *IEEE Communications Letters*, vol. 22, no. 4, pp. 836–839, 2018.

[112] M. Zheng, W. Liang, H. Yu, and M. Song, "Smcss: A quick and reliable cooperative spectrum sensing scheme for cognitive industrial wireless networks," *IEEE Access*, vol. 4, pp. 9308–9319, 2016.

[113] S. Nallagonda, R. Mamidi, and A. Bhowmick, "Analysis of energy-efficient cooperative spectrum sensing with improved energy detectors and multiple antennas over nakagami-q/n fading channels," *International Journal of Communication Systems*, vol. 34, no. 5, p. e4731, 2021, e4731 dac.4731.

[114] M. Ranjeeth, S. Anuradha, and S. Nallagonda, "Optimized cooperative spectrum sensing network analysis in nonfading and fading environments," *International Journal of Communication Systems*, vol. 33, no. 5, p. e4262, 2020, e4262 IJCS-17-0487.R1.

[115] C. Ji and Q. Qi, "Cooperative spectrum sensing algorithm based on evolutionary game theory," *IEEE Access*, vol. 10, pp. 71 557–71 565, 2022.

[116] T. Wimalajeewa and P. K. Varshney, "Polarity-coincidence-array based spectrum sensing for multiple antenna cognitive radios in the presence of non-gaussian noise," *IEEE Transactions on Wireless Communications*, vol. 10, no. 7, pp. 2362–2371, 2011.

[117] M. Karimzadeh, A. M. Rabiei, and A. Olfat, "Soft-limited polarity-coincidence-array spectrum sensing in the presence of non-gaussian noise," *IEEE Transactions on Vehicular Technology*, vol. 66, no. 2, pp. 1418–1427, 2017.

[118] L. D. S. Costa, D. A. GUIMARÃES, and B. F. Uchôa-Filho, "On the signal-to-noise ratio wall of energy detection in spectrum sensing," *IEEE Access*, vol. 10, pp. 16 499–16 511, 2022.

[119] O. M. Eltabie, M. F. Abdelkader, and A. M. Ghuniem, "Incorporating primary occupancy patterns in compressive spectrum sensing," *IEEE Access*, vol. 7, pp. 29 096–29 106, 2019.

[120] C.-H. Liu, J. A. Tran, P. Pawelczak, and D. Cabric, "Traffic-aware channel sensing order in dynamic spectrum access networks," *IEEE Journal on Selected Areas in Communications*, vol. 31, no. 11, pp. 2312–2323, 2013.

[121] X. Luo, W. Zhao, H. Li, M. Jin, and G. Cui, "Fusion test statistics based mixture detector for spectrum sensing," *IEEE Transactions on Vehicular Technology*, vol. 71, no. 3, pp. 3315–3319, 2022.

[122] A. Sabra and M. Berbineau, "Experimental assessment of eigenvalue-based spectrum sensing using usrp-based mimo testbed for cognitive radio applications," *IEEE Sensors Letters*, vol. 6, no. 10, pp. 1–4, 2022.

[123] J. Wu, P. Li, J. Bao, and H. Ge, "Quick multiband spectrum sensing for delay-constraint cognitive uav networks," *IEEE Sensors Journal*, vol. 22, no. 19, pp. 19 088–19 100, 2022.

[124] Z. Wang, S. Lyu, L. Liu, and Y. Xia, "Learning-aided markov chain monte carlo scheme for spectrum sensing in cognitive radio," *IEEE Transactions on Vehicular Technology*, vol. 71, no. 10, pp. 11 301–11 305, 2022.

[125] Z. Du, X. Chen, H. Zhang, and B. Yang, "Compressed-sensing-based periodic impulsive feature detection for wind turbine systems," *IEEE Transactions on Industrial Informatics*, vol. 13, no. 6, pp. 2933–2945, 2017.

[126] B. Bhavana, S. Namburu, T. Panigrahi, and S. L. Sabat, "Robust methods for wideband compressive spectrum sensing under non-gaussian noise," *IEEE Communications Letters*, vol. 25, no. 10, pp. 3398–3402, 2021.

[127] Q. Li and Z. Li, "A novel sequential spectrum sensing method in cognitive radio using suprathreshold stochastic resonance," *IEEE Transactions on Vehicular Technology*, vol. 63, no. 4, pp. 1717–1725, 2014.

[128] X. Zhu, B. Champagne, and W.-P. Zhu, "Cooperative spectrum sensing based on the rao test in non-gaussian noise environments," in *2013 International Conference on Wireless Communications and Signal Processing*, 2013, pp. 1–6.

[129] M. Liu, N. Zhao, J. Li, and V. C. M. Leung, "Spectrum sensing based on maximum generalized correntropy under symmetric alpha stable noise," *IEEE Transactions on Vehicular Technology*, vol. 68, no. 10, pp. 10 262–10 266, 2019.

[130] A. Margoosian, J. Abouei, and K. N. Plataniotis, “An accurate kernelized energy detection in gaussian and non-gaussian/impulsive noises,” *IEEE Transactions on Signal Processing*, vol. 63, no. 21, pp. 5621–5636, 2015.

[131] F. Tan, X. Song, C. Leung, and J. Cheng, “Collaborative spectrum sensing in a cognitive radio system with laplacian noise,” *IEEE Communications Letters*, vol. 16, no. 10, pp. 1691–1694, 2012.

[132] W. Zhang, C. Zhang, G. An, and J. Li, “Logarithmic similarity measure based cooperative spectrum sensing under impulsive noise,” *Progress In Electromagnetics Research C*, vol. 100, pp. 45–57, 2020.

[133] I. Song, D. Kim, S. Lee, and S. Yoon, “Selection-based detectors and fusion centers for cooperative cognitive radio networks in heavy-tailed noise environment,” *Journal of Communications and Networks*, vol. 19, no. 3, pp. 259–269, 2017.

[134] J. Tang, Y. Li, and Q. Wu, “Non-gaussian noise cooperative spectrum sensing scheme based on rao test,” in *2015 International Conference on Network and Information Systems for Computers*, 2015, pp. 545–548.

[135] H. Qu, X. Xu, J. Zhao, F. Yan, and W. Wang, “A robust hyperbolic tangent-based energy detector with gaussian and non-gaussian noise environments in cognitive radio system,” *IEEE Systems Journal*, vol. 14, no. 3, pp. 3161–3172, 2020.

[136] L. Jiang, Y. Li, Y. Ye, Y. Chen, M. Jin, and H. Zhang, “Unilateral left-tail anderson darling test-based spectrum sensing with laplacian noise,” *IET Communications*, vol. 13, no. 6, pp. 696–705, 2019.

[137] N. I. Miridakis, T. A. Tsiftsis, and G. Yang, “Generalized energy detection under generalized noise channels,” *IEEE Wireless Communications Letters*, vol. 9, no. 12, pp. 2020–2024, 2020.

[138] B. Li, S. Li, A. Nallanathan, and C. Zhao, “Deep sensing for future spectrum and location awareness 5g communications,” *IEEE Journal on Selected Areas in Communications*, vol. 33, no. 7, pp. 1331–1344, 2015.

[139] B. Li, S. Li, A. Nallanathan, Y. Nan, C. Zhao, and Z. Zhou, “Deep sensing for next-generation dynamic spectrum sharing: More than detecting the occupancy state of primary spectrum,” *IEEE Transactions on Communications*, vol. 63, no. 7, pp. 2442–2457, 2015.

[140] N. Biswas, G. Das, and P. Ray, “Optimal hybrid spectrum sensing under control channel usage constraint,” *IEEE Transactions on Signal Processing*, vol. 66, no. 14, pp. 3875–3890, 2018.

[141] N. Biswas, Z. Wang, L. Vandendorpe, and H. Mirghasemi, “On joint cooperative relaying, resource allocation, and scheduling for mobile edge computing networks,” *IEEE Transactions on Communications*, vol. 70, no. 9, pp. 5882–5897, 2022.

[142] W. Yin and D. Xu, "Design and performance analysis of bandwidth-adaptive continuous spectrum sensing," *IEEE Systems Journal*, vol. 16, no. 4, pp. 5258–5269, 2022.

[143] N. C. Beaulieu and Y. Chen, "Improved energy detectors for cognitive radios with randomly arriving or departing primary users," *IEEE Signal Processing Letters*, vol. 17, no. 10, pp. 867–870, 2010.

[144] J. Wang, R. Chen, J. Huang, F. Shu, Z. Chen, and G. Min, "Multiple-antenna spectrum sensing method with random arrivals of primary users," *IEEE Transactions on Vehicular Technology*, vol. 67, no. 9, pp. 8978–8983, 2018.

[145] M. Jin, Q. Guo, Y. Li, J. Xi, and Y. Yu, "Energy detection with random arrival and departure of primary signals: New detector and performance analysis," *IEEE Transactions on Vehicular Technology*, vol. 66, no. 11, pp. 10 092–10 101, 2017.

[146] T. Düzenli and O. Akay, "A new spectrum sensing strategy for dynamic primary users in cognitive radio," *IEEE Communications Letters*, vol. 20, no. 4, pp. 752–755, 2016.

[147] T. Duzenli and O. Akay, "A new method of spectrum sensing in cognitive radio for dynamic and randomly modelled primary users," *IETE Journal of Research*, vol. 68, no. 2, pp. 957–965, 2022.

[148] H. Pradhan, S. S. Kalamkar, and A. Banerjee, "Sensing-throughput tradeoff in cognitive radio with random arrivals and departures of multiple primary users," *IEEE Communications Letters*, vol. 19, no. 3, pp. 415–418, 2015.

[149] L. Tang, Y. Chen, E. L. Hines, and M.-S. Alouini, "Performance analysis of spectrum sensing with multiple status changes in primary user traffic," *IEEE Communications Letters*, vol. 16, no. 6, pp. 874–877, 2012.

[150] M. R. Amini, M. Mahdavi, and M. J. Omidi, "Discrete-time markov chain analysis of energy efficiency in a cr network regarding primary and secondary traffic with primary user returns," *IEEE Access*, vol. 6, pp. 22 305–22 323, 2018.

[151] K. Chang and B. Senadji, "Spectrum sensing optimisation for dynamic primary user signal," *IEEE Transactions on Communications*, vol. 60, no. 12, pp. 3632–3640, 2012.

[152] B. Li, J. Hou, X. Li, Y. Nan, A. Nallanathan, and C. Zhao, "Deep sensing for space-time doubly selective channels: When a primary user is mobile and the channel is flat rayleigh fading," *IEEE Transactions on Signal Processing*, vol. 64, no. 13, pp. 3362–3375, 2016.

[153] S. MacDonald, D. C. Popescu, and O. Popescu, "Analyzing the performance of spectrum sensing in cognitive radio systems with dynamic pu activity," *IEEE Communications Letters*, vol. 21, no. 9, pp. 2037–2040, 2017.

[154] J. Unnikrishnan and V. V. Veeravalli, “Algorithms for dynamic spectrum access with learning for cognitive radio,” *IEEE Transactions on Signal Processing*, vol. 58, no. 2, pp. 750–760, 2010.

[155] M. Hossain and J. Xie, “Hide and seek: A markov-based defense strategy against off-sensing attack in cognitive radio networks,” *IEEE Transactions on Network Science and Engineering*, vol. 7, no. 4, pp. 3028–3041, 2020.

[156] Y. Sun, B. L. Mark, and Y. Ephraim, “Collaborative spectrum sensing via online estimation of hidden bivariate markov models,” *IEEE Transactions on Wireless Communications*, vol. 15, no. 8, pp. 5430–5439, 2016.

[157] Z. Wang, L. Liu, and K. Li, “Dynamic markov chain monte carlo-based spectrum sensing,” *IEEE Signal Processing Letters*, vol. 27, pp. 1380–1384, 2020.

[158] N. I. Miridakis, T. A. Tsiftsis, and G. Yang, “Moment-based spectrum sensing under generalized noise channels,” *IEEE Communications Letters*, vol. 25, no. 1, pp. 89–93, 2021.

[159] B. Jamali and A. Babakhani, “A fully integrated 50–280-ghz frequency comb detector for coherent broadband sensing,” *IEEE Transactions on Terahertz Science and Technology*, vol. 9, no. 6, pp. 613–623, 2019.

[160] A. Bergman, T. Langer, and M. Tur, “Coding-enhanced ultrafast and distributed brillouin dynamic gratings sensing using coherent detection,” *Journal of Lightwave Technology*, vol. 34, no. 24, pp. 5593–5600, 2016.

[161] J. A. Estrada, S. Johannes, D. Psychogiou, and Z. Popović, “Tunable impedance-matching filters,” *IEEE Microwave and Wireless Components Letters*, vol. 31, no. 8, pp. 993–996, 2021.

[162] T. Sibbett, H. Moradi, and B. Boroujeny, “Normalized matched filter for blind interference suppression in filter bank multicarrier spread spectrum systems,” *IEEE Access*, vol. 10, pp. 64 270–64 282, 2022.

[163] G. Guo, M. Mandal, and Y. Jing, “A robust detector of known signal in non-gaussian noise using threshold systems,” *Signal Processing*, vol. 92, p. 2676–2688, 11 2012.

[164] A. Papoulis, *Probability Random Variables, and Stochastic Processes.* Newyork, London: McGraw-Hill Book Company, 1965.

[165] J. So, “Energy-efficient cooperative spectrum sensing with a logical multi-bit combination rule,” *IEEE Communications Letters*, vol. 20, no. 12, pp. 2538–2541, 2016.

[166] H. Wu, F. Yao, Y. Chen, Y. Liu, and T. Liang, “Multibit-quantization-based collaborative spectrum sensing scheme for cognitive sensor networks,” *IEEE Access*, vol. 5, pp. 25 207–25 216, 2017.

[167] S. Hu, Q. Luo, F. Li, Z. Liu, Y. Gao, and J. Wu, "Practical implementation of multi-user transform domain communication system for control channels in cloud-based cognitive radio networks," *IEEE Access*, vol. 6, pp. 17 010–17 021, 2018.

[168] R. Sarikhani and F. Keynia, "Cooperative spectrum sensing meets machine learning: Deep reinforcement learning approach," *IEEE Communications Letters*, vol. 24, no. 7, pp. 1459–1462, 2020.

[169] N. S. Moayedian, S. Salehi, and M. Khabbazian, "Fair resource allocation in cooperative cognitive radio iot networks," *IEEE Access*, vol. 8, pp. 191 067–191 079, 2020.

[170] W. Yin and H. Chen, "Decision-driven time-adaptive spectrum sensing in cognitive radio networks," *IEEE Transactions on Wireless Communications*, vol. 19, no. 4, pp. 2756–2769, 2020.

[171] J. Zhang, Z.-Q. He, H. Rui, and X. Xu, "Multiband joint spectrum sensing via covariance matrix-aware convolutional neural network," *IEEE Communications Letters*, vol. 26, no. 7, pp. 1578–1582, 2022.

[172] P. Cai and Y. Zhang, "Intelligent cognitive spectrum collaboration: Convergence of spectrum sensing, spectrum access, and coding technology," *Intelligent and Converged Networks*, vol. 1, no. 1, pp. 79–98, 2020.

[173] G. Huang and J. K. Tugnait, "On cyclostationarity based spectrum sensing under uncertain gaussian noise," *IEEE Transactions on Signal Processing*, vol. 61, no. 8, pp. 2042–2054, 2013.

[174] B. Okyere, L. Musavian, and R. Mumtaz, "Performance analysis of physical layer network coding in massive mimo systems with m-qam modulations," *IEEE Transactions on Vehicular Technology*, vol. 70, no. 5, pp. 4631–4645, 2021.

[175] E. Biglieri, K. Yao, and C.-A. Yang, "Fading models from spherically invariant processes," *IEEE Transactions on Wireless Communications*, vol. 14, no. 10, pp. 5526–5538, 2015.

[176] E. Biglieri and M. Lops, "Linear-quadratic detectors for spectrum sensing," *Journal of Communications and Networks*, vol. 16, no. 5, pp. 485–492, 2014.

[177] E. Biglieri, E. Grossi, and M. Lops, *Random-Set Theory and Wireless Communications.* Now Foundations and Trends, 2012.

[178] E. Biglieri, V. Tarokh, and M. K. Simon, "Special issue on coding and signal processing for mimo system," *Journal of Communications and Networks*, vol. 5, no. 2, pp. 93–95, 2003.

[179] E. Biglieri and M. Lops, "Multiuser detection in a dynamic environment– part i: User identification and data detection," *IEEE Transactions on Information Theory*, vol. 53, no. 9, pp. 3158–3170, 2007.

[180] E. C. Molina, "An expansion for laplacian integrals in terms of incomplete gamma functions, and some applications," *The Bell System Technical Journal*, vol. 11, no. 4, pp. 563–575, 1932.